Conference Proceedings

Workshop

Adaptive Structures at Shore

23rd & 24th of May 2022
Hamburg, Germany

Editor

J. Grabe

Hamburg University of Technology
Institute of Geotechnical Engineering and Construction Management

Publications by the Institute of
Geotechnical Engineering and Construction Management

52

Editor:

Univ.-Prof. Dr.-Ing. Jürgen Grabe
Hamburg University of Technology
Institute of Geotechnical Engineering and Construction Management
Harburger Schloßstraße 36
D – 21079 Hamburg
e-mail: *grabe@tuhh.de*

ISBN-13: 978-3-936310-54-2 (first edition)
DOI: https://doi.org/10.15480/882.4468 (first edition)

Printery

Druckzentrum Neumünster GmbH
Rungestraße 4
D – 24537 Neumünster

Published in the same series:

1. J. Grabe (eds.), 2000: Verbrennungsrückstände. Conference Proceedings, ISBN 3-936310-00-9
2. J. Grabe (eds.), 2001: Schaden- und Risikomanagement im Tiefbau. Conference Proceedings, ISBN 3-936310-01-7
3. J. Grabe, 2003. Bodenmechanik und Grundbau. ISBN 3-936310-03-3
4. J. Grabe (eds.), 2003: Euronormen in der Geotechnik – Was ändert sich? Conference Proceedings, ISBN 3-936310-04-1
5. J. Grabe (eds.), 2003: Bodenverdichtung, Experimente - Modellierung - Geräteentwicklung - Baustellenberichte - F+E-Bedarf. Conference Proceedings, ISBN 3-936310-05-X
6. M. Kelm, 2004: Nummerische Simulation der Verdichtung rolliger Böden mittels Vibrationswalzen. Dissertation, ISBN 3-936310-06-8
7. J. Grabe (eds.), 2004: Kaimauern - Messungen und Numerik. Conference Proceedings, ISBN 3-936310-07-6
8. J. Stein, 2005. Experimentelle und numerische Untersuchungen zum Düsenstrahlverfahren. Promotion, ISBN 3-936310-09-2
9. J. Grabe (eds.), 2005: Grenzschicht Wasser und Boden - Phänomene und Ansätze. Conference Proceedings, ISBN 3-936310-10-6
10. J. Grabe (eds.), 2005: FEM in der Geotechnik - Qualität, Prüfung, Fallbeispiele - Conference Proceedings, ISBN 3-936310-11-4
11. B. Mardfeldt, 2006: Zum Tragverhalten von Kaikonstruktionen im Gebrauchszustand. Dissertation, ISBN 3-936310-12-2
12. J. Grabe (eds.), 2006: Optimierung in der Geotechnik - Strategien und Fallbeispiele. Conference Proceedings, ISBN-13: 978-3-936310-13-9
13. T. Bierer, 2007: Bodenschwingungen aus Straßenverkehr auf unebener Fahrbahn im Zeitbereich - experimentelle und theoretische Untersuchungen. Dissertation, ISBN-13: 978-3-936310-14-6
14. J. Grabe (eds.), 2007: Bemessen mit Finite-Elemente-Methoden. Conference Proceedings, ISBN-13: 978-3-936310-15-3
15. K.-P. Mahutka, 2008: Zur Verdichtung von rolligen Böden infolge dynamischer Pfahleinbringung und durch Oberflächenrüttler. Dissertation, ISBN-13: 978-3-936310-16-0
16. J. Grabe (eds.), 2008: Seehäfen für Containerschiffe zukünftiger Generationen. Conference Proceedings, ISBN-13: 978-3-936310-17-7

17. F. König, 2008: Zur zeitlichen Traglastentwicklung von Pfählen und der nachträglichen Erweiterung bestehender Pfahlgründungen. Dissertation, ISBN-13: 978-3-936310-18-4

18. S. Henke, 2008: Herstellungseinflüsse aus Pfahlrammung im Kaimauerbau. Dissertation, ISBN-13: 978-3-936310-19-1

19. J. Grabe (eds.), 2009: Spundwände – Profile, Tragverhalten, Bemessung, Einbringung und Wiedergewinnung. Conference Proceedings, ISBN-13: 978-3-936310-20-7

20. J. Dührkop, 2009: Zum Einfluss von Aufweitungen und zyklischen Lasten auf das Verformungsverhalten lateral beanspruchter Pfähle in Sand. Dissertation, ISBN-13: 978-3-936310-21-4

21. O. Möller, 2009: Zum Langzeit-Kompressionsverhalten weicher organischer Sedimente. Dissertation, ISBN-13: 978-3-936310-22-1

22. J. Grabe (eds.), 2011: Ports of container ships of future generations. Conference Proceedings, ISBN-13: 978-3-936310-23-8

23. S. Kinzler, 2011: Zur Parameteridentifikation, Entwurfs- und Strukturoptimierung in der Geotechnik mittels numerischer Verfahren. Dissertation, ISBN-13: 978-3-936310-24-5

24. G. Qiu, 2012: Coupled Eulerian Lagrangian Simulations of Selected Soil-Structure Problems. Dissertation, ISBN-13: 978-3-936310-25-2

25. X. Ma, 2013: Nutzung der oberflächennahen Geothermie mittels Energiepfählen und Erdwärmesonden. Dissertation, ISBN-13: 978-3-936310-26-9

26. J. Grabe (eds.), 2013: Proceedings of the Conference on Maritime Energy COME 2013. Conference Proceedings, ISBN-13: 978-3-936310-28-3

27. J. Grabe (eds.), 2013: Bemessen mit numerischen Methoden. Conference Proceedings, ISBN-13: 978-3-936310-29-0

28. T. Pucker, 2013: Stoffmodell zur Modellierung von stetigen Materialübergängen im Rahmen der Optimierung geotechnischer Strukturen. Dissertation, ISBN-13: 978-3-936310-30-6

29. S. Henke, 2013: Untersuchungen zur Pfropfenbildung infolge der Installation offener Profile in granularen Böden. Habilitation, ISBN-13: 978-3-936310-31-3

30. J. Grabe (eds.), 2014: Ports for Container Ships of Future Generations. Conference Proceedings, ISBN-13: 978-3-936310-32-0

31. J. Grabe (eds.), 2014: Offshore Basishäfen, Conference Proceedings, ISBN-13: 978-3-936310-33-7

32. C. Rudolph, 2015. Untersuchungen zur Drift von Pfählen unter zyklischer, lateraler Last aus veränderlicher Richtung, Dissertation, ISBN-13: 978-3-936310-34-4

33. J. Grabe (eds.), 2015: Morphodynamics 2015, Conference Proceedings, ISBN-13: 978-3-936310-35-1

34. T. Hamann, 2015: Zur Modellierung wassergesättigter Böden unter dynamischer Belastung und großen Bodenverformungen am Beispiel der Pfahleinbringung, Dissertation, ISBN-13: 978-3-936310-36-8

35. B. Schümann, 2015: Beitrag zum dynamischen Dreiphasenmodell für Boden auf Basis der Finite-Elemente-Methode, Dissertation, ISBN-13: 978-3-936310-37-5

36. M. Milatz, 2015: Untersuchungen zum Einfluss der Kapillarität auf das hydraulisch-mechanische Verhalten von granularer Tragschichten für Verkehrswege, Dissertation, ISBN-13: 978-3-936310-38-2

37. H. Kaya, 2016: Bodenverschleppung und Spaltbildung infolge der Einbringung von Profilen in Dichtungsschichten aus Ton, Dissertation, ISBN-13: 978-3-936310-39-9

38. J. Grabe (eds.), 2017: Proceedings of the Conference on Maritime Energy COME 2017. Conference Proceedings, ISBN-13: 978-3-936310-40-5

39. B. Kocak, 2017: Zur numerischen Modellierung von hydraulisch-mechanisch gekoppelten Prozessen in gesättigten granularen Böden mittels Smoothed Particle Hydrodynamics, Dissertation, ISBN-13: 978-3-936310-41-2

40. K. Siegl, 2017: Zur Pfahldynamik von gerammten Großrohrpfählen und der daraus resultierenden Wellenausbreitung in Wasser und im Meeresboden, Dissertation, ISBN-13: 978-3-936310-42-9

41. J. Grabe (eds.), 2017: Numerical Methods in Geotechnics, Conference Proceedings, ISBN-13: 978-3-936310-43-6

42. J. Grabe (eds.), 2018: Digitale Infrastruktur und Geotechnik (DIG 2018), Conference Proceedings, ISBN-13: 978-3-936310-44-3

43. D. Osthoff, 2018: Zur Ursache von Schlosssprengungen und zu einbringbedingten Lageabweichungen von Spundwänden, Dissertation, ISBN-13: 978-3-936310-45-0

44. E. Heins, 2018: Numerical based identification of the pile-soil interaction in terms of the axial pile bearing capacity, Dissertation, ISBN-13: 978-3-936310-46-7

45. K.-F. Seitz, 2021: Zur Topologieoptimierung von geotechnischen Strukturen und zur Tragfähigkeitssteigerung des Baugrunds durch Scherfugenverfestigung, Dissertation, ISBN-13: 978-3-936310-47-4

46. D. Plenker, 2021: Physical and numerical investigations of the dynamic interaction of saturated granulates and fluid, Dissertation, ISBN-13: 978-3-936310-48-1

47. J. Grabe, J.-O. Backhaus & P. Vogel, 2021: Bauprojektmanagement, ISBN-13: 978-3-936310-49-8

48. M. Kanitz, 2021: Experimental and numerical investigations of particle-fluid systems in geotechnical engineering, Dissertation, ISBN-13: 978-3-936310-50-4

49. J.-O. Backhaus, 2021: A methodology for the numeric time-cost forecast and pareto optimization of large injection projects in tunneling, Dissertation, ISBN-13: 978-3-936310-51-1

50. S. N. Sinduri, 2021: Optimisation of deep compaction as liquefaction mitigation measure, Dissertation, ISBN-13: 978-3-936310-52-8

51. J. Bubel, 2022: Zum Versagen von Unterwasserböschungen im Seegang, Dissertation, ISBN-13: 978-3-936310-53-5

Table of Contents

MONITORING AND AUTOMATION

BRIDGES

QUAY WALLS

FLOATING STRUCTURES

Preface

Coastal regions will experience unavoidable challenges in the future due to global climate change. Long-term forecasts of the associated changes in the boundary conditions of maritime structures in their planned service life are unreliable due to the range of possible global warming scenarios. Adaptive and resilient structures are a possible solution to this predicament.

To enable a structure to adapt to its environment, a long and short term prediction of the impacts and resulting loads, as well as knowledge of the existing material resistances, is necessary. The development of efficient methods for material healing in order to (re-)establish the required resistances, and the associated extension of the service life of the structures play a decisive role, especially in the case of structures in water that are difficult to access. With knowledge of the impacts and resistances, the numerical modelling of the structures allows topology- and structure-optimisation in the design process and an assessment of the degree of utilisation of the overall system during its service life. Thus, innovative modelling methods enable the evaluation of the need for active adaptation under the given boundary conditions. In practice, the actual adaptation of a structure must be realised by means of active and semi-active components integrated into the design. Therefore, corresponding control and regulation methods are required. Furthermore, an adaptable structure in the water requires automated monitoring in real time to assess its status. Long-term stable, smart sensor systems are therefore essential.

The workshop intends to outline the state of research in the different disciplines involved in the development of adaptive structures.

My special thank goes to the authors for their contribution, all doctoral students and staff of the Institute of Geotechnical Engineering and Construction Management as well as the administration of Hamburg University of Technology for their participation and support.

I am looking forward to the numerous precious contributions, presentations and constructive discussions.

Sincerely yours,

Jürgen Grabe

Hamburg, 12$^{\text{th}}$ of April 2022

Future Ecosystems and Biodiversity linked to Marine engineering structures

Karen Wiltshire

The contribution was not available by the time of printing.

Adaptive Structures in Architecture

Walter Haase, Christina Eisenbarth, Katrin Chwalek, Lucio Blandini

Abstract: This article describes the motivation, the project and the research goals of the Collaborative Research Centre (CRC) 1244, an interdisciplinary cooperation between various insti-tutes of the University of Stuttgart and partners, with the aim of developing adaptive buildings that achieve a significantly higher level of comfort with significantly less material and operating energy.

1 The Collaborative Research Centre (CRC) 1244

1.1 Motivation

Innovative solutions are needed in the building sector to be able to achieve the EU's climate targets and become climate neutral by 2050 (European Commission, 2019). In 2020 alone, 37 % of global energy-related CO_2 emissions were emitted in the construction sector (United Nations Environment Programme, 2021). These emissions result from the operation of buildings, the production of the necessary building materials and the construction process itself. Thus, the building sector has a great responsibility yet a great potential to reduce emissions that contribute to climate change. In addition, the building sector consumes about 3 billion tons of raw materials and is responsible for 40 % of solid waste (Dalla Valle, 2021). Certain raw materials essential to the construction process are now scarce, such as sand, one of the most widely used raw materials on earth, but its consumption exceeds the natural renewal rate (United Nations Environment Programme, 2014). The increase in the world population from 7.7 billion people in 2019 to an expected 9.7 billion people in 2050 (United Nations et al., 2019) will require the construction of more housing and infrastructure buildings, leading to immense demand for resources. One approach to solve this problem is to design buildings adaptively. Adaptive buildings provide adaptation mechanisms in the structural system and the façade. In the load-bearing structure, the stress state or the vibration behavior is significantly improved, which means that the mass of the load-bearing structure can be drastically reduced (Geiger et al., 2020). The adaptive façade reacts to varying external influences or changing user requirements in such a way that the user comfort is increased and the energy expenditure for conditioning is minimized by adapting the physical properties of the building skin. Considering the above-mentioned challenges, more living space should be created in the future with less use of resources and fewer emissions (Sobek et al., 2021).

1.2 Introduction

In the Collaborative Research Centre (CRC) 1244, research has been conducted on the topic of adaptivity since 2017 in close interdisciplinary cooperation to find out how, in the context of a growing world population and diminishing resources, more living space can be created with less material in the future. The goal of CRC 1244 is to find answers to the pressing ecological and social questions of our time for the building industry. The aim is to optimize the energy, material and emissions balance of the supporting structure and façade throughout the entire life cycle of the building through adaptivity.

2 Adaptivity in the High-Rise Building Demonstrator

2.1 Adaptivity at the D1244

Adaptivity is the targeted modification of physical, mechanical or geometric properties of various components (Sobek et al., 2021). The development of novel adaptivity concepts is being researched and tested within the framework of CRC 1244 at the demonstrator high-rise building, the D1244, which can be seen in Figure 1. Here, adaptive systems are developed that actively change their properties with the help of controlled processes. Unique to the D1244 is the integration of active elements into the load-bearing structure and, in the future, also into the façade. It is important to consider adaptivity at the beginning of the design process in order to be able to develop the optimal adaptive supporting structure or façade system (Sobek et al., 2021). The original concept for CRC 1244 was developed under the leadership of Prof. Werner Sobek, who was both the spokesperson for the first research phase of CRC 1244 and the architect of the experimental high-rise building.

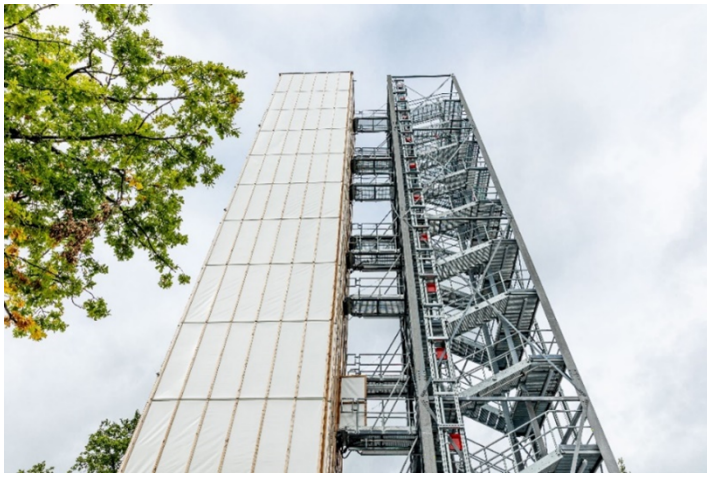

Figure 1: The D1244 high-rise building / Universität Stuttgart, Uli Regenscheit

2.2 The Adaptive Support System

The adaptive load-bearing system of the D1244 changes its geometry and stiffness in such a way that stresses, deformations and the vibration behaviour can be optimised when forces occur. In this context, the integrated regulation and control technology in the building gives the adaptive system the possibility to cause these system changes through its actuators integrated into the supporting structure. Through the use of sensors, the building can react to external influences such as wind or earthquakes and recognise the forces acting on the building in a fraction of a second - it can specifically counteract them and significantly improve the load transfer. This achieves a damping of vibrations, a reduction in deformations and a reduction in the stress on the load-bearing system - making it possible to build significantly lighter.

Figure 2: The D1244 high-rise building / Universität Stuttgart, Uli Regenscheit

2.3 Novel Adaptive Façade Systems

The façade of the D1244, which was initially designed as a temporary membrane envelope, will gradually be replaced by adaptive envelope elements. An adaptive façade system reacts both to changing external influences in its environment and to the respective different user requirements and accordingly adapts its physical properties such as light transmission, thermal transmittance, acoustic properties or microclimatic effectiveness on the urban space, to name but a few, to the respective needs (Romano et al., 2018). The aim is to maximize indoor comfort for users, achieve energy savings and thus reduce emissions (Attia et al., 2020; Leistner at al., 2020). Complete recyclability of the systems is mandatory (Sobek et al., 2021). Such novel adaptive envelope systems are being developed within the framework of CRC 1244. The different variants of adaptive façades are being tested at D1244 to determine their potential and to demonstrate the positive influence and interaction of people and architecture in interior and urban spaces. For the 11th floor of D1244, an ETFE façade system is being developed with different intermediate layers that control the appearance, thermal transmittance and shading properties of the façade. One promising infill is the Pneumatically Actuated Origami Sun Shading (PAOSS) system, which

will be installed on the southwest side (Eisenbarth et al., 2021). Pneumatic actuators integrated into the origami structure allow the textile elements to be opened and closed to control light transmission and prevent glare (Figure 3).

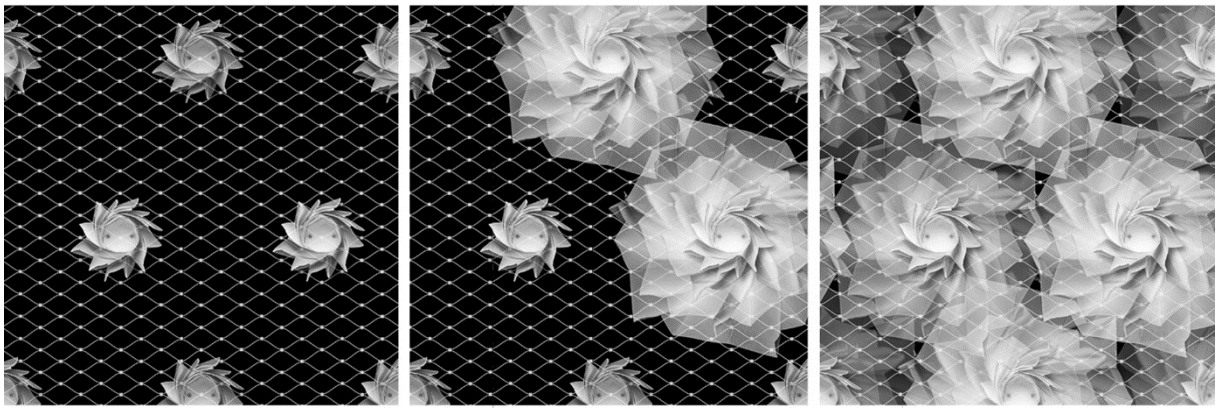

Figure 3: PAOSS sun-shading system. In closed state (left), in partially actuated state as selective glare protection (middle) and in open state as full sun protection (right) (source: ILEK)

A new hydroactive façade system, also based on textiles, is being tested on the 9th and 10th floors. The aim of the socalled „HydroSKIN“ is to retain rainwater and improve the urban microclimate around the building (Eisenbarth et al., 2022).

Adaptive envelope concepts open up a completely new spectrum of functions and forms in the façade sector.

3 Outlook and Objectives

By developing novel adaptivity concepts for all areas of the built environment, CRC 1244 stands for sustainable architecture that takes responsibility for economic, ecological and socio-cultural issues. The basis for defining this goal is the shared conviction of all partners that material and energy consumption in the building process must be extremely reduced in the near future - while at the same time increasing user comfort. A holistic and interdisciplinary strategy is to be developed that brings together technological and architectural approaches through adaptivity (Sobek et al, 2021).

4 Acknowledgements

The research presented in this paper was funded by the German Research Foundation (DFG) - project number 279064222 - SFB 1244. The authors would like to thank the DFG for founding and supporting the SFB 1244 and all the staff involved for their dedicated work.

References

[1] Attia S., Lioure R., Declaude Q. (2020): Future trends and main concepts of adaptive facade systems. Energy Science and Engineering 8 (9)

[2] Dalla Valle A. (2021): Change Management Towards Life Cycle AE(C) Practice. Springer International Publishing

[3] Eisenbarth, C., Haase, W. Klett, Y., Blandini, L. and Sobek, W. (2021): PAOSS - Pneumatically Actuated Origami Sun Shading, Journal of Facade Design and Engineering, vol. 9, no. 1, 147–162, 2021, doi: 10.7480/jfde. 2021.1.5535.

[4] Eisenbarth, C., Haase, W., Blandini, L. and Sobek, W. (2022): Potentials of Hydroactive Lightweight Façades for Urban Climate Resilience, Civil Engineering Design, doi: 10.1002/cend.202200003 (in press).

[5] European Commission (2019): Economic and Social Committee and the Committee of the Regions: The European Green Deal.

[6] Geiger F., Gade J., Von Scheven M., Bischoff M. (2020): Optimal Design of Adaptive Structures versus Optimal Adaptation of Structural Design. in: Proc. of the 21st IFAC World Congress, Berlin, Germany

[7] Leistner S., Honold C., Maierhofer M., Haase W., Blandini L., Sobek W., Roth D., Binz H., Menges A. (2020): Research on integral design and planning processes for adaptive buildings. Architectural Engineering and Design Management, 0(0):1-20

[8] Romano R., Aelenei L., Aelenei D., Mazzucchelli E. S. (2018): What is an adaptive façade? Analysis of Recent Terms and definitions from an international perspective. Journal of Facade Design and Engineering, 6(3):65-76

[9] Sobek W., Sawodny O., Bischoff M., Blandini L., Böhm M., Haase W. et al. (2021): Adaptive Hüllen und Strukturen. Bautechnik, 98(3): 208–221

[10] United Nations, Department of Economic and Social Affairs, Population Division (2019): World Population Prospects 2019: Highlights, (ST/ESA/SER.A/423)

[11] United Nations Environment Programme (2014): Sand, rarer than one thinks. In: Environmental Development 11

[12] United Nations Environment Programme (2021): Global Status Report for Buildings and Construction: Towards a Zero-emissions, Efficient and Resilient Buildings and Construction Sector

Authors

Dr.-Ing. Walter Haase
Managing Director of the Collaborative Research Centre 1244
University of Stuttgart
Institute for Lightweight Structures and Conceptual Design
Pfaffenwaldring 7 & 14
70569 Stuttgart
T +49 711 - 685 68310 / - 685 62276
F +49 711 - 685 66968
e-mail: walter.haase@ilek.uni-stuttgart.de
Web: www.ilek.uni-stuttgart.de/
Web: www.sfb1244.uni-stuttgart.de/

Christina Eisenbarth
Doctoral Researcher at the Collaborative Research Centre 1244
University of Stuttgart
Institute for Lightweight Structures and Conceptual Design
Pfaffenwaldring 14
70569 Stuttgart
T 49 711 - 685 66138
F +49 711 - 685 66968
e-mail: christina.eisenbarth@ilek.uni-stuttgart.de
Web: www.ilek.uni-stuttgart.de/
Web: www.sfb1244.uni-stuttgart.de/

Katrin Chwalek
Doctoral Researcher at the Collaborative Research Centre 1244
University of Stuttgart
Institute for Lightweight Structures and Conceptual Design
Pfaffenwaldring 14
70569 Stuttgart
T +49 711 - 685 63796
F +49 711 - 685 66968
Web: www.ilek.uni-stuttgart.de/
Web: www.sfb1244.uni-stuttgart.de/

Prof. Dr. Ing. M.Arch. Lucio Blandini
Director of the Institute for Lightweight Structures and Conceptual Design
University of Stuttgart
Institute for Lightweight Structures and Conceptual Design
Pfaffenwaldring 7 & 14
70569 Stuttgart
T +49 711 - 685 63796
F +49 711 - 685 66968
e-mail: christina.eisenbarth@ilek.uni-stuttgart.de
Web: www.ilek.uni-stuttgart.de/
Web: www.sfb1244.uni-stuttgart.de/

Rising on ice - Antarctic Station Neumayer III

Andreas Nitschke, Thomas Matz

Abstract: The Antarctic research station Neumayer III was put into operation in 2009 after two years of construction. It is the first German above-ground Antarctic research station. The following article describes the requirements and solutions for such a building in Antarctica. In particular, the site conditions on the Ekström Ice Shelf required novel adjustments to the building's design and construction.

1 Overview Antartica

Antarctica is the continent south of the 60th parallel and, at 14 million km2, is around one and a half times the size of Europe. The landmass is almost completely (98 %) covered by ice up to 4500 m thick. The ice shield contains 90 % of the ice and 70 % of the freshwater reserves worldwide. The ecosystem of Antarctica is almost untouched. The conditions in the Antarctic are decisive for the global climate. Antarctica is inhabited in summer/winter by around 4000/1000 scientists in more than 80 research stations.

With the Antarctic Treaty of 1959, Antarctica was placed under special protection by the international community. The aim is to maintain the ecological balance and to use Antarctica for

peaceful purposes. Military exercises and the exploitation of mineral resources are prohibited, territorial claims are suspended. By the Environmental Protection Protocol (Madrid Protocol; entered into force in 1998), more extensive requirements were placed on activities in Antarctica.

As part of the increased attention being paid to Antarctica, the activities there are also becoming a stage for the participating states and their efforts to protect the climate. The newer Antarctic stations are showing a trend towards architecturally designed buildings and the use of the latest technology to reduce energy consumption and pollution.

The map (Figure 1) shows the location of the year-round stations. For better accessibility, most stations are located near the coast.

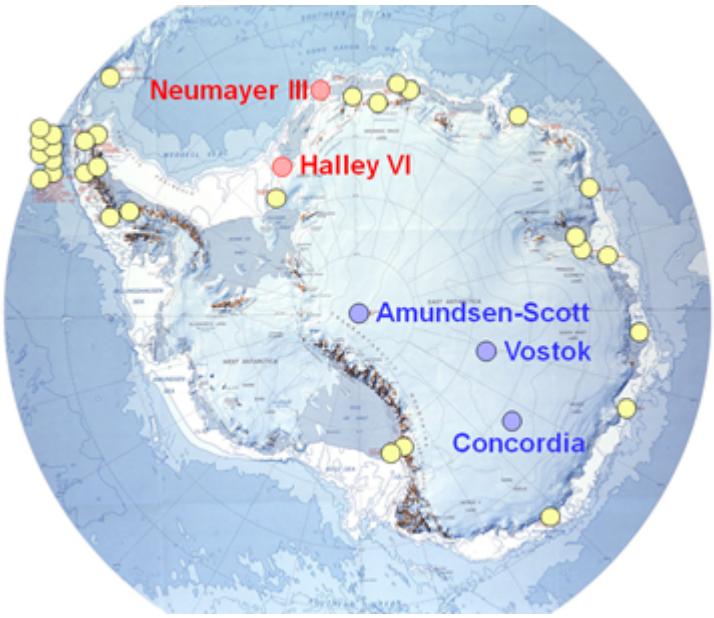

Figure 1: year-round Antarctic Stations (foundation: on rock in yellow, on inland ice in blue, on ice shelf in red)

2 Conditions for working in Antarctica

2.1 Remoteness

Like no other continent, Antarctica is characterized by its remoteness and hostility to life. Accessibility is only given in the Antarctic summer from November to March. The landmass is surrounded by a belt of pack ice that can only be crossed by ship in summer. The ship passage takes about 10-15 days in good conditions and can be delayed by several days depending on the ice conditions. Accessibility by larger aircraft is limited to a few airports and is mainly used for passenger transport. From the larger airfields, the neighbouring stations, which are often several 100 km away, can then be reached by feeder flight. Air traffic is also extremely dependent on the

weather conditions and is only possible in summer. Conversely, this means that neither material nor people can be brought in or out of Antarctica in winter. The last dates for leaving the country must be adhered to, otherwise, there is a risk of overwintering. Transports into, within and out of the Antarctic are very complex in every respect, both in terms of time and the available capacities as well as economically. The subsequent delivery of material or the replacement of personnel is hardly possible.

2.2 Location on Ice shelf causes special demands

Most Antarctic stations are located near the coast in ice-free regions, socalled oases. Few stations are founded on ice and like the German Neumayer stations and the British Halley VI.

Shelf ice is defined as that portion of coastal glaciers that is already floating and moving towards the ocean. Ice plates breaking off at the edge of the shelf ice form tabular icebergs, some of which can reach considerable dimensions. The shelf ice is in constant motion, both overall towards the sea and relatively through distortion and torsion. The German Antarctic stations are located at Atka Bay on the Ekström Ice Shelf. Figure 2 shows the ice movements in the construction area of the Neumayer III station. The annual flow movement is approx. 120 m/a and deformations of 2 % per year were to be considered. The thickness of the ice shelf at Neumayer Station is about 200 m.

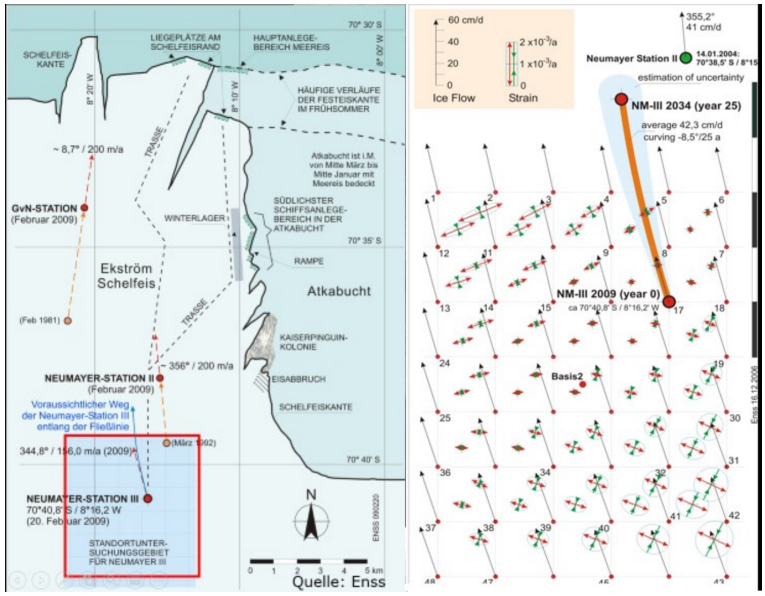

Figure 2: Location and movement on Shelf ice of Neumayer Stations

2.3 Climate and Seasons

2.3.1 Summer and Winter

Astronomically speaking, the sun stays above the horizon between 19 November and 24 January (polar day) and below the horizon between 19 May and 27 July (polar night). During summer working in shifts around the clock is possible, as far as other weather conditions allow. During winter working outside is very limited due to darkness and adverse winds and temperatures. The intensity and duration of solar irradiation can be significant, especially during the 24 hours of a polar day. For the design case of warming in the summer, this has to be considered. The mean solar radiation in December and January is 346 W/m^2 and 286 W/m^2 respectively, while radiation drops to 121 W/m^2 on average over the full year. Working outside is only possible in summer. But even then, days lost due to snowstorms and low temperatures must be considered.

2.3.2 Wind and Temperature

The strong winds and low temperatures are the determining climate factors for all activities carried out by human beings in the Antarctic. The highest wind velocities recorded at Neumayer are 27.3 m/s (10 minutes-average) in the summer season and 39.9 m/s (1 minute-average) in winter. Gust wind velocities according to Table 1 can be calculated with these wind data for the reference height of 10 m.

Table 1: Gust wind velocities

	5 sec gust	2 sec gust	1 sec gust
50-year-event	58.8m/s	61.4m/s	63.2m/s
100-year-event	60.6m/s	63.2m/s	65.1m/s

The design of the station considers wind velocities up to 63 m/s. The distribution of wind directions and velocities is shown in Figure 3. The main wind directions are between 075° and 105° and between 210° and 270°.

The mean temperatures at the station, measured 2 m above ground, are -16.1 °C (year), -22.6 °C (winter, July) and -3.9 °C (summer, January). Extreme temperatures so far were -47.3 °C and +4.3 °C. For the design, ambient temperatures between –50 °C and +30 °C had to be considered. In areas below the snow surface temperatures will not fall below –25 °C. The combination of temperatures and wind velocities, the so called wind-chill-factor, is crucial for outdoor working conditions.

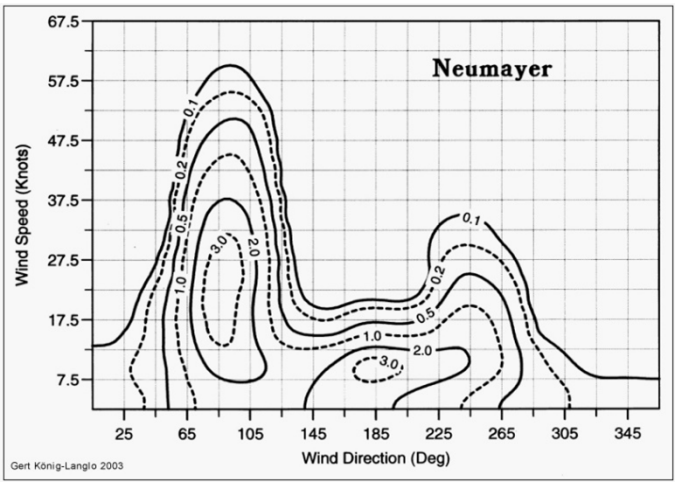

Figure 3: Relative occurrence of wind directions and velocities in % of observations (Nitschke, 2006)

2.3.3 Snowdrift and accumulation

Snowdrift starts at wind velocities of about 6 m/s (21.6 km/h) and therefore occurs on more than 50 % of all days in the station area. It increases with larger wind velocities. Most of the drifting snow is found close to the ground. Snow masses moved by drifts and transported over long distances are considerable. Drift snow builds up around obstacles, mainly at the front and rear ends (wind tails), and reaches the top height of the obstacles quickly. Excavation pits can be filled expeditiously with snow at wind velocities of 10 m/s (Beaufort 5) and more. Consequently, the structure should create as few wind tails as possible and thereby help to avoid the undesirable accumulation of snow. Snowfall and snowdrift mainly contribute to the accumulation, which comprises precipitation, drift snow deposition, hoar and evaporation. The accumulation rate at the station site varies considerably and is 0.73 m/a on average, corresponding to 280 kg/(m^2a). As a design value, 0.80 m/a has been used.

2.4 Reliability of Materials and Methods

In particular, the seclusion and inaccessibility in winter require structures with a high level of reliability and operational safety. Since the number of on-site personnel is limited and generally more oriented towards ongoing operations, the benchmark must be simplicity and redundancy. This sometimes contradicts the operator's desire for the latest digitised standard for the technical systems. "State of the art" versus "simple and proven" must be balanced carefully. The innovation often lies in a new combination of proven solutions from other application areas.

This applies both to the materials to be used, for which long-term experience under comparable conditions should be available, and to the methods and processes used in building construction. In the case of the materials, the approvals for use at very low temperatures are often not available and only cover the usual area of application in the country of origin. Necessary environmental

and framework conditions for construction processes, e.g. sufficient temperatures for concreting or weather protection for welding, must be clarified in detail and in advance.

2.5 Prefabrication, Mock-Up, Transport and Mounting on site

Due to the boundary conditions by limited capacities in terms of personnel and construction time, the construction of Antarctic stations requires a high degree of prefabrication of the parts of the building, which should only be assembled and not built in the Antarctic. Rooms and systems are usually prefabricated in containers ready for operation in the home country. Screw connections with a few, rather large screws should be provided for steel components. Connections such as gluing, welding, soldering should be avoided or their applicability must be checked in advance. For complex sections, a trial assembly at the factory is recommended.

When packing and transporting the individual parts, the entire transport chain and especially the last few meters on the construction site must be taken into account, as only limited lifting equipment is available here. The weight and dimensions of the individual parts are often determined by the loading conditions and must be considered at the planning stage. It should also be considered that the parts are transported through all climatic zones and condensation from the tropics can turn into ice in the Antarctic.

The individual parts are to be locked in such a way that no snow can penetrate during interim storage in the Antarctic. The Antarctic snow is very fine and dry and can be blown into every crack. If the parts are then installed inside the station, the melting of the snow can cause damage to electrical systems. The same applies to assembly sections, which must be well secured against the ingress of snow, particularly if the outer shell is not closed.

If the measure is spread over several seasons, the construction site must be made particularly winter-proof. All parts are to be well secured against the storm and openings are to be closed, otherwise, the rooms behind are completely filled with snow. Subsequent intervention during the winter is not possible due to the climatic conditions.

3 The German Neumayer Stations

The research areas of the Neumayer stations include meteorology, geophysics and air chemistry. The climate changes at this location have been observed in uninterrupted long-term series of measurements for 50 years.

The German stations (Georg von Neumayer 1981-1992, Neumayer II to 2009 and Neumayer III since 2009) were single buildings that contained all the functions and technical systems in one structure like a ship, which is particularly beneficial for small teams in winter. However, special safety precautions must be taken here and the separation of living, working and machine

technology is not possible. Single buildings are more common for newer stations in special environments.

3.1 Subsurface Construction of Georg von Neumayer und Neumayer II

Due to their location on the ice shelf, the stations are exposed to high wind velocities combined with low temperatures and strong snowdrifts. The earlier stations addressed this by being below the surface of the ice. The design principle was containers in corrugated iron tubes that were covered with snow. This allowed the high wind loads to be avoided. The snow has an insulating effect against the outside temperatures, so that inside the stations temperature was balanced to some minus degrees. Figure 4 shows a photo of the Neumayer II station from the construction period.

Figure 4: Neumayer II under construction (D. Enß Hansa 9/1992, Page 3-15)

These stations were accessible via stair towers, which were also the only signs of the station above ground (see Figure 5). Over the course of its operational life, around 0.8 m of snow was deposited on the surface each year, so that the stations sank deeper in relation to the surface. On the one hand, this meant that the stair towers had to be regularly lengthened, and on the other hand, the snow load on the corrugated iron tubes kept increasing. Both effects made it necessary to close the station after 17 years. Figure 5 shows the deformations of the ceilings that were present when Neumayer II was dismantled.

After abandoning the stations, all large parts of the stations that could not be dismantled and removed through the stair towers remain in the ice and drift with the ice movement to the cliff edge, where they then break off with an iceberg and ultimately, when it melts, will sink into the sea. The location of the stations deep under the ice meant considerable restrictions in terms of comfort and psychological stress for the staff. Especially in winter, when the station could

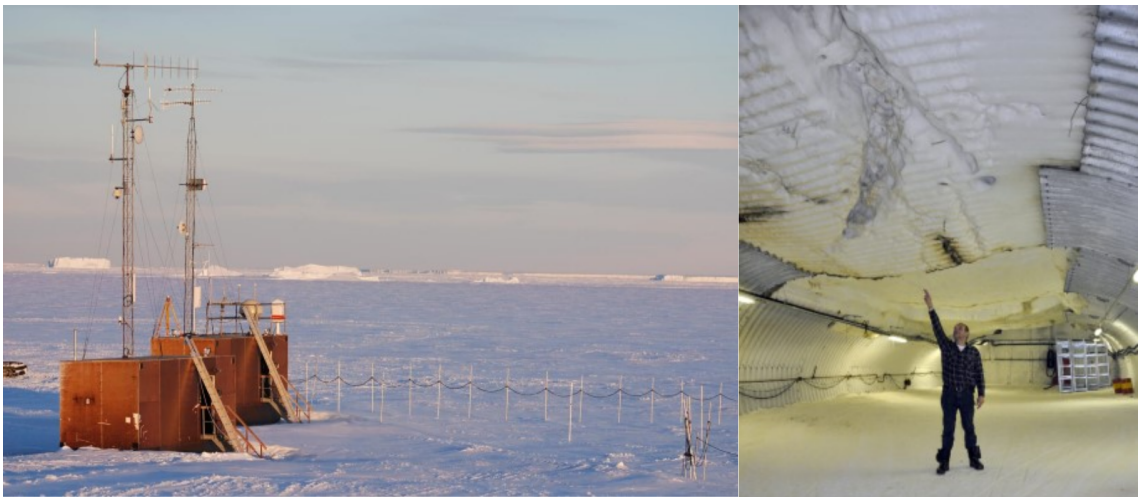

Figure 5: Neumayer II under construction (D. Enß Hansa 9/1992, Page 3-15)

not be left for a long time due to the weather, one had to rely on one another in a small space with less privacy and without daylight. To leave the station via the stair towers, all the necessary material and equipment always had to be carried up. The ventilation and exhaust of the rooms many meters below the surface were demanding.

4 Antarctic Station Neumayer III

The disadvantages of the subsurface construction and the environmental requirements that have increased with the Madrid Protocol, which prescribe the recycling of systems that are no longer required, made an above-ground construction necessary for the Neumayer III station. The following challenges had to be mastered.

- Founding the building on smooth snow
- Avoiding sinking of the building by lifting
- Balancing of stresses due to distortion of the Shelf Ice
- Avoiding snow accumulation in the vicinity of the building
- Bearing the high wind loads

The construction principle of the Neumayer III station is described below and the solutions for the above points are discussed.

Table 2: Characteristic Numbers

Crew winter /summer		10/50 Pers.
Platform	Length: (about half the length of Polarstern)	68 m
	Width:	24m
Trench section:	Length:	76 m
	Width:	26m
	Depth:	8m
Container modules on the platform		100 pc.

Table 3: Protected usable areas in the station m^2

Area allocation	Air-conditioned	Cold	Total
U2 garage	13.8	1,658.8	1,672.6
U1 garage	428.8	646.5	1,075.3
D1 platform	854.7	426.7	1,281.4
D2 platform	820.9	13.8	834.7
D3 platform	0.0	26.8	26.8
Total NM-III	2,118.2	2,772.6	4,890.8
For comparison, NM II	914.0	2,015.0	2,929.0

4.1 Construction Principle

The Antarctic station Neumayer III (NM III) is divided into a part below the snow surface, the so-called garage, and an elevated part, the platform. The garage and platform are con-nected by the staircase suspended from the structure. Figure 7 shows a cross-section through the station in the staircase area.

4.1.1 Garage

The garage is divided into two levels. Level U1 is the foundation level and the garage floor on which the vehicles are parked. Level U1 is not heated, the temperature follows the outside temperature and averages around -15°C. Level U2 is located under the garage roof between the supporting structure. Technical facilities such as hydraulic systems, the snow melting plant, workshops and storage rooms are housed here. The room temperatures are kept above zero degrees.

The garage roof ends even to the snow surface and forms level 0. Around the roof pane, vertical steel plates are attached, which are hydraulically pressed against the snow wall. Garage level U1 is accessible to vehicles via a snow ramp on the north side, which can be closed with a cover. The cover can be opened hydraulically via a portal bock. The intermediate level U2 can be reached via the staircase.

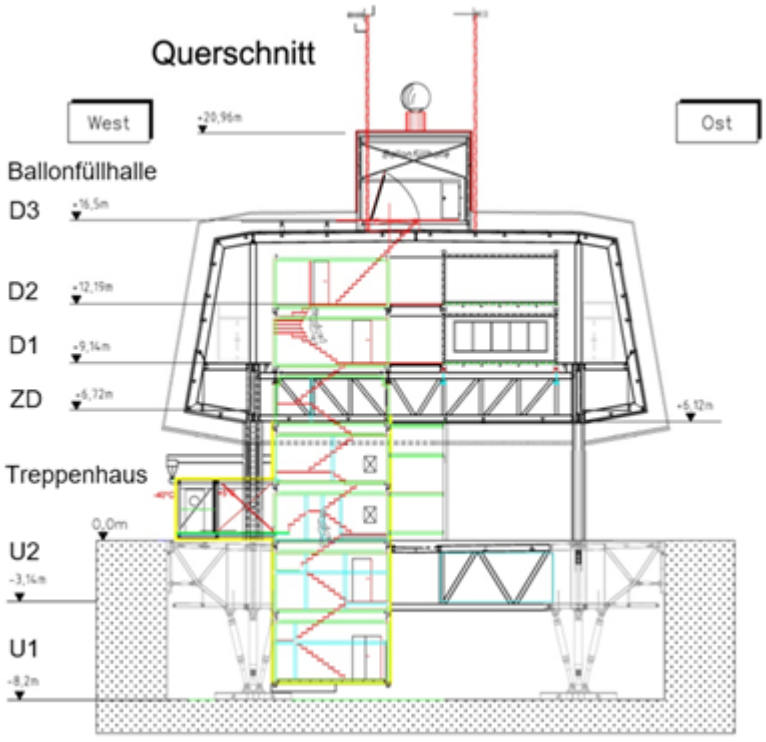

Figure 6: Cross-section Neumayer III

Figure 7: NM III, Garage, hydraulically driven Side Skirts

4.1.2 Platform

The platform is divided into several levels from bottom to top

- ZD the tween deck at the level of the supporting girder structure
- D1+D2 the living and research areas in two layers of living cells

- D3 the roof level with research facilities, antennas etc.
- the balloon inflation hall with the roof exit

The generators and control rooms are arranged on the platform in the northern area, separated from the living and working rooms. The firefighting equipment, fuel tanks and storage are in the tween deck. The platform is enclosed by an aerodynamically shaped facade made of cold store panels.

The space between the facade and the living cells is called the gallery and serves as an additional area and as a temperature buffer. In this way, a good temperature gradient from the outside to the inside can be maintained. While it can be as low as – 40 °C outside the station, the temperature in the gallery does not fall below freezing and normal room temperature can be maintained in the living and working areas.

4.1.3 Load Bearing Structure

In the longitudinal direction, the station is divided into seven fields plus cantilevers. The platform rests on sixteen columns made of cross-welded HEB beams. These stand on the girder grid of the garage roof, which rests on 32 hydraulic cylinders arranged in pairs. To absorb horizontal forces, the pairs of hydraulic cylinders, socalled bipods, are arranged in a V-shape. Steel spindles are located between the hydraulic cylinders, which act as safety supports and take on the loads should the hydraulic pressure drop unexpectedly. To be able to absorb the horizontal loads in both directions, four of the bipods are arranged in the longitudinal direction and 12 in the transverse direction. The bipods stand on steel foundation plates with dimensions of 3 m x 4 m or 4 m x 4 m. Figure 9 shows the foundation scheme. Horizontal forces can also be absorbed by the side skirts of the roof pane.

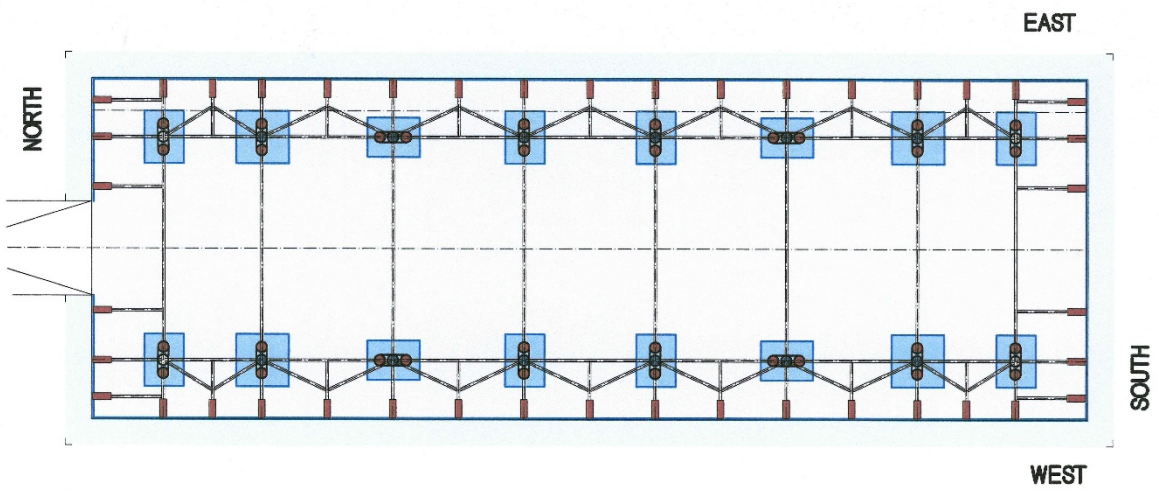

Figure 8: NM III, Garage, hydraulically driven Side Skirts

4.2 Founding the building on smooth snow

The foundation loads under the bipods average 1500 kN or 125 kN/m^2.

In the area of the Neumayer Station there is an annual increase in the snow of about 0.8 m. This snow is very fine-grained and dry on the surface, comparable to a fine powder-like flour. It is not suitable for the foundation of a structure with high foundation loads. It is only through the layers that are deposited over the years that the snow is compacted and solidified in such a way that it has sufficient load-bearing capacity. The load-bearing capacity depends on the density of the snow, which is reached after about 5-10 years of compression. The foundation level had to be arranged approx. 10 x 0.8 m = 8.0 m below the snow surface, which goes well with the height of the garage.

Another property of snow or ice under high loads is important for the foundation of the station. Under constant load, ice has a three-phase viscoelastic settlement behaviour. In the first phase, the rate of settlement decreases and approaches a constant value in the second phase. After a certain time, the third phase follows, in which the rate of settlement increases exponentially and ultimately leads to ground break/failure.

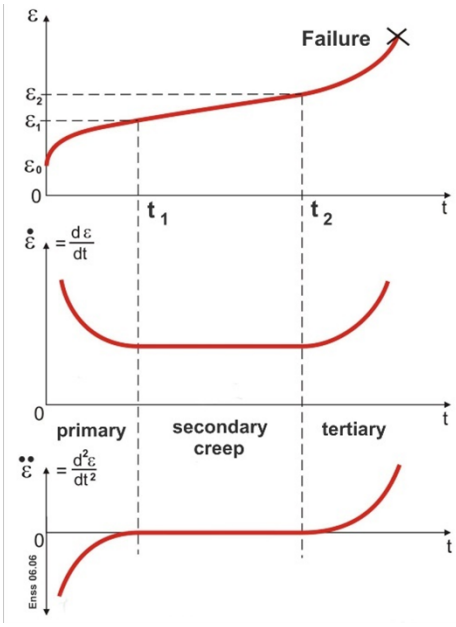

Figure 9: Creeping behavior of Ice/Snow

In Geduhn et al. (2006), it was shown that under the conditions and loads present at the Neumayer station, the limit stress between linear and non-linear viscoelastic creep behaviour can be set at approx. 180 kN/m^2. This limit should not be exceeded in the long term, otherwise, there is a risk of exponentially growing deformations. The duration of the first creep phase has been calculated in Geduhn et al. (2006) to last approximately six years before the second and third phases begin with the risk of creep rupture. However, because of the annual lifting and lining of the station foundations with new snow (see Chap. 5.3), the loading point moves away from the layer at risk of fracture and simultaneously the load pressure is reduced as a result of the load spread

(Figure 11). This means that the settlements remain permanently in the primary phase and a creep fracture can be ruled out.

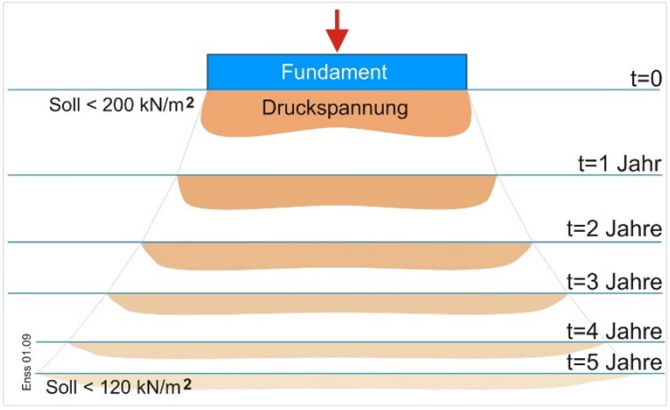

Figure 10: Creeping behavior of Ice/Snow

4.3 Avoiding sinking of the building by lifting

As described above, the station stands on hydraulic cylinders to which the foundation plates are coupled. The supporting structure of the station is designed so stiffly that the omission of single supports is acceptable in terms of load and deformation. This allows individual supports to be raised and lined with snow. The foundation slabs are then set down again and the new snow is compacted under them to such an extent that it can bear weight again.

The lifting process starts with all hydraulic cylinders being extended and the garage roof being lifted out of the snow surface. The safety spindle supports are fixed in the high position. Then the trestle of the ramp cover is raised so that the access opening for snow clearing vehicles is open again. With these snow groomers the snow is then pushed in, to fill up the garage floor. On the outside, the garage roof is also filled with snow on the sides to seal the pit again and to enable the horizontal loads to be transferred via the side skirts. The foundation slabs are raised individually and in pilgrim steps, lined with snow and set down again. A video of the lifting process is linked on the AWI website. (https://www.youtube.com/watch?v=H57xqUmlCdk&t=80s). Figure 12 shows a situation where one foundation has already been raised and relined while the others are still in their home position.

During the entire process, the deflections of the structure and the oil pressures are precisely monitored and kept within the permissible limits by the hydraulic system. The permissible deflections for the supporting structure are between 10 mm and 30 mm, but for the facade elements, the relative movements may only be in the range of a few millimetres due to the needed tightness of the shell.

To monitor the deformations, measuring cylinders are arranged on the bipods, which are connected via hoses based on the principle of a hose water level. Here, the various deviations from the target position are automatically monitored and displayed on an overview tableau.

Figure 11: NM III, Lifting process, 2nd Bipod already lifted

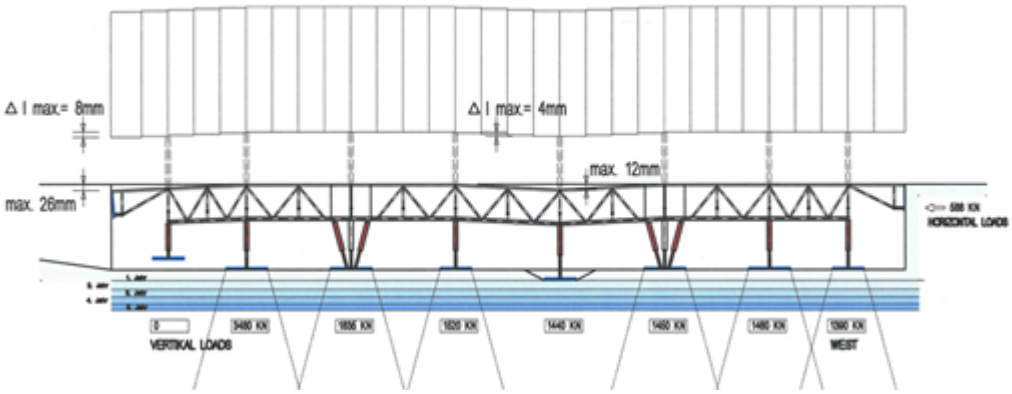

Figure 12: NM III, limits of allowable deformations

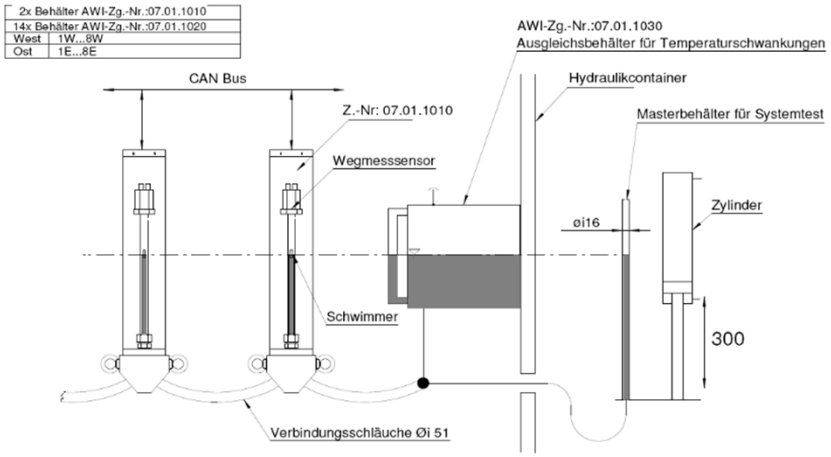

Figure 13: NM III, supervision of vertical movements by hose water level

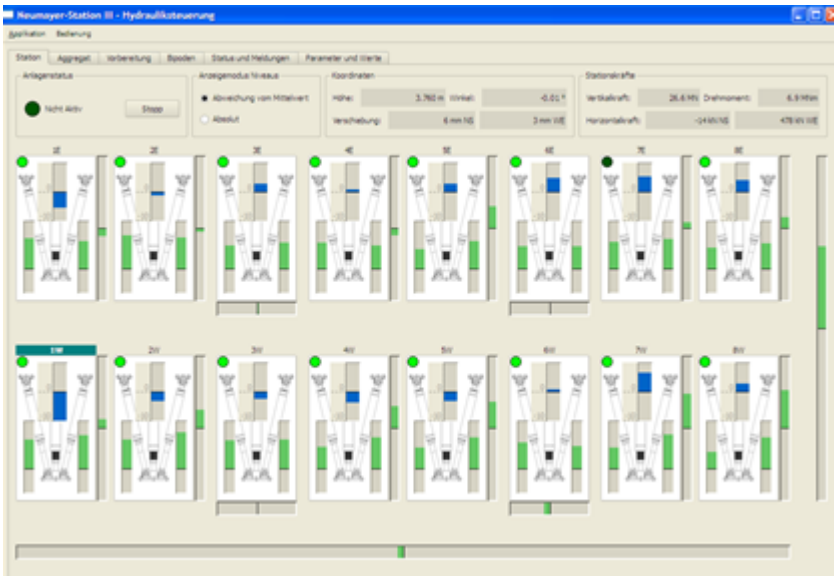

Figure 14: NM III, display for supervision of settlements/movements

4.4 Balancing of stresses due to distortion of the Shelf Ice

The movement of the ice shelf, the settlement of the foundations and the viscous flow of snow into the garage result in constraints within the structure, which must be compensated if they should not lead to overloading. Vertical deformation and twisting of the supports and foundations are recorded by the hose level system described above and can be compensated by controlling the bipods. Horizontal shifts in the level of the garage floor are reflected in the misalignment of the supports, which are regularly checked by using spirit levels or observing changes in the pressure of the hydraulic cylinders. If the critical values are reached, the stress can be relieved by raising and lowering the foundation plates. The same also applies to pressure on the edge of the roof, which can be compensated for by loosening and then pressing again the hydraulic side skirts against the snow walls. The pressures in the cylinders and the deformations are checked regularly.

4.5 Avoiding snow accumulation in the vicinity of the building

To prevent the building from snow accumulation, the platform was raised six meters high above ground level. This creates a nozzle effect under the structure, which ensures that no snow remains on the garage roof. In extensive simulation calculations and wind tunnel tests, the height of the stilts and the shape of the facade were optimised. For the latter, the focus of optimisation was the altitude of the stagnation point, where the airflow splits upwards and downwards. Figure 17 shows the comparison of a numerical simulation with a photo from the wind tunnel test.

Both images show good congruency. The flow, here from the left, shows a reduction in flow speed on the windward side, which leads to snow accumulation in front of the station. The wind

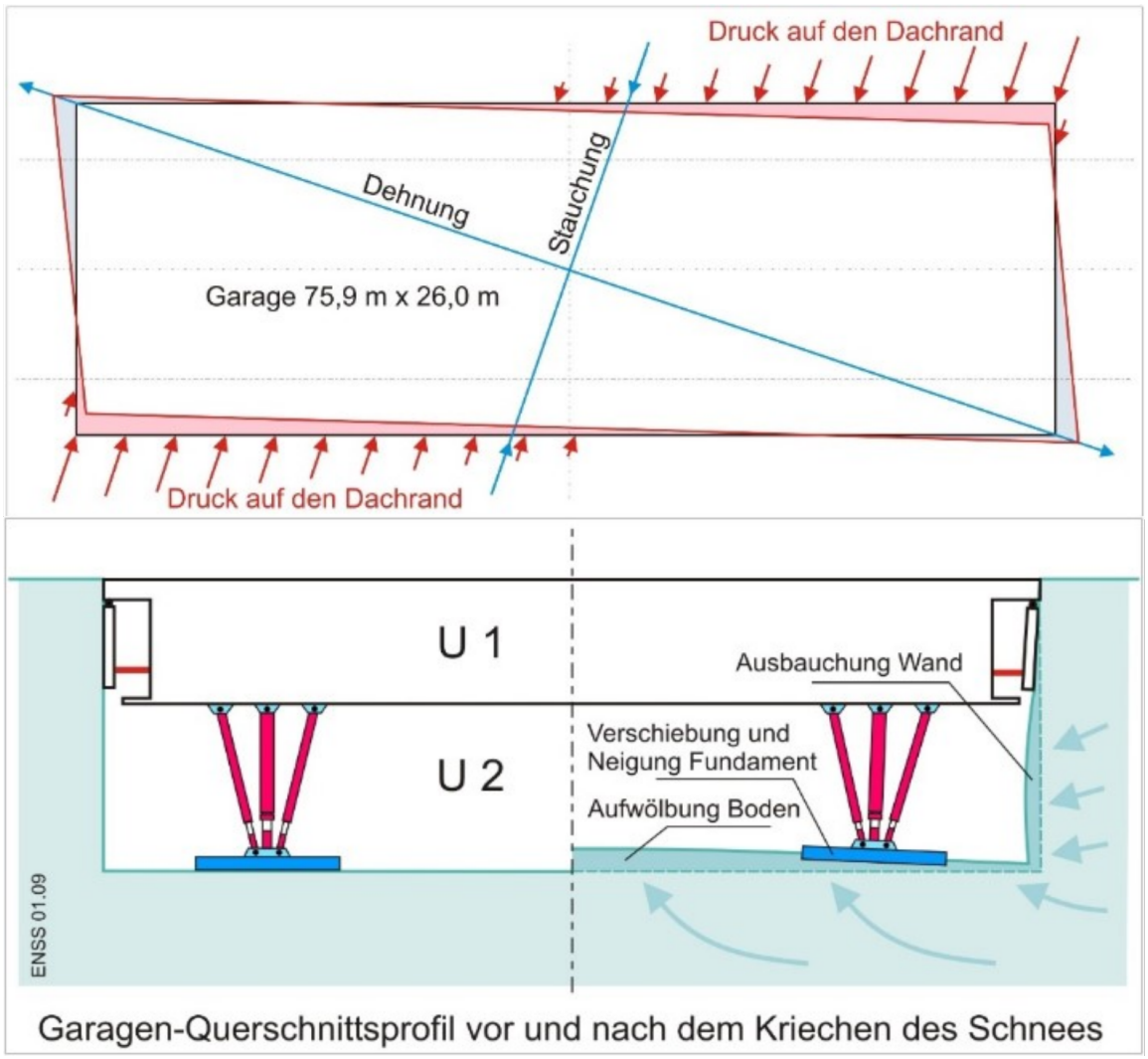

Figure 15: NM III, distortion of Garage walls due to creeping ice shelf

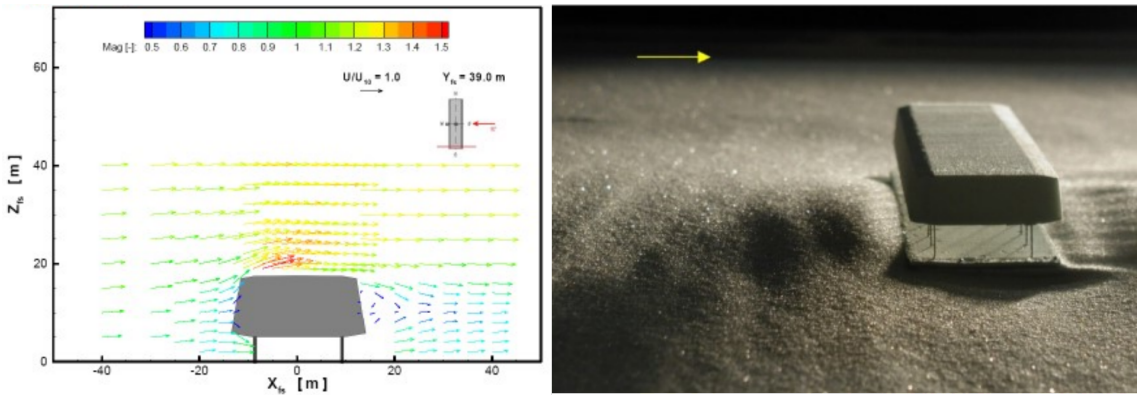

Figure 16: NM III, Simulations and wind tunnel tests

tunnel test additionally shows snow being eroded behind the garage ceiling, which did not occur in nature, since the consistency of the snow on the ground differs from that of the drift snow.

During the last years of station operation, there are moderate accumulations of snow in the vicinity, beside the east side. The garage roof remains snow-free. Although the snow accumulation on the east side corresponds to the results of the preliminary investigation, it still has adverse effects. Due to the additional load, the east wall of the garage is dented more than the west wall and must be removed more frequently. The snow mound also makes it difficult to bypass the station. For this reason, snow is cleared regularly by the station staff. Figure 18 shows a photograph of the snow accumulation on the eastern side.

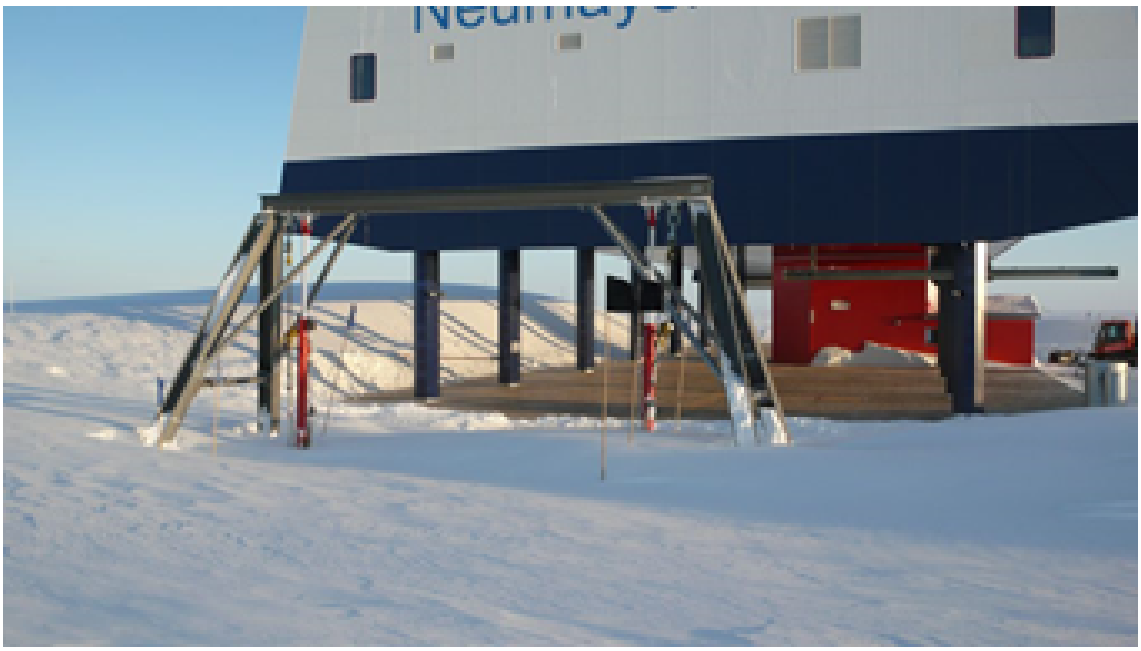

Figure 17: NM III, snow accumulation mound on the east side

4.6 Bearing the high wind loads

As part of the numerical simulations and wind tunnel tests, the dynamic pressures on the outer skin of the station were also recorded and used as a basis for the static calculations. The wind loads are absorbed by the shell and transferred to the snow via the support system (bipods, side skirts). With a design wind speed of 48.2 m/s (174 km/h), the static wind load is 245 t (1.63 kN/m^2) and the dynamic wind load is up to 345 t. The calculated natural frequency for transverse and longitudinal vibrations is 2.4 Hz.

5 Summary

The German Antarctic station Neumayer III was established in 2009 as a successor to the previous stations Georg von Neumayer and Neumayer II on the Ekstrom Ice Shelf. It is thus continuing almost 50 years of uninterrupted research at this location. In winter, it accommodates ten crew members to maintain the functions and the long-term series of measurements, and in summer up to 40 further researchers and guests can be hosted.

Due to the location on the constantly moving ice shelf and the demanding climatic conditions of low temperatures down to -45 °C, wind velocities of up to 175 km/h and significant snowfall of 0.8 m/a, the adaptability of the building is challenged by high demands.

The garage below creates storage space for the machines and technical equipment and at the same time achieves a foundation level that offers sufficient strength for the high building loads of a total of 2600 t. The structure is braced horizontally in the ice pit of the garage by means of hydraulically controlled side shields at the level of the edge of the roof. The raised platform offers the researchers good working and living conditions with sufficient daylight.

Sinking in the snow is countered by an annual lifting and lining of the entire building using hydraulic supports. At the same time, the relining of the foundations counteracts the risk of foundation failure due to the viscoelastic creep behaviour of the ice. The forced stresses that result from the ongoing deflection of the glacier subsoil are relieved by consistent monitoring and controlled load redistribution before they reach critical values.

The snowdrifts due to high snowdrift were minimised by elevating the platform and keeping it as far away from the building as possible.

References

[1] Geduhn M., Enss D.; (2006): Bearing Capacity of 20 Single Column Shallow Foundations of the Antarctic Station Neumayer III over 30 Years Service Life; Paper No. OMAE2006-92444

[2] Nitschke A., Gernandt H., El Naggar S., Siegmund R.;(2006): Design and Construction of the planned Research Station Neumayer III in the Antarctic. Paper No. OMAE2006-92445

Pictures

Alfred-Wegener-Institut
Helmholtz-Zentrum für Polar- und Meeresforschung
Am Handelshafen 12
27570 Bremerhaven
+49 (0)471 4831-0
+49 (0)471 4831-1149
Web: http://www.awi.de

Authors

Dipl.-Ing. Andreas Nitschke
Ramboll Deutschland GmbH
Jürgen-Töpfer-Straße 48
Harburger Schlostrae 20
22763 Hamburg
Tel.: +49 (0) 40 – 32818-123
Fax: +49 (0) 40 – 32818-139
e-mail: andreas.nitschke@ramboll.com
Web: https://de.ramboll.com

Dipl. Ing. (FH) Thomas Matz
Antarctic Operations, Technical Coordination Neumayer-Station III
Logistics and Research Platforms
Am Alten Hafen 26
27568 Bremerhaven
Tel.: +49 (0) 471 4831-1164
Fax: +49 (0) 471 4831-1355
e-mail: thomas.matz@awi.de
Web: http://www.awi.de

Seamless modeling of the hydrodynamics across the scales

Vera Fofonova, Norbert Hoffmann, Sergey Danilov, Marco Klein, Karen Helen Wiltshire

Abstract: With the increased power of modern computers numerical models become more often used for answering present and future climate relevant questions. Nevertheless, the spread of simulated states between individual models indicates substantial restrictions in simulating realistic ocean. Common model biases in ocean models are attributed to insufficient spatial resolution and shortcomings of parameterizations that aim to represent unresolved processes. Making progress on this largely depends on accurate representation of the physical environment in a coupled coastal-open ocean system. However, the interface between the deep ocean, shelf ocean and coastal alongshore areas in the current Earth System Modelling has not yet been appropriately represented. A traditional coupling requires the introduction of the so called sponge layer (zone, where the different solutions are forced in agreement), which heavily damps variability and interaction between the large-scale and regional components. Along with this, the water mass exchange between shelf and ocean is performed through cascading processes, which are hardly reproduced by both regional and global solutions. Additionally, the wave model should be coupled to the coastal model to reproduce the shallow water dynamics and surge events. In this paper we suggest a concept of a numerical platform to overcome significantly identified challenges and to provide high quality prognoses of extreme events in the coastal zones.

1 Concept

There is an increasing urgency and growing need for better quality estimates of circulation and dynamics on the ocean shelf to answer major present and future scientific, ecosystem and societal issues posed by changing climate. Numerical simulations are a powerful instrument in answering these questions. Making progress in this direction largely depends on the accurate representation of the physical environment in a coupled coastal-shelf-open ocean system. An accurate model representation of physical processes is a prerequisite for reliable simulation of biogeochemical cycles and ecosystem dynamics. Over recent years, considerable efforts have been invested into the development of regional models (e.g., GETM, SCHISM/SELFE, DELFT3D, ROMS, FVCOM) and their practical applications (e.g., Burchard and Bolding 2002, Zhang and Baptista 2008, Zhang et al. 2016, Shchepetkin and McWilliams 2005, Chen et al. 2006). These models are used by different institutions to study currents, sediment transport and ecosystem dynamics. They are well-established tools equipped with necessary parameterizations and modules that

may be required in shelf or coastal modeling. However, they are regional models with open boundaries. When it comes to applying them for studying long-term trends and variability in the regional seas, they have to be coupled to a large-scale modeling system. Although the global ocean circulation models can go to smaller scales by increasing resolution, they cannot reproduce many aspects of coastal dynamics, mainly due to limitations imposed by the vertical dynamics (mixing, vertical advection, etc.) and the inability to maintain stability with very thin layers of water and reproduce a rich variety of coastal physical processes (sediment dynamics, flooding events, etc.). The coastal functionality can be added to the global ocean circulation model, but at the high cost of losing the computational efficiency of the global solution. On the other hand, regional models are often too dissipative and computationally expensive for global simulations.

Here, we aim to suggest a numerical platform that would be able to fill this gap. We propose to integrate into the Earth System Modelling framework the coastal branch FESOM-C (e.g., Androsov et al., 2019) of the Finite-volumE Sea ice-Ocean Model FESOM (e.g., Danilov et al., 2017) complemented by a high quality sea wave model, simulating the evolution of wave spectrum. FESOM is the first mature ocean climate model which operates on unstructured meshes and allows for variable resolution in an otherwise global climate configuration. Since FESOM-C and FESOM rely on similar numerical solutions, share the same code infrastructure and work on unstructured meshes, it is possible to couple them without traditional nesting and in most efficient way. The next important step is to include the spectral wave model into this chain, the impact of which on currents, water levels, sediment dynamics and local ecosystem in shallow areas is hard to overestimate. The wave model facilitates correct exchange of momentum between atmosphere and ocean. To increase the fidelity of the proposed platform, radar observations can be also integrated into the system.

Our platform would bridge the scales creating a system, which transfers the high quality deep ocean and large scale atmospheric signals to the wide range of smaller scale processes without traditional nesting. This development goes beyond the existing state of the art modelling platforms and their applications. It would make possible high quality predictions of storm surges and related flooding, which are of major concern in such heavily populated coastal areas with a marine anthropogenic landscape (e. g. , wind farms, bridges, etc.) as the North Sea coast.

2 FESOM

FESOM (Finite-volumE Sea ice-Ocean Model FESOM 2.0, Danilov et al. 2017, Scholz et al. 2019) is a global sea-ice ocean circulation model which operates on unstructured meshes. It's recent configuration exploits 4 km resolution in the North Sea (Fig. 1). It allows to simulate the global ice-ocean system with extremely high resolutions in the regions of interest at affordable computational cost. Coupled with other Earth system components FESOM builds an AWI-CM climate model. Hence, AWI-CM allows for long-term climate integrations using an eddy-resolving ocean. Earlier versions of AWI-CM (using Finite Element version of FESOM) have contributed to several CMIP6 and OMIP-2 endorsed model intercomparison projects. The new version of FESOM 2.0 promises higher efficiency of the new climate setup compared to its predecessor (FESOM 1.4).

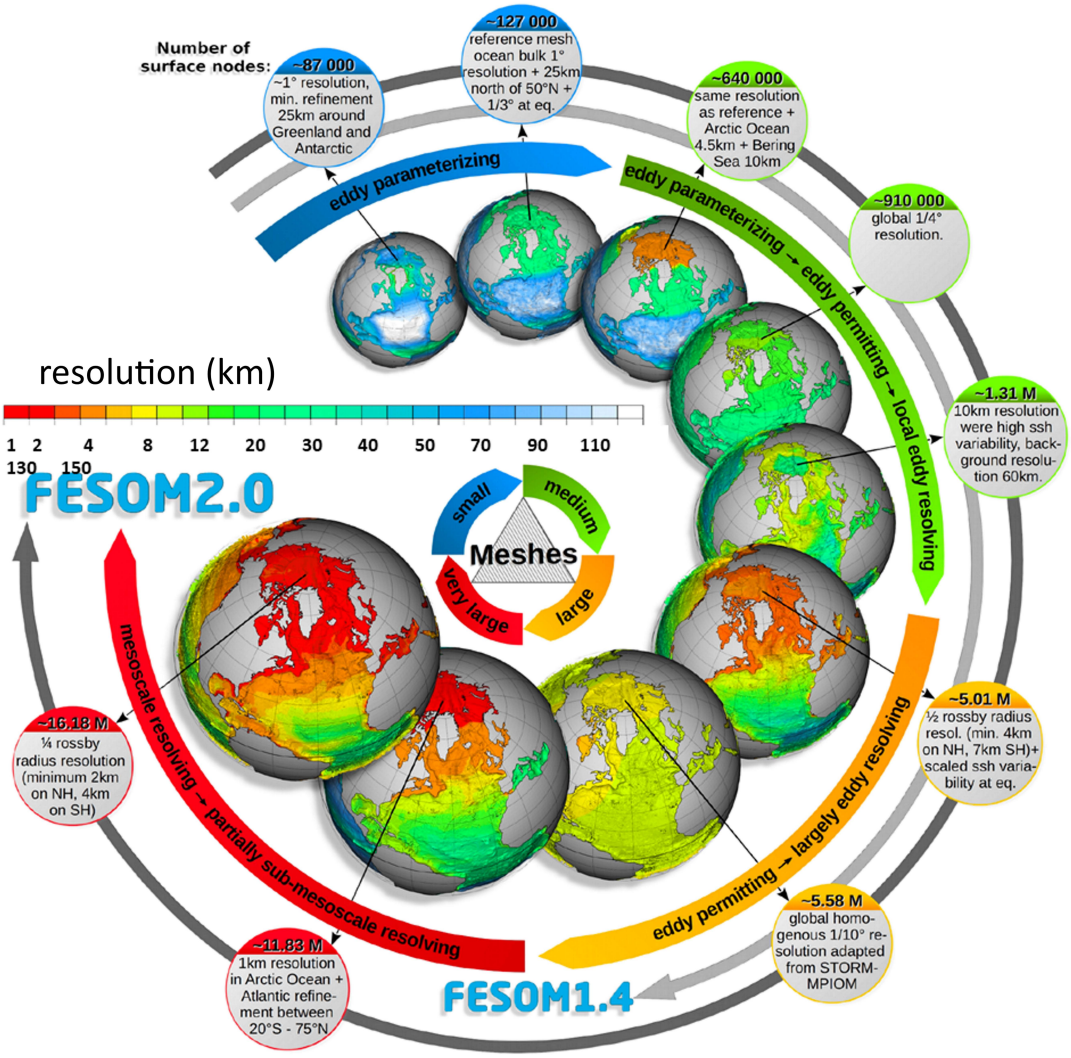

Figure 1: The global meshes, which are used by FESOM2. Adopted from Scholz et al. (2019).

3 FESOM-C

FESOM-C is a recently designed Coastal branch of the global Finite VolumE Sea-ice Ocean Model FESOM (Danilov et al., 2017; Androsov et al., 2019; Fofonova et al., 2019; Kuznetsov et al., 2020; Fofonova et al., 2021). Being developed for large scale ocean applications, FESOM still parameterizes many coastal processes which are resolved in FESOM-C and are required for proper representation of the exchange between the marginal seas and the global ocean. During the last 5 years, the physical core of the coastal FESOM-C module has been developed in AWI and tested in numerous idealized and realistic experiments including sea level rise studies (Fig. 2). However, the two-way final coupling of FESOM-C with FESOM and wave model has been not performed yet.

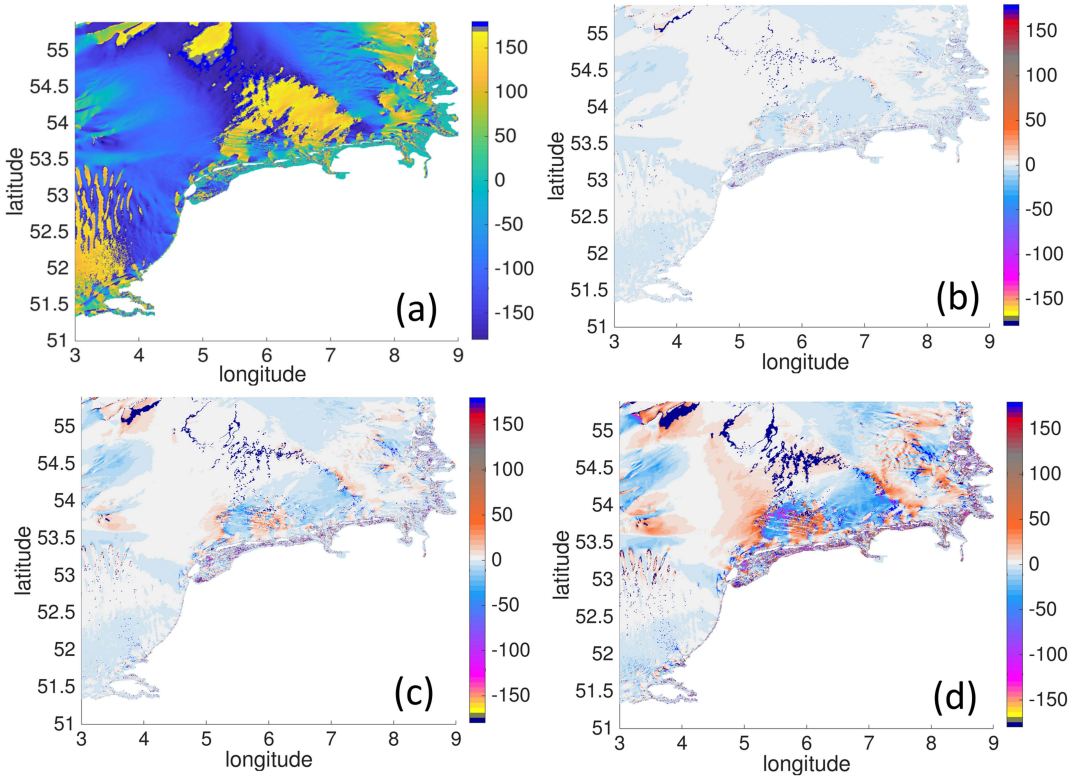

Figure 2: (a) Tidal residual currents angle, deg, with x-axes (positive angle is counted anti-clockwise). Changes of the residual currents angle compared to reference one (positive angle is counted anti-clockwise), deg: (b) +10 cm sea level rise scenario. (c) +30 cm sea level rise scenario. (d) +75 cm sea level rise scenario.

FESOM-C solves 3D primitive equations in the Boussinesq, hydrostatic, and traditional approximations for the momentum, continuity, and density constituents, and it uses a terrain-following coordinate in the vertical. It has the cell vertex finite-volume discretization (quasi-B-grid) and works on any configurations of triangular, quadrangular, or hybrid meshes (Danilov and Androsov, 2015; Androsov et al., 2019). The schemes to compute vertical eddy viscosity and diffusivity can be chosen via the coupled General Ocean Turbulence Model (Burchard et al., 1999) developed in Leibniz Institute for Baltic Sea Research Warnemünde (IOW). The numerical scheme of FESOM-C splits the fast and slow motions into barotropic and baroclinic subsystems (Lazure and Dumas, 2008). It uses an asynchronous time stepping, assuming that integration of temperature and salinity is half-step-shifted with respect to momentum. For modeling wetting and drying (defining the element of the grid to be covered by water or dry) we use the method proposed by Stelling and Duinmeijer (2003), the algorithm to account for wetting and drying (if an appropriate flag is on) is performed on each time step of the external mode. (The inclusion of the wetting and drying algorithm is important for the realistic simulations of the dynamics in the intertidal zones.) Three schemes have been implemented in FESOM-C for horizontal advection (Androsov et al., 2019): upwind, Miura (Miura, 2007), and MUSCL-type (van Leer, 1979). The tracer advection schemes are running in combination with the FCT (flux-corrected transport) algorithm. The typical time step for the barotropic mode for the North Sea applications is of the order of 1–10 seconds.

4 Wave Model

Recently an increased interest has emerged on the potential of computer simulation based phase resolved wave prediction. Techniques to predict ocean waves with a temporal horizon of a few minutes should have a large impact on extreme events prediction and on applications in ocean engineering, like the operation of vessels and structures, the control of devices and vehicles, routing. The physical model is restricted to potential theory, for which the resulting wave elevation equations are solved by applying a higher order spectral method (HOS). To achieve real time capability, not only the simulation itself needs to be highly efficient, but also the determination of initial conditions from both measurement data and larger scale ocean predictions. We suggest to use a data assimilation procedure based on the full nonlinear potential flow wave evolution equation in a nonlinear manner. We assume that surface elevation data is recorded over time, such that temporal derivatives can be evaluated directly, while a Newton-Krylov method is employed for surface elevation and surface potential consistent both with the nonlinear evolution equations and the data at hand. In this study the prediction of wave states is to be accomplished through numerical simulation of spatial initial conditions determined by the above described procedure. To achieve low computational times, we restrict the method to potential flow and simulate on the basis of the well known HOS approach. Figure 3 shows characteristic results of wave predictions as well as the corresponding error measures.

A key message here is that nonlinear simulation is preferable to linear simulation in forecasting, and that nonlinear simulation is only slightly more expensive in terms of computing time than linear simulation. Real time two-dimensional sea state prediction is achievable on present software and hardware architectures. The prediction times seem to be on the order of a few minutes (Köllisch, 2018, Klein, 2020). In frame of the suggested platform we will integrate background information on ocean background flow, as it can be accessed from the oceanographic simulation tools described in the first part of this paper, and varying bottom topography. Also first work on incomplete and sparse data has already been started (Desmars, 2021) and will hopefully be leading to even more accurate and even less computationally expensive approaches.

5 Conclusion

In this work we proposed a concept of the multi-scale ocean model without traditional nesting which includes appropriate coastal dynamics including wave dynamics and also efficiently operates at continental slopes and in the deep ocean. This will be achieved through exploiting the unstructured grid approach of FESOM and its coastal module FESOM-C additionally equipped by full nonlinear potential flow wave evolution equation. We couple these general circulation and regional ocean models respecting the local conservation of fluxes between them. The realization of this concept will open new horizons in the extreme events prediction on the shelf including sea level rise and storm surges events.

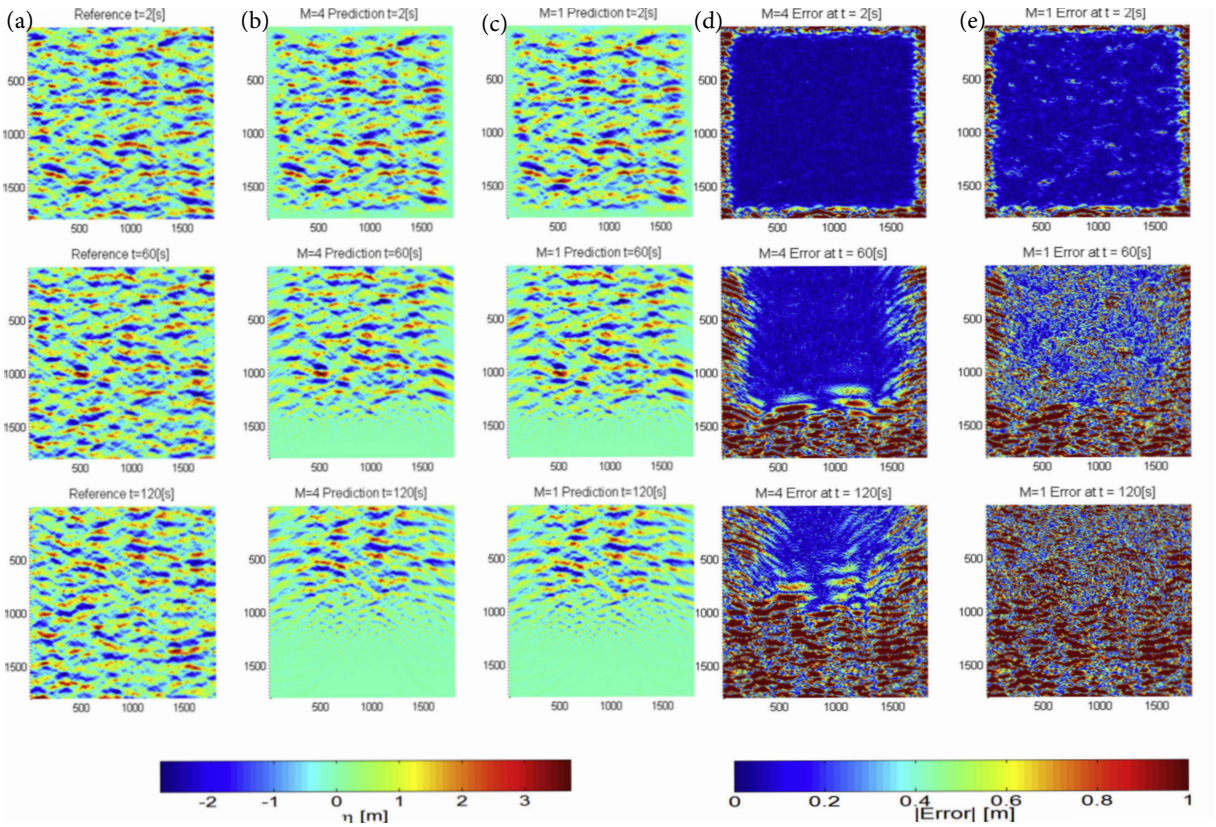

Figure 3: Wave prediction: the three left diagram columns, (a), (b), (c), present surface elevation snapshots for given reference data, (a), and the corresponding nonlinear, (b), as well as linear, (c), predictions at different time steps (from top to bottom). Error measures: the error measures between the predictions and the reference are shown in the two right diagram columns, (d) and (e), in particular, comparing nonlinear predictions, (d), and linear one, (e), with the references for different time steps (from top to bottom). The superiority of the nonlinear wave prediction simulation is obvious. Adopted from Köllisch, 2018.

References

[1] Androsov, A., Fofonova, V., Kuznetsov, I., Danilov, S., Rakowsky, N., Harig, S., Brix, H., and Wiltshire, K. H. (2019): FESOM-C v.2: coastal dynamics on hybrid unstructured meshes, Geosci. Model Dev., 12: 1009–1028.

[2] Burchard, H., Bolding, K. (2002): GETM, a General Estuarine Transport Model, EUR 20253 EN, European Commission, JRC23237.

[3] Burchard, H., Bolding, K., and Ruiz-Villarreal, M. (1999): GOTM, a general ocean turbulence model. Theory, implementation and test cases., Tech.Rep. available at: `https://www.io-warnemuende.de/tl_files/staff/burchard/pdf/papers/report.pdf`(last access: 9 November 2021).

[4] Chen, C., Beardsley, R., and Cowles., G. (2006): An unstructured grid, finite-volume coastal ocean model (FVCOM) system, Oceanography, 19:78–89.

[5] Danilov, S. and Androsov, A. (2015): Cell-vertex discretization of shallow water equations on mixed unstructured meshes, Ocean Dynam., 65: 33–47, https://doi.org/10.1007/s10236-014-0790-x.

[6] Danilov, S., Sidorenko, D.,Wang, Q., and Jung, T. (2017): The Finite-volumE Sea iceâOcean Model (FESOM2), Geosci. Model Dev., 10: 765–789, https://doi.org/10.5194/gmd-10-765-2017.

[7] Desmars, N., et al., (2021): Reconstruction of Ocean Surfaces From Randomly Distributed Measurements Using a Grid-Based Method, International Conference on Offshore Mechanics and Arctic Engineering, American Society of Mechanical Engineers, 85161.

[8] Fofonova, V., Androsov, A., Sander, L., Kuznetsov, I., Amorim, F., Hass, H. C., and Wiltshire, K. H. (2019): Non-linear aspects of the tidal dynamics in the Sylt-Romo Bight, south-eastern North Sea, Ocean Sci., 15: 1761–1782, https://doi.org/10.5194/ os-15-1761-2019.

[9] Fofonova, V., Kärnä, T., Klingbeil, K., Androsov, A., Kuznetsov, I., Sidorenko, D., Danilov, S., Burchard, H., and Wiltshire, K. H. (2021): Plume spreading test case for coastal ocean models, Geosci. Model Dev., 14: 6945–6975, https://doi.org/10.5194/ gmd-14-6945-2021.

[10] Klein, M., et al., (2020): On the deterministic prediction of water waves, Fluids, 5.1:9.

[11] Köllisch, N., et al., (2018): Nonlinear real time prediction of ocean surface waves, Ocean Engineering, 157:387–400.

[12] Kuznetsov, I., Androsov, A., Fofonova, V., Danilov, S., Rakowsky, N., Harig, S., and Wiltshire, K. H. (2020): Evaluation and application of newly designed finite volume coastal model FESOM-C, effect of variable resolution in the Southeastern North Sea, Water (Switzerland), 12: 1412, https://doi.org/10.3390/w12051412,2020.

[13] Lazure, P. and Dumas, F. (2008): An external-internal mode coupling for a 3D hydrodynamical model for applications at regional scale (MARS), Adv. Water Resourc., 31: 233–250, https://doi.org/10.1016/j.advwatres.2007.06.010.

[14] Miura, H. (2007): An upwind-biased conservative advection scheme for spherical hexagonal-pentagonal grids, Mon. Weather Rev., 135: 4038–4044.

[15] Scholz, P., Sidorenko, D., Gurses, O., Danilov, S., Koldunov, N., Wang, Q., Sein, D., Smolentseva, M., Rakowsky, N., and Jung, T. (2019): Assessment of the Finite-volumE Sea ice-Ocean Model (FESOM2.0)–Part 1: Description of selected key model elements and comparison to its predecessor version, Geosci. Model Dev., 12: 4875–4899, https://doi.org/10.5194/gmd-12-4875-2019.

[16] Shchepetkin, A. F., and McWilliams, J. C. (2005): The regional oceanic modeling system (ROMS): a split-explicit, free-surface, topography-following-coordinate oceanic model, Ocean modelling, 9: 347–404.

[17] Stelling, G. S. and Duinmeijer, S. P. A. (2003): A staggered conservative scheme for every Froude number in rapidly varied shallow water flows, Int. J. Numer. Meth. Fl., 43: 1329–1354, https://doi.org/10.1002/fld.537.

[18] van Leer, B. (1979): Towards the Ultimate Conservative Difference Scheme, V. A Second Order Sequel to Godunov's Method, J. Comput. Phys., 32: 101–136.

[19] Zhang, Y., and Baptista, A. M. (2008): SELFE: a semi-implicit Eulerian Lagrangian finite-element model for cross-scale ocean circulation, Ocean modelling, 21: 71–96.

[20] Zhang, Y. J., Ye, F., Stanev, E. V., Grashorn, S. (2016): Seamless cross-scale modeling with SCHISM, Ocean modelling, 102:64–81.

Authors

Dr. Vera Fofonova
Alfred-Wegener-Institut, Helmholtz-Zentrum für Polar- und Meeresforschung
Küstenökologie/Klimadynamik
Bussestr. 24
27570 Bremerhaven
Tel.: +49(471)4831-1722
e-mail: vera.fofonova@awi.de
Web: https://www.awi.de/en/about-us/organisation/staff/single-view/vera-fofonova.html

Prof. Dr. Norbert Hoffmann
Technische Universität Hamburg
Institut für Strukturdynamik
Schlossmühlendamm 30
21073 Hamburg
Tel.: +49(40)42878-3120
e-mail: norbert.hoffmann@tuhh.de
Web: https://tore.tuhh.de/cris/rp/rp00364

Prof. Dr. Sergey Danilov
Alfred-Wegener-Institut, Helmholtz-Zentrum für Polar- und Meeresforschung
Klimadynamik
Bussestr. 24
27570 Bremerhaven
Tel.: +49(471)4831-1764
e-mail: sergey.danilov@awi.de
Web: https://www.awi.de/en/about-us/organisation/staff/single-view/sergey-danilov.html

Dr. Marco Klein
Technische Universität Hamburg
Institut für Strukturdynamik
Schlossmühlendamm 30
21073 Hamburg
Tel.:+49(40)42878-2467
e-mail: marco.klein@tuhh.de
Web: https://tore.tuhh.de/cris/rp/rp03241

Prof. Dr. Karen Helen Wiltshire
Alfred-Wegener-Institut, Helmholtz-Zentrum für Polar- und Meeresforschung
Küstenökologie
Hafenstrasse 43
25992 List/Sylt
Tel.: +49(4651)956-4112
e-mail: karen.wiltshire@awi.de
Web: https://www.awi.de/ueber-uns/organisation/mitarbeiter/detailseite/karen-helen-wiltshire.html

Adaption of steel and concrete structures allowing longer lifecycles

Sylvia Keßler, Johannes Gescher, Marcus Rutner

Abstract: Any structure at shore – steel or reinforced concrete structures – are exposed to severe environmental and loading conditions. Here the engineering challenge is to design and to maintain the structures during their entire service-life without major intervention. The objective is to comply with the safety requirements and at the same time to minimize the carbon footprint with a reasonable consumption of natural resources. This paper provides an overview about different strategies to ensure service life of existing structures under severe environment with the focus on the material level.

1 Service-life limitations of on- and offshore structures

The design objective of civil engineering structures is that the structure is able to achieve the design service life without major repair measures being necessary. Thus, the structure shall perform appropriately under all combinations of action expected in the years to come, which could cover a period of some decades to more than hundred years. It is a challenge to accomplish this goal, especially for steel or reinforced concrete structures in contact with water or even worse, in contact with seawater (Kessler and Lasa, 2019). In such conditions, structures are exposed to a combination of several stresses such as waves, frost, chlorides, and sulfates, static and dynamic loads; whereby one of which would lead to serious deterioration rates, see Figure 1. In combination, the situation becomes worse with serious effects on the durability (Yao et al., 2017, Kessler et al., 2017), serviceability and load bearing capacity.

However, the current design codes (Eurocode 0 & 2, 2021) consider loads on a purely singular basis, the interactions and thus the intensification of an attack does not receive sufficient attention. Consequently, many steel or reinforced concrete structures require repair measures during their design service life. Steel and reinforced concrete structures must demonstrate adaptability to any singular and any combination of environmental stresses and mechanical loads over the entire design service life, mostly with the assistance of proper maintenance and repair. Maintenance and repair cover the activities necessary to retain the performance of the structure above the required performance during its service life. These actions include (i) maintenance planning for existing structures; (ii) assessment of structure including inspection/investigation and evaluation of the performance of structure; (iii) planning and designing repair in case it is required due to damage,

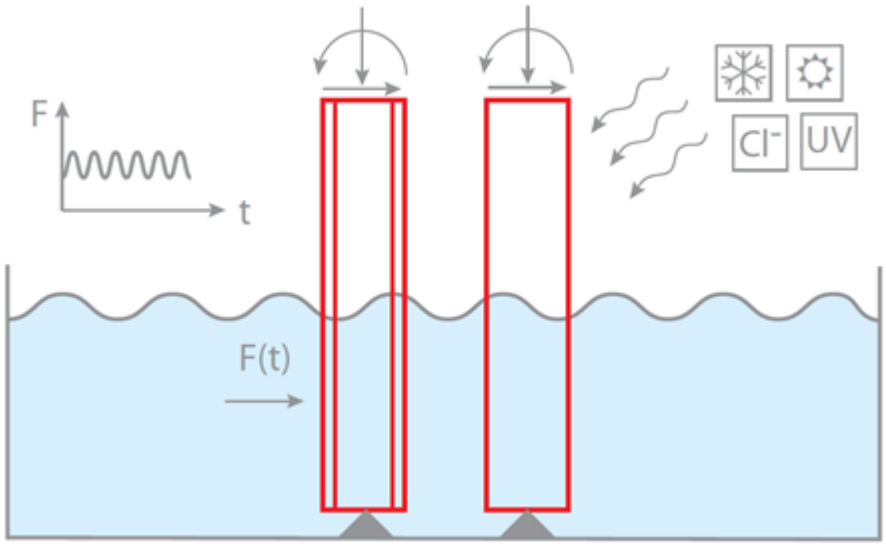

Figure 1: Exposure conditions of steel and reinforced structures in seawater

deterioration and (iv) execution of repair including preparation, execution, and documentation (ISO 16311, 2014).

The performance requirements refer to a condition for design, or an actual, potential, or intended option for intervention, aiming at meeting a specified performance criterion during the service life with appropriate reliability (fib Bulletin, 2022). In order to control the achievement of the performance requirements, the definition of performance indicators is beneficial. Performance indicators are measurable parameters (i.e., characteristic of materials and structures) that quantitatively describe a property of the structure and/or of the aspect of its performance for its purpose to qualify fitness of the structure during service life (fib Bulletin, 2022). In addition, there are requirements independent of the basic functionality of the structure that describe the user expectation on the structures in form of key performance indicators (KPI's). Key performance indicators aim to specify further functional requirements during the service life linked to e.g., reliability, availability, maintainability, safety, security, health, environment, economics and politics (Hajdin et al., 2018). In order to achieve the design service life of structures built in contact with water or seawater, proper maintenance and repair is necessary to withstand any change in mechanical or environmental stresses and in this way to ensure structural adaptability. The objectives of this paper are (i) to provide a short overview of the challenges when designing structures under severe conditions, (ii) to compile inspections and monitoring tool and (iii) to discuss possible repair measures beyond the current state-of-the-art in practice. This discussion includes not only the impact on the performance indicators but also their impact on the key performance indicators. Since each repair measure could impair the availability of structures, contributes to the carbon footprint of the structure (Kessler, 2020), and requires expenses for the repair measure itself and possible social costs due to detour or due to congestions of persons and goods.

2 Major deterioration mechanisms of on and off shore structures

Among others, the two major deterioration mechanisms of structures exposed to water or seawater are corrosion and fatigue. Corrosion is an electrochemical process of a metal, in civil engineering mostly steel, which interacts with the medium or a biological system (water, seawater, and concrete — any kind of electrolyte) to release electrons and iron ions which results in material loss and the loss of the cross section of the structural component. Consequently, corrosion impairs the functionality of the affected element. The corrosion process of steel in concrete is a bit more complex, since concrete is an alkaline electrolyte which leads to a formation of a passive film on the rebar that protects the steel from corrosion in the first place. Thus, the corrosion mechanism consists of two phases, the initiation and the propagation phase. During the initiation phase, chlorides from the seawater can easily diffuse through the porous concrete. As soon as a critical chloride concentration reaches the first reinforcement layer, the destruction of the passivation film starts and the initiation of the corrosion process can take place. With the beginning of the corrosion activity, the propagation phase starts. Beside the loss of steel cross section, corrosion of steel in concrete is able to induce cracks in the concrete cover due to the increasing formation of iron oxides, which require a greater volume as its source material. The result is the structural damage of the concrete impairing the serviceability, the safety of the users and in an advanced stage the load bearing capacity. Cracked concrete structures are particularly at risk since cracks enable an easy access of chlorides to the reinforcement leading to a shortened initiation time (Hiemer et al., 2018). Civil metal infrastructure, which is subjected to cyclic loading, ages through material fatigue very locally and predominantly in structural joints, which eventually may lead to premature structural failure. Cyclic loading in combination with local notch effects causes cyclically changing stress concentrations at the notch tip, which induce constantly changing plastic deformations eventually resulting in crack initiation, crack propagation and finally failure. In case of a welded joint, on top of notch effects the material toughness decreases inside the heat-affected zone, which results in a higher susceptibility for crack growth. Both deterioration mechanisms in combination, called corrosion fatigue, are leading to a much shorter fatigue life (Gehlen et al., 2016). Metal corrosion processes can be massively accelerated by the activity of microorganisms especially in a seawater environment, which is naturally rich in sulfate. It is assumed that microbially influenced corrosion contributes to at least 10-20 % of total corrosion damage (Flemming HC, 1995; Dinh HT et al., 2004). Interestingly, although the accelerating activity of the microorganisms is clearly accepted, the fundamental principles are still largely under debate within the scientific community. Fe0 has a rather negative electrode potential enabling the reduction of a variety of electron acceptors ranging from oxygen to even protons under anoxic conditions. Hence, while in oxic waters rust forms, anoxic conditions lead to a layer of hydrogen on the steel surface.

$$Fe^0 + 2H^+ \rightarrow Fe^{2+} + H_2 \tag{1}$$

Both of these layers limit further corrosion either simply by passivating the material or establishing a layer of hydrogen which prevents further Fe0 oxidation. The best-studied microbial

induced corrosion process is catalyzed by sulfate reducing microorganisms. These organisms respire with sulfate as terminal electron acceptor of their respiratory chain and depend on anoxic conditions. Within the respiratory process, sulfate is reduced to hydrogen sulfide. Some of these organisms can grow chemolithoautotrophically, meaning that they can use an inorganic electron donor like hydrogen and are capable of using carbon dioxide as only carbon source to build biomass. For many years, it was suggested that the simple depletion of hydrogen from the steel surface would be sufficient for accelerated corrosion and this hypothesis is still regarded in many current manuscripts (Tang et al., 2019). Nevertheless, this hypothesis was never able to explain that also sulfate reducing bacteria that are not able to use hydrogen as electron donor can still accelerate corrosion and that the rate limiting step for hydrogen production is not its desorption from the surface but the adsorption. Hence, it is meanwhile assumed that the product of bacterial sulfate production H2S plays a critical role by building metalsulfide films on the steel surface accelerating the cathodic hydrogen producing reaction. Moreover, these films might also catalyze oxygen reduction, which will accelerate corrosion significantly under conditions of fluctuating oxic/anoxic conditions. Finally, the metalsulfides are cathodic to the steel material. Hence, once in contact electron transfer will lead to rapid galvanic corrosion (Little et al., 2020).

The abovementioned mechanisms are examples for microbial induced corrosion based on the consumption or production of metabolites. These processes are generally referred to as chemical microbially influenced corrosion (CMIC) (Emerson, 2019). In recent years, it was hypothesized for a number of anaerobic but otherwise metabolically quite different microorganisms that besides indirect mechanisms also a direct uptake of electrons from Fe^0 would be possible (Enning et al., 2012; Uchiyama et al., 2010; Kato et al., 2015; Dinh et al., 2004; Venzlaff et al., 2013). Hence, these organisms are supposed to respire directly with electrons from Fe^0 and are not using hydrogen formed abiotically on the surface of the metal. Still, it is an experimental challenge to distinguish whether the organisms thrive with hydrogen or not as it is always produced on the metal surface. Recently, more evidence came from a strain that was genetically engineered in a way that it is not able to use hydrogen as electron donor anymore (Tang et al., 2019). The experiments conducted with a strain from the genus Geobacter were clear evidence that this direct electron transfer is indeed possible as even a strain that was not able to use hydrogen was still able to thrive on Fe^0 surfaces. Also, while the strain with the ability to grow with hydrogen was growing planktonically in the medium, the mutant grew on the metal surface bolstering the hypothesis that contactdepended direct electron uptake supported growth of the organism.

3 Inspectability of on and off shore structures

Each maintenance and repair measure require the proper assessment of the structures' condition based on frequent inspection and, if applicable, continuous monitoring. In case of structures built in seawater, the challenge is often the accessibility (Cassiani et al., 2021). Major parts are under the sea level whereas the parts above are prone to wind and waves endangering the inspection personnel. In addition, structures suffering from corrosion and/or fatigue show only in an advanced stage visual sign of damage. However, visual condition survey forms the basis of any assessment with the objective of crack detection and observation of any irregularities;

from damage detection to damage identification up to damage localization (Kessler and Gehlen, 2017).

Depending on the expected deterioration mechanisms more specific inspection techniques and monitoring sensors are of advantage, see Table 1.

In metal structures, the discrete crack means closure of the structure, while for concrete structures, the focus is on the maximum crack width preventing the penetration of water into the cracks. Hence, for metal structures, crossplotting the reduction in structural capacity and the damage increase over the lifetime shows that with larger defect size the growth rate of defects dramatically increases while the structural capacity decreases. Hence one challenge certainly is to detect a potential defect within a certain given inspection window to be able to take appropriate measures. There are various damage detection techniques available. Beside visual inspection, dye penetrant testing, magnetic particle testing, there are nondestructive insitu structural evaluation methods that operate with signals sent through the thickness, e.g. ultrasonic testing. These techniques require the equipment to be moved over the whole plate or connection to be inspected, which is time consuming, labor intensive and of reduced applicability in case of limited accessibility. Further, there are structural evaluation methods that employ a number of sensors attached or embedded in the structure sending signals along the structural members or connection, hence covering a larger area and volume within one measurement, however, potential limitations are signal strength, boundary conditions, etc. All structural health monitoring methods have in common to a) detect defects, b) to define the defect size, c) to measure the defect growth rate, and d) to localize the defect.

4 Engineering strategies to elongate the life time of structures

There are many engineering strategies to elongate the service life of structures. In the following, the focus is on such strategies, which are still under development.

4.1 (Artificial) Self-healing of concrete

As mentioned above, any concrete crack due load-dependent or load-independent actions could lead to a premature initiation of reinforcement corrosion in presence of chlorides. Thus, crack healing is the first step in postponing or even preventing corrosion. Concrete has an inherent ability to heal cracks, the so-called autogenous self-healing of concrete (de Rooij et al., 2013). The autogenous self-healing is the combination of several effects, such as continued hydration, carbonation, swelling and mechanical blocking of the crack pathway, which all together leading to crack closure or at least to a crack width reduction. The success of this process has its limitations since the maximum healable crack width is about 300 µm under certain boundary condition demanding continuous water exposure. Thus, structural durability and reliability cannot rely on the autogenous self-healing effect of concrete. However, there are several methods

Damage Mechanism	Inspection Technique/ Monitoring	Damage Parameter	Damage Indicator
Carbonation-induced corrosion Chloride-induced corrosion Corrosion propagation	Permeability Chloride level sensors pH Sensors Electrical potential Polarization resistance Corrosion rate sensors	Moisture Chloride presence Electrical resistivity	pH value at rebar Chloride concentration at rebar Concrete resistivity Corrosion potential Polarization resistance Corrosion rate Steel cross section loss Concrete cracking level Concrete spalling level
Fatigue	NDT via attached piezoelectric sensors e.g. Vibroacoustic Modulation method or Lamb wave approach Ultrasonic testing Acoustic emission test Radiographic test Eddy current test Magnetic particle test Dye penetrant test	Denotes (non)linear signal modulation which correlates with the fatigue defect size Detects cracks at the surface	Modulation Index or Damage Index

Table 1: Example of the assessment chain: From damage mechanism to damage indicators, in accordance to (fib Bulletin, 2022)

available in order to enhance or to trigger artificially the self-healing capacity of concrete (de Belie et al., 2018). One option for enhancement is the optimization of the concrete mixture by the use of mineral additions, crystalline admixtures or the addition of polymers with or without superabsorbent properties. The implementation of mineral addition leads to a lower hydration rate but for a much longer period, which supports the self-healing due to continued hydration. Crystalline admixtures reduce the permeability of concrete since they react in presence of water to crack-clogging precipitates. In contrast, superabsorbent polymers are able to absorb fluids, as their name indicate, with the inherent capacity to swell, which results in a crack blocking effect. Whereas, the pure addition of polymers could lead to a delayed hydration since the polymer partly shield the cement from the water. Any delay of the hydration results in a higher self-healing capacity for cracks formed at a young age. However, the self-healing ability increases even more with the encapsulation of a healing agent added to the fresh concrete. The idea behind it is that during concrete cracking the capsule breaks as well and releases the healing agent directly in the crack. Possible healing agents are epoxy, bacteria spores, sodium or colloidal silicate and so on. Cracks in concrete are often the starting point of reinforcement corrosion activity. Healing the crack in a short period after cracking is certainly beneficial to avoid the corrosion initiation. However, the self-healing mechanism itself shall not trigger reinforcement corrosion leading to an even more severe situation than an open crack (Van Belleghem et al., 2018, Kessler and Jonkers, 2018). Therefore, the application of self-healing strategies require a proper control of effectiveness through inspection tools and/or monitoring.

4.2 Tool-based procedures

A promising method is the Vibroacoustic Modulation method (VAM) introduced in the late 1990s (Donskoy and Sutin, 1999; Donskoy et al., 2001). However, only very recently, a physics-based approach has been developed to explain the Vibroacoustic Modulation methodology (Dorendorf et al., 2022). The method allows small size crack detection through global sensing. This is achieved through the attachment of sensors and receivers, i.e. piezoelectric disks, on the surface of a structure. The piezoelectric discs experiencing an alternating current insert acoustic waves (bending and compression waves) of certain frequency into the structure. The acoustic waves capture the total cross section; hence, sense defects not only at the surface but also at internal defects. The acoustic signal passing the defect is being modulated, hence, carries the information about the defect with it to the receiving piezo-electric sensor. Vibroacoustic Modulation (VAM) not only allows detection of the defect, the defect size and defect growth rate, but also enables the localization of defects (Li et al., 2014). Recent papers (Dorendorf et al., 2022; Lim and Son, 2017; Oppermann et al., 2021) show very promising results in respect to necessary conditions for successful measurement, interpretation of results, the data evaluation and transmission and also pose remaining question and challenges. Some of the open questions are about use of burst signals in VAM, which may lead to precise defect localization measurement, further, the separation of the nonlinear signal and the detectability of microsized defects.

4.3 Nanolaminated coating

Nanostructured materials and nanostructured metal multilayers are known for possessing superior material properties in comparison to bulk materials, such as increased strength, wear resistance, corrosion resistance, fatigue resistance and magnetic properties (Mastorakos et al., 2011; Misra, 2006; Aliofkhazraei et al., 2021). These superior properties have been attributed to the Hall-Petch effect and to the number of coherent or incoherent interfaces, which act as barriers, impeding the propagation of deformation carriers such as dislocations, phase transformation bands and shear bands, as investigated in (Misra et al., 2005; Nieh and Wadsworth, 2001; Misra et al., 1998). Applying nanolaminated metals in structural engineering might lead to promising approaches (Brunow and Rutner, 2020). An evaluation of most processing methods of nanolaminate coatings and thin films, among others PVD, CVD or ALD, however shows limitations in respect to scalability of the nanolaminate processing and applicability in large-scale structures. Using electrodeposition for the bottom-up fabrication of nanostructured materials comes with advantages and disadvantages compared to vapor deposition techniques (Aliofkhazraei et al., 2021; Kanani, 2020). The electrodeposition process is prone to quality variations in the produced coatings, due to small changes in the preparation process (Ebrahimi and Liscano, 2001). The single bath process utilizes the difference in current densities for deposition of multilayer coatings consisting of different metals from one single electrolyte. However, the low costs and the scalability of the electro-deposition process in comparison to vapor deposition processes makes electrodeposition suitable for a large scale or even insitu application, such as a postweld treatment method (Brunow and Rutner, 2020).

In first proof of concept studies, thin metal nanolaminate coating was deposited on a welded joint aiming at increasing the lifetime of the joint under fatigue loading (Brunow et al., 2022). Test samples were 8 mm thick S235 steel plate samples with a butt weld (double v groove). A single bath electroplating process with a pulsed direct current method was used to coat the sample with a Cu/Ni nanolaminate with a total thickness of approximately 7.5 μm consisting of a 1 μm thick Ni base layer and 160 Cu/Ni bilayers with a thickness of 39 nm and 47 nm, respectively. The samples were tested in tension-tension fatigue with a stress range of 255 MPa, which is 94 % of the measured yield strength of the samples (271 MPa). The number of specimen was small; hence, results of this first study can only be seen as a first tendency. The nanolaminate-coated specimen showed a significant increase in lifetime compared to the as welded specimen. Five hypotheses on how and why nanolaminate coatings increase the fatigue resistance of welded metal specimen have been introduced in (Brunow et al., 2022).

4.4 Biological Strategies

Although the metabolic activity of microorganisms is mostly considered to be the driver of corrosion, some studies show the potential of microbial biofilms as a sustainable measure for corrosion protection. Interestingly, there is often no precise understanding of the underlying mechanism. Overall, (I) the depletion of oxygen at the material surface by aerobic respiring organisms, (II) the release of antimicrobial substances and (III) the formation of corrosion

inhibitors are discussed as mechanisms of action. However, to date, experiments have tended to be conducted with pure cultures and under static laboratory conditions. In this respect, the questions arise (i) how the interaction of the anticorrosive biofilms with the natural surrounding microbiome affects the corrosion protection; (ii) how desired biofilms can be settled on the materials in a longterm stable manner; and (iii) which formulation multi-species biofilms could have in order to be able to bring about a stabilization of the anticorrosive properties through the diversity-related stabilization of the applied or grown microbial community. Nevertheless, field experiments give evidence that the corrosion protective activity of microorganisms or microbial communities adhering on the steel surface can be transferred to natural environments as well. A recent study by In't Zandt and colleagues provided evidence that such protective layers could consist for instance of so called syntrophic and methanogenic organisms. The authors raise the hypothesis that mainly methanogens contribute to steel protection. These organisms use either CO_2 and H_2 or acetate and build CH_4 as final product. The main steel protecting activity might be a result of autotrophy of the organisms. CO_2 fixation by microorganisms is always combined with an increase in the local pH around the organisms. Hence, although methanogens will thrive using the hydrogen layer on the steel surface they will also provide alkalinity to the steel surface, which will cause mineralization reactions leading to shielding and protection of the steel surface. The syntrophic microorganisms build a tight relation with the methanogens; they convert dissolved low molecular weight organic compounds into the substrates for the methanogens, which is likely the reason for the colocalization of the two organism groups.

5 Future Perspectives

The maintenance of existing metal and reinforced concrete structures under severe on and off shore conditions is a challenge. However, there are several strategies under development, which are reviewed in this manuscript, in order to ensure the service life of structures. Here, we see clear directions and perspective for future research and development studies. Self-healing materials, especially self-healing concrete is one mechanism, which, when successfully applied, could be a very sustainable measure to ensure the durability of reinforced concrete structure. Additionally, this measure does not require access to the structure and thus increases the safety of the engineers involved. As we are within a full socioeconomic migration towards a bioeconomy, it will become more and more important to find biohybrid or biobased solutions for all kinds of challenges including corrosion inhibition. So far, we have not fundamentally understood in detail how this process works but have evidence for a variety of processes that might play a role to varying extends. Nevertheless, it seems possible that biofilms on surfaces can be regarded as functional materials that can be applied with user-defined characteristics. To this end, a biofilm could be seen as some kind of anticorrosion paint that can be applied to a service. If the right organism's mixture is chosen that can thrive under the designated conditions, it does not seem unlikely that these anticorrosion biofilm-paints will have a long lasting effect on the reactivity of surfaces within water. Metal nanolaminates shows superior material properties compared to bulk metals. Exploring on how metal nanolaminated coatings can contribute to locally strengthen the weak parts of a metal global structure, such as welded structural joints, against fatigue or even the combined action of fatigue and corrosion opens up an interesting field of research.

References

[1] M. Aliofkhazraei , F.C. Walsh , G. Zangari , H. Köçkar , M. Alper , C. Rizal , L. Magagnin, V. Protsenko , R. Arunachalam , A. Rezvanian , A. Moein , S. Assareh , M.H. Allahyarzadeh (2021) Appl. Surf. Sci. Adv. 6:100141

[2] N. De Belie, E. Gruyaert, A. Al-Tabbaa, P. Antonaci, C. Baera, D. Bajare, A. Darquennes, R. Davies, L. Ferrara, T. Jefferson, C. Litina, B. Miljevic, A. Otlewska, J. Ranogajec, M. Roig-Flores, K. Paine, P. Lukowski, P. Serna, JM Tulliani, S. Vucetic, J. Wang, H.M. Jonkers (2018) A Review of Self-Healing Concrete for Damage Management of Struc-tures Adv. Mater. Interfaces 5, 1800074, DOI: 10.1002/admi.201800074

[3] Van Belleghem, B.; Kessler, S.; Van den Heede, P.; Van Tittelboom, K., De Belie, N. (2018) Chloride induced reinforcement corrosion behavior in self-healing concrete with encapsulated polyurethane. Cement and Concrete Research 113:130-139 https://doi.org/10.1016/j.cemconres.2018.07.009

[4] Brunow, J., Rutner, M. (2020) Fügen von nanostrukturierten metallischen Querschnitten – Einsatz als Makroquerschnitt im konstruktiven Ingenieurbau. Tagungsband Deutscher Ausschuss für Stahlbau, DASt-Kolloquium, Karlsruhe

[5] Brunow, J., Gries, S., Krekeler, T., Rutner, M. (2022) Material mechanisms of Cu/Ni nanolaminate coatings resulting in lifetime extensions of welded joints. Scripta Materi-alia. 212 DOI: https://doi.org/10.1016/j.scriptamat.2022.114501

[6] Cassiani JD, Dugarte M, Arteta CA, Kessler S. (2021) Durability assessment of a tunnel structure with two-sided chloride ingress - A case study located in a tropical environ-ment. Structural Concrete1(14) https://doi.org/10.1002/suco.202100550

[7] Dinh HT, Kuever J, Mussmann M, Hassel AW, Stratmann M, Widdel F. (2004) Iron corrosion by novel anaerobic microorganisms. Nature 427:829–832

[8] D. Donskoy, A. Sutin, (1999) Vibro-acoustic modulation non-destructive technique. J Intell Mater Syst Struct, 9(9):765-771

[9] D. Donskoy, A. Sutin, A. Ekimov (2001) Nonlinear acoustic interaction on contact inter-faces and its use for non-destructive testing. NDT&E International, 34: 231-239

[10] F. Ebrahimi, A.J. Liscano (2001) Mater. Sci. Eng. A 301: 23-34

[11] D. Emerson (2019) The role of iron-oxidizing bacteria in biocorrosion: a review. Journal of Bioadhesion and Biofilm Research 34(9) https://doi.org/10.1080/08927014.2018.1526281

[12] Enning D, Venzlaff H, Garrelfs J, Dinh HT, Meyer V, Mayrhofer K, Hassel AW, Stratmann M, Widdel F. (2012) Marine sulfate-reducing bacteria cause serious corrosion of iron under electroconductive biogenic mineral crust. Environ Microbiol 14:1772-1787

[13] Eurocode 0 (2021) Basis of structural design; German version EN 1990:2002 + A1:2005 + A1:2005/AC:2010

[14] Eurocode 2 (2021) Design of concrete structures - Part 1-1: General rules - Rules for buildings, bridges and civil engineering structures; German and English version prEN 1992-1-1:2021

[15] Flemming HC. (1995) Eating away at the infrastructure: the heavy cost of microbial corrosion. Water Qual Int 4:16-19

[16] fib Bulletin XX TG 3.3 (2022) 'Existing concrete structures: Life management, test-ing and structural health monitoring' (under revision)

[17] C. Gehlen, K. Osterminski, and T. Weirich (2016) High-cycle fatigue behaviour of reinforcing steel under the effect of ongoing corrosion. Structural Concrete, 17(3): 329-337, DOI: 10.1002/suco.201500094.

[18] R. Hajdin, M. Kušar, S. Mašović, P. Linneberg, J. Amado, and N. Tanasić, (2018) TU1406 COST Action: Quality Specifications for Roadway Bridges, Standardization at a European Level: WG3 - Technical Report: Establishment of a Quality Control Plan, 2018. https://www.tu1406.eu/wp-content/uploads/2018/09/tu1406_wg3_digital_vf.pdf

[19] Hiemer, F, Jakob, D, Keßler, S, Gehlen, C. (2018) Chloride induced reinforcement corrosion in cracked and coated concrete: From experimental studies to time-dependent numerical modeling. Materials and Corrosion 69:1526-1538 https://doi.org/10.1002/maco.201810148

[20] ISO 16311 (2014) Maintenance and repair of concrete structures

[21] N. Kanani (2020) Galvanotechnik-Grundlagen, Verfahren und Praxis einer Schlüsseltechnologie, 3rd ed., Hanser, München

[22] Kato S, Yumoto I, Kamagata Y. (2015) Isolation of acetogenic bacteria that induce biocorrosion by utilizing metallic iron as the sole electron donor. Appl Environ Microbi-ol 81:67-73

[23] Kessler, S.; Gehlen, C. (2017) Reliability evaluation of half-cell potential measure-ment using POD. Journal of Infrastructure Systems 23(2) http://dx.doi.org/10.1061/(ASCE)IS.1943-555X.0000334

[24] Kessler, S., Thiel, C., Grosse, C., Gehlen, C (2017) Effect of freeze-thaw damage on chloride ingress in concrete, Materials and Structures 50:121, DOI: 10.1617/s11527-016-0984-4

[25] Kessler, S.; Jonkers, H.M. (2018) Corrosion behaviour of the reinforcement through application of self-healing filler material in cracked concrete. 4th International Confer-ence on Service Life Design for Infrastructures (SLD4) Delft, Netherlands

[26] Kessler, S.; Lasa, I. (2019) Study on Probabilistic Service Life of Florida Bridges, Materials Performance 58(10):46-51

[27] Kessler, S. (2020) Comparative Life-Cycle Analysis of Two Repair Measures for Chloride Contaminated Concrete Structures, Proceeding XV International Conference on Durability of Building Materials and Components DBMC 2020, https://congress.cimne.com/dbmc2020/frontal/default.asp

[28] Li, Z., Wang, Z., Xiao, L., Qu, W. (2014) Damage Detection and Locating Using Tone Burst and Continuous Excitation Modulation Method, Proc. of SPIE Vol. 9064, doi: 10.1117/12.2044998

[29] Lim, H.J., Sohn, H. (2017) Necessary Conditions for Nonlinear Ultrasonic Modulation Generation Given a Localized Fatigue Crack in a Plate-Like Structure, Materials 10, 248, doi:10.3390/ma10030248

[30] BJ Little, J Hinks, DJ. Blackwood (2020) Microbially influenced corrosion: Towards an interdisciplinary perspective on mechanisms, International Biodeterioration & Bio-degradation 154, https://doi.org/10.1016/j.ibiod.2020.105062

[31] I.N. Mastorakos, A. Bellou, D.F. Bahr, H.M. Zbib (2011) J. Mater. Res. 26:1179-1187

[32] A. Misra, M. Verdier, Y.C. Lu, H. Kung, T.E. Mitchell, M. Nastasi, J.D. Embury, (1998) Scr. Mater. 39:555-560

[33] A. Misra, J.P. Hirth, R.G. Hoagland, (2005) Acta Mater. 53(4):817-824

[34] A. Misra (2006) Nanostructure Control of Materials, Elsevier, 146-176

[35] T. Nieh, J. Wadsworth (2001) Scr. Mater. 44:1825-1830

[36] P. Oppermann, L. Dorendorf, B-C. Renner, M. Rutner (2020) Nonlinear Modulation with Low-Power Sensor Networks using Undersampling, Structural Health Monitoring. 20(6): 3252-3264 DOI: https://doi.org/10.1177/1475921720982885

[37] M. de Rooij, K. van Tittelboom, N. De Belie, E. Schlangen (2013) Self-Healing Phe-nomena in Cement-Based Materials: State-of-the-Art Report of RILEM.

[38] HY Tang, DE Holmes, T. Ueki, PA Palacios, DR Lovley (2019) Iron Corrosion via Direct Metal-Microbe Electron Transfer. Applied and Environmental Science. 10(3), https://doi.org/10.1128/mBio.00303-19

[39] Uchiyama T, Ito K, Mori K, Tsurumaru H, Harayama S. (2010) Iron-corroding meth-anogen isolated from a crude-oil storage tank. Appl Environ Microbiol 76:1783-1788

[40] Venzlaff H, Enning D, Srinivasan J, Mayrhofer KJJ, Hassel AW, Widdel F, Strat-mann M. (2013) Accelerated cathodic reaction in microbial corrosion of iron due to di-rect electron uptake by sulfate-reducing bacteria. Corros Sci 66:88-96

[41] Yao, Y.; Wang, L.;. Wittmann, F.H.; De Belie, N.; Schlangen, E.; Alava, H.E.; Wang, Z.; Kessler, S.; Gehlen, C.; Yunus, B.M.D.; Li, Y.; Li, W.; Setzer, M.J.; Xing, F.; Cao, Y. (2017) Test methods to determine durability of concrete under combined environmental actions and mechanical load: final report of RILEM TC 246-TDC. Materials and Struc-tures 50:123, DOI 10.1617/s11527-016-0983-5

Authors

Univ.-Prof'in Dr.-Ing. Sylvia Keßler
Professur für Konstruktionswerkstoffe und Bauwerkserhaltung
Helmut-Schmidt-Universität
Universität der Bundeswehr Hamburg
Holstenhofweg 85
22043 Hamburg
e-mail: sylvia.kessler@hsu-hh.de
www: www.hsu-hh.de/kwb

Univ.-Prof. Dr. Johannes Gescher
Technische Universität Hamburg
Institut für technische Mikrobiologie (TMI)
Kasernenstraße 12
21073 Hamburg
e-mail: johannes.gescher@tuhh.de
www: www.gescher-lab.de

Univ.-Prof. Dr.-Ing. habil. Marcus P. Rutner
Technische Universität Hamburg
Institut für Metall- und Verbundbau
Denickestr. 17
21073 Hamburg
e-mail: marcus.rutner@tuhh.de
www: www.tuhh.de/mvb/

Modern computational techniques for modelling, simulation and optimization of large and flexible structures

Roland Wüchner, Kai-Uwe Bletzinger

The contribution was not available by the time of printing.

Multifield and multiscale problems: Challenges in modelling, simulation and optimization of marine structures

Alexander Düster, Thomas Rung

Abstract: This paper outlines the challenges in computational modelling, simulation and optimization of marine structures. We briefly address aspects of fluid-soil interaction as well as fluid-structure interaction being relevant for marine structures. By means of several examples, current modelling, simulation and optimization approaches are discussed and related challenges are highlighted.

1 Introduction

The modelling, simulation and optimization of adaptive structures in water represent a major challenge for numerical methods. The reason for this is on the one hand the *multifield problem*, which requires the consideration of the interaction of two or even more fields for reliable modelling, e.g. fluid(s), structure(s) and soil (cf. Fig. 1). The fluid-structure interaction (FSI) is the most prominent example, which plays an important role for marine structures. The fluid loads resulting from wind and waves interact with the structure and influence its motion and deformation. If the structures are located in areas with seasonal sea ice, the wind and wave loads are accompanied by ice contact loads and the influence of sub-zero temperatures. With regard to the foundation of offshore structures, the interaction of the water and the structure with the soil must also be taken into account. Since offshore structures are often the habitat of organic structures or aqua-cultures, their interplay with the loads and the motion of these structures is of relevance.

The simulation of the multifield problem requires the coupled solution of the individual sub-fields. This naturally leads to a considerable computational effort, since the numerical solution of the decoupled sub-fields is already fairly complex and the interaction of different fields is difficult to model and often confined to small, dynamically changing regions which are hard to resolve. In conjunction with fluid-soil interaction, for example, additional mixing processes have to be considered. In the case of the soil-structure interaction, the non-linear, path-dependent behavior of the heterogeneous soil poses a supplementary challenge. State-of-the-art approaches aim to couple efficient solutions for the individual fields in such a way that their interaction can be simulated reliably, stably at reasonable computational cost.

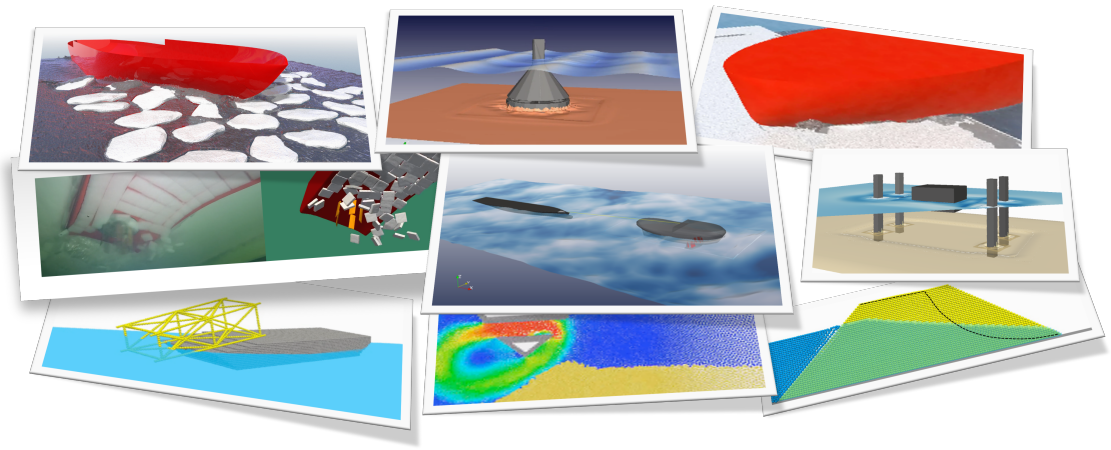

Figure 1: Computational modelling of marine engineering multifield problems.

In addition to the multifield problem, the *multiscale problem* introduces further difficulties. Multiscale phenomena already occur in the individual sub-fields, e.g. flow turbulence, and are usually taken into account by physical models. The problem is exacerbated when multiple fields or multiple continua are coupled because different length and time scale regimes might prevail in the individual continua. As an example, the outer dimensions of marine engineering structures often exceed the dimensions of the details relevant for their stability and strength by several orders of magnitude. The local compressive stresses are a case in point, since they are needed for evaluating the stability of thin-walled structures. Furthermore, fatigue strength calculations also require the evaluation of local stresses. The deformations of marine structures caused by fluid loads refer to diverse time scales. With attention being directed to transient loads, extreme waves must also be taken into account for the stability and the strength of marine structures and occur at very long intervals. On the other hand, the entire stress history is relevant for the assessment of durability.

In conclusion, a reliable prediction of stresses using the finite element method (FEM) for a structural mechanics analysis or the finite volume method (FVM) for the fluid dynamic analysis requires fine spatial and temporal discretizations. However, in an engineering context, a direct resolution of all relevant spatial and temporal scales is hardly possible with current simulation methods due to the resulting computational effort. To this end, skillful combinations of discretization methods and physical models are to be developed, which allow a reliable computation of problems that involve a large spectrum of time and length scales, taking into account the interaction between individual fields.

Due to the increasing complexity of adaptive structures, their reliability and durability will play a crucial role in dimensioning. *Constraint optimization methods* can be used to ensure these baseline constraints and –at the same time– minimizing the resource requirements and/or enhancing the economic efficiency. For this purpose, gradient-based PDE-constraint topology and shape optimizations are perhaps most suitable. The biggest benefits are superior efficiency, essentially because the optimization can be formulated such that the effort decouples from the number of optimization parameters, a seamless integration into existing PDE solvers and a rich

design space. These optimizations usually refer to *adjoint methods* based on an augmented objective function, additionally taking into account geometric and state-related constraints to customize buildings and structures (Allaire et al., 2021; Jameson, 1995; Bazilevs et al., 2013; Heners et al., 2017; Kühl et al., 2021; Kühl et al., 2022) Optimization procedures increase the complexity and computational cost of a coupled multifield and multiscale simulation, particularly for time-dependent problems. For this purpose, feasible simulation-based optimization methods dedicated to coupled dynamic multifield problems must be developed. In order to realize a numerical optimization procedure, the modelling, the numerics and their implementation are closely interlinked. A robust procedure can also be combined with other methods of engineering analysis: Using data assimilation strategies, the optimization tools can be coupled with the results of sensor-acquired data, either to increase the predictive realism or to support the sensor design and location. Similarly, it is possible to take into account (measured) uncertainties to increase the robustness of an optimization.

The present contribution aims to outline the status and prospects of multifield / multiscale simulations dedicated to the optimization (control) of marine structures. The paper is organized as follows: Section 2 presents an approach for fluid-soil interaction relevant for marine structures. The material modelling is addressed and the applied simulation approach is briefly explained. Furthermore, results for an adjoint multiphase shape optimization are presented. In Section 3 the fluid-structure interaction – which plays an important role for marine structures – is briefly addressed. To this end, a partitioned solution approach is applied to the simulation of a self-aligning floating offshore wind turbine. By means of this example, remaining challenges of such modelling and simulation approaches are discussed. Finally, the paper is summarized in Section 4 and an outlook on required future developments is given.

2 Fluid-soil interaction

2.1 Material modelling

When attention is directed to the simulation of immiscible and inert flows composed of air and water phases, that interact with a soil phase, fluid dynamic approaches to treat the multi-continua problem are conceivable. In the last decade, several fluid-based simulation models for describing the fluid-soil interaction with a focus on soil erosion and sediment transport have been published, e.g. in Ulrich et al. (2013) or in Zubeldia et al. (2018). In particular, Lagrangian particle simulations were initially used to describe the large local deformations of the ground and the soil-water interface and mimic the interfacial mixing of continua. To give an example consider the scour formation in a harbor basin near the quay induced by the transverse thrusters of a maneuvering ship, which was investigated in (Ulrich et al., 2013) . Similar problems occur during the lowering of wind turbine foundations, the jacking of installation ships or the release of jackets from a barge, cf. Figs. 1 and 2.

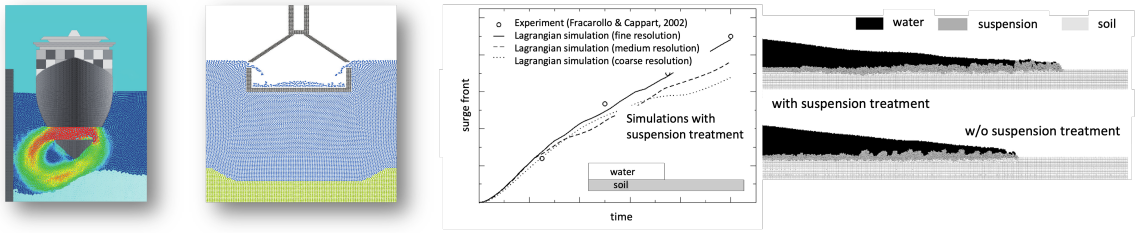

Figure 2: Particle-based Lagrangian modelling of fluid-soil interaction. Scouring induced by a transverse thruster of a departing ship (left), gravity foundation release (centre) and comparison of predicted and measured surge front of a water column breaking above soil (right).

The majority of the approaches refer to a fluid-based (viscous) description and combine (i) elements for describing the nonlinear (viscous) behavior when a yield strength limit is exceeded, (ii) established yield strength formulations with (iii) strategies for describing suspensions and (iv) greatly simplified soil models in the sub-critical regime below the yield strength.

2.2 Simulation approach

Though Lagrangian particle methods have reached a considerable level of maturity for violant flows, cf. Shadloo et al. (2016), they still lack some necessary ingredients to efficiently predict multiscale phenomena, e.g. adaptive, dynamic and anisotropic resolution capabilities and a sufficient level of mathematical consistency (Leonardi et al., 2016). Therefore, Eulerian methods are predominantly used in marine engineering simulations. They reconstruct the phase fields to be examined in space with the help of indicator functions on the basis of so-called level set (Osher and Sethian, 1988) or volume-of-fluid (VoF) methods (Hirt and Nichols, 1981). The majority of the approaches are based on VoF strategies with compressive convection approximations, e.g. described in Ubbink and Issa (1999), to avoid spurious mixing. When attention is restricted to problems where interface physics is secondary to the principal phenomena, VoF-methods represent a reasonable compromise between accuracy, algorithmic flexibility and efficiency. Nonetheless, particle-based fluid-soil-modelling strategies suggested in Ulrich et al. (2013) or Zubeldia et al. (2018) can be transferred to Eulerian multiphase approaches, as reported by Luo-Theilen and Rung (2019). Related studies addressed the interaction of air-water flows with the soil phase and multiple rigid bodies, as occurring, for example, during a dynamic jack-up process or the gravity foundation lowering illustrated in Fig. 3.

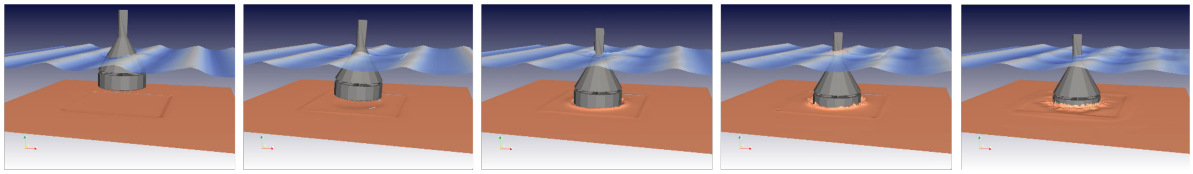

Figure 3: Eulerian modelling of the interaction between two immiscible fluids (air, water) and a soil phase for the example of a gravity foundation lowered in seaways (observation snap shots recorded from left to right).

A less widespread Eulerian approach are diffusive phase field methods, which are also known as Cahn-Hilliard (CH) phase field models (Cahn and Hilliard, 1958; Lowengrub and Truskinovsky, 1998; Garcke et al., 2015). As outlined by Kühl et al. (2021), Cahn-Hilliard methods can be understood as an extension of the classical VoF method (CH-VoF) that are able to better describe the interface physics. Despite their interface focus, CH-VoF methods are also well suited for engineering simulations which often (zonally) under-resolve the interface, since modeled phase separation and coalescence processes can easily be introduced. Significant technical merits of CH-VoF methods arise in conjunction with adjoint optimization methods discussed below.

2.3 Optimization approach

In addition, to a more comprehensive interface model, CH-VoF methods offer excellent prospects for simulation-driven gradient-based optimizations. In particular, they provide a unique access to a consistent adjoint formulation and facilitate the required stability at large Reynolds and Froude numbers to be considered in marine engineering (Kühl et al., 2021). At the same time, the CH-VoF strategy forms a bridge between the two classical optimization approaches, i.e. shape and topology optimizations, as outlined in Garcke et al. (2018) for a simple single-phase flow example. Moreover, global and local technical constraints are readily integrated into the optimization process – e.g. the preservation of the displacement or the center of buoyancy, cf. Kröger et al. (2018).

A comprehensive simulation-based optimization method dedicated to geotechnical multifield / multiphase problems is yet to be developed. However, enriching CH-VoF-based adjoint multiphase methods by appropriate soil models (cf. Sec. 2.1) seems promising to optimize the motion of (deformable) semi-/immersed bodies to control the soil loads along the water bottom or the structural loads. As demonstrated in Kühl et al. (2021) and depicted by Fig. 4, fully consistent adjoint multiphase optimization methods can be used to optimize the shape of objects to control the deformation or the loads on an interface. The focus of such efforts will initially be on the differentiable description of all phase transitions and their consistent discretization. Moreover, an efficient, simulation-accompanying reconstruction of dynamic processes is required that might employ memory saving, incremental model reduction techniques (Brand, 2002).

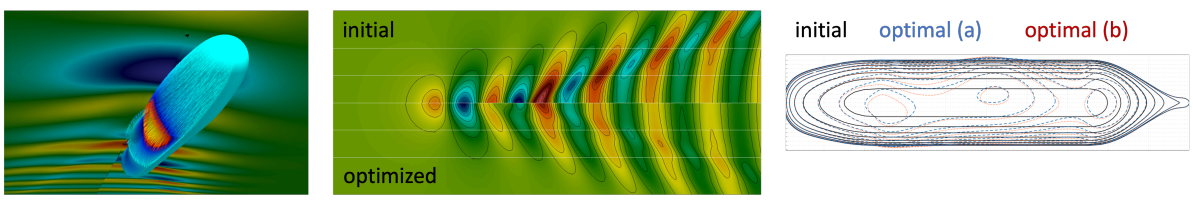

Figure 4: Adjoint multiphase shape optimization of a generic immersed body aiming at a reduced free-surface elevation for a prescribed length and displacement; elevation of the free surface and shape sensitivities (left), surface elevation (centre) and side view of initial and optimal shapes (right).

3 Fluid-structure interaction

3.1 Solution approach

Multifield problems require the consideration of coupled partial differential equations, see Schrefler et al. (2017). For the numerical treatment of fluid-structure interaction (FSI) problems both monolithic (Bazilevs et al., 2013) as well as partitioned approaches (Bungartz and Schäfer, 2006; Bungartz et al., 2010) proved to be successful solution strategies. Adjoint Methods for optimizing problems of fluid-structure interaction are presented, for example, in Bazilevs et al. (2013); Heners et al. (2017). In König et al. (2016) a partitioned solution approach was developed which can be applied to different kinds of multifield problems. In the next section we will present an example related to the fluid-structure interaction of an adaptive structure.

3.2 Floating offshore structures

Offshore structures are subject to complex dynamic loads. Considering a floating wind turbine (FWT), its motion and deformation is induced by fluid loads caused by wind and waves. These fluid loads can, however, be used for self-alignment of the FWT to increase the energy harvested from the wind. For this purpose, the foundation of the FWT is attached to a turret buoy anchored to the sea floor, see Figure 5.

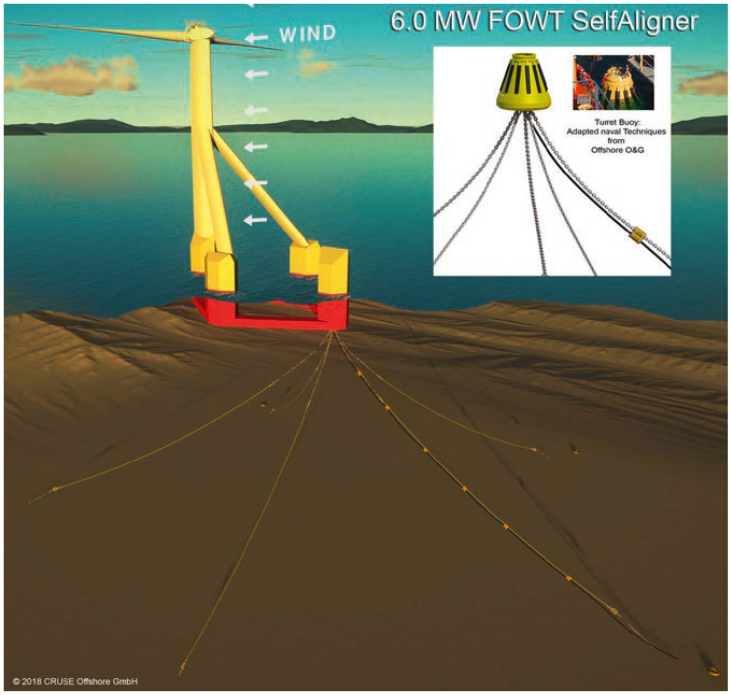

Figure 5: Concept of a self-aligning 6 MW floating wind turbine, see Abdel-Maksoud et al. (2019); Wiegard et al. (2021).

Through a profiled tower and a downwind rotor a moment is created that turns the system into the wind and enables passive control. Thus an active yaw system is not required, resulting in a technically simpler and cheaper construction. This concept was examined in Abdel-Maksoud et al. (2019); Cruse et al. (2021); Wiegard et al. (2019, 2021).

A reliable simulation of the FWT requires modelling of a multifield problem in which the fluid-structure interaction must be taken into account. In Figure 1 the results of a partitioned solution approach for the self-aligning floating wind turbine are depicted. The fluid (wind and waves) is modelled with the boundary element code panMARE (Bauer and Abdel-Maksoud, 2012; Abdel-Maksoud et al., 2019), discretizing the potential flow theory. The structure of the FWT is discretized with the finite element method utilizing the commercial finite element code ANSYS (ANSYS Academic Research Mechanical, Release 18.2). Both solvers are coupled in a partitioned solution approach, exchanging fluid loads and deformations in an implicit coupling scheme using comana, see König et al. (2016). Figure 6 presents the von Mises stresses in the structure computed for extreme waves up to 13.6 m. From this it is evident that the stresses exceed locally the yield stress of normal strength steel, requiring a modification of the structure, see Wiegard et al. (2021).

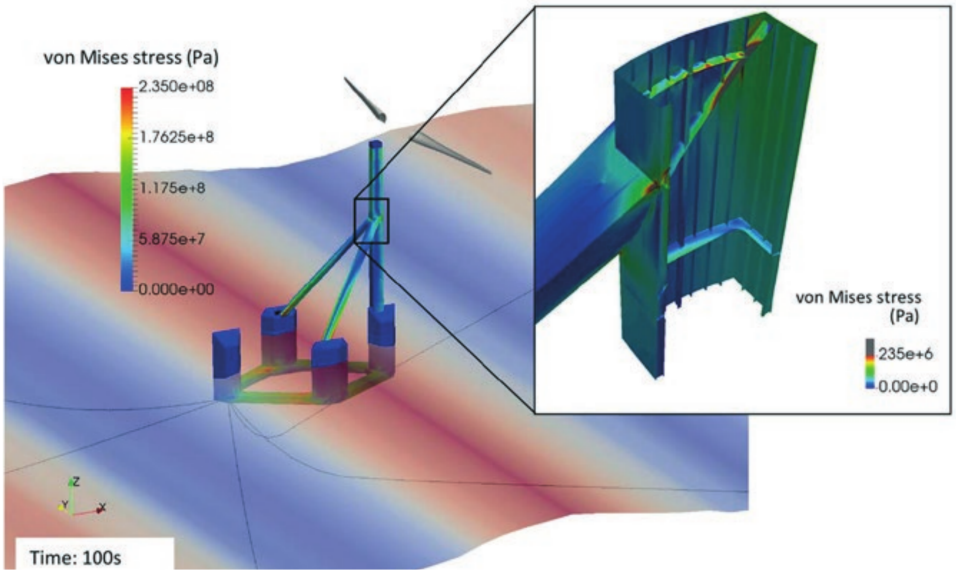

Figure 6: Simulation of the fluid-structure interaction of a floating wind turbine based on a detailed finite element model of the structure, see Abdel-Maksoud et al. (2019).

There are still many challenges, since the required simulation methods are not sufficiently developed. Depending on the task even more modelling aspects have to be included, such as the anchoring of the FWT in the seabed using suction buckets. For the design of the FWT different issues are to be taken into account, such as mechanical stability (due to local buckling) and fatigue. The challenge here lies in the different length scales which need to be considered. Several orders of magnitude have to be spanned between the dimensions of the structure under consideration and its details to be examined, for example a weld seam. This multiscale problem in combination with the already very computationally intensive simulation of the multifield problem significantly increases the complexity of the overall computational approach.

The problem should therefore be examined in more depth, since the required simulation methods to be developed are also needed for many related problems of adaptive structures in the water.

4 Conclusions and outlook

In this contribution we briefly addressed several aspects of the modelling, simulation and optimization of marine structures. To this end, we focused on the fluid-soil as well as fluid-structure interaction. By means of several examples, current simulation approaches were discussed, related challenges were highlighted and future prospects were outlined. Due to the complexity of coupled marine engineering problems and the wide range of involved scales, the solution itself is already a great challenge. To enable coupled simulation models for design optimization, calls for innovative and efficient advancements of computational models.

References

[1] Abdel-Maksoud, M., A. Düster, A. Bockstedte, G. Haake, S. Siegfriedsen, and J. Cruse (2019). HYSTOH – Hydrodynamische und strukturmechanische Optimierung eines Halbtauchers für Offshore-Windenergie-Anlagen. In Tagungsband der Statustagung Maritime Technologien 2019, pp. 173–184. Schriftenreihe Projektträger Jülich.

[2] Allaire, G., C. Dapogny, and F. Jouve (2021). Chapter 1 - Shape and Topology Optimization. In Geometric Partial Differential Equations - Part II, Volume 22 of Handbook of Numerical Analysis, pp. 1 – 132. Elsevier.

[3] Bauer, M. and M. Abdel-Maksoud (2012). A Three-Dimensional Panel Method for the Simulation of Sheet Cavitation in Marine Propeller Flows. In Proceedings in Applied Mathematics and Mechanics.

[4] Bazilevs, Y., M.-C. Hsu, and M. Bement (2013). Adjoint-Based Control of Fluid-Structure Interaction for Computational Steering Applications. Procedia Computer Science 18, 1989–1998.

[5] Bazilevs, Y., K. Takizawa, and T. Tezduyar (2013). Computational Fluid-Structure Interaction: Methods and Applications. Wiley Series in Computational Mechanics. John Wiley & Sons.

[6] Brand, M. (2002). Incremental singular value decomposition of uncertain data with missing values. In European Conference on Computer Vision, pp. 707–720. Springer.

[7] Bungartz, H., M. Mehl, and M. Schäfer (Eds.) (2010). Fluid-Structure Interaction II, Modelling, Simulation, Optimisation, Volume 73 of Lecture Notes in Computational Science and Engineering. Springer.

[8] Bungartz, H. and M. Schäfer (Eds.) (2006). Fluid-Structure Interaction, Modelling, Simulation and Optimisation, Volume 53 of Lecture Notes in Computational Science and Engineering. Springer.

[9] Cahn, J. and J. Hilliard (1958). Free energy of a nonuniform system, i. interfacial free energy. Journal of Chem Physics 28, 258–267.

[10] Cruse, J., M. Abdel-Maksoud, A. Düster, A. Bockstedte, G. Haake, and S. Siegfriedsen (2021). Design of Floating Offshore Wind Turbine (FOWT) “SelfAligner". In J. Park and D. Whang (Eds.), EKC 2019 Conference Proceedings. Science, Technology, and Humanity: Advancement and Sustainability, Singapore, pp. 55–67. Springer.

[11] Garcke, H., C. Hecht, M. Hinze, and C. Kahle (2015). Numerical approximation of phase field based shape and topology optimization for fluids. SIAM Journal on Scientific Computing 37, A1846–A1871.

[12] Garcke, H., M. Hinze, C. Kahle, and K. Lam (2018). A phase field approach to shape optimization in navier-stokes flow with integral state constraint. Advances in Computational Mathematics 44, 1345–1383.

[13] Heners, J., L. Radtke, M. Hinze, and A. Düster (2017). Adjoint shape optimization for fluidstructure interaction of ducted flows. Computational Mechanics 61, 259–276.

[14] Hirt, C. and B. Nichols (1981). Volume of fluid (vof) method for the dynamics of free boundaries. Journal of Computational Physics 39, 201–225.

[15] Jameson, A. (1995). Optimum Aerodynamic Design Using CFD and Control Theory. AIAA Paper. AIAA–95–1729–CP.

[16] König, M., L. Radtke, and A. Düster (2016). A flexible C++ framework for the partitioned solution of strongly coupled multifield problems. Computers & Mathematics with Applications 72, 1764–1789.

[17] Kröger, J., N. Kühl, and T. Rung (2018). Adjoint volume-of-fluid approaches for the hydrodynamic optimisation of ships. Ship Technology Research 65, 47–68.

[18] Kühl, N., M. Hinze, and T. Rung (2021). Cahn-Hilliard Navier-Stokes simulations for marine free-surface flows. Experimental and Computational Multiphase Flow.

[19] Kühl, N., J. Kröger, M. Siebenborn, M. Hinze, and T. Rung (2021). Adjoint complement to the volume-of-fluid method for immiscible flows. Journal of Computational Physics 440, 110411.

[20] Kühl, N., P. M. Müller, and T. Rung (2022). Adjoint Node-Based Shape Optimization of Free Floating Vessels. arXive:2202.04480. preprint.

[21] Leonardi, M., J. Dominguez, and T. Rung (2016). An approximately consistent sph simulation approach with variable particle resolution for engineering applications. Engineering Analysis with Boundary Elements 106, 555–570.

[22] Lowengrub, J. and L. Truskinovsky (1998). Quasi–Incompressible Cahn–Hilliard Fluids and Topological Transitions. In Proceedings of the Royal Society of London A: Mathematical, Physical and Engineering Sciences, Volume 454, pp. 2617–2654. The Royal Society.

[23] Luo-Theilen, X. and T. Rung (2019). Numerical analysis of the installation procedures of offshore structures. Ocean Engineering 179, 116–127.

[24] Osher, S. and J. Sethian (1988). Fronts propagating with curvature-dependent speed: Algorithms based on hamilton-jacobi formulations. Journal of Computational Physics 79, 12–49.

[25] Schrefler, B., L. Simoni, and B. Markert (2017). Multifield Problems. In E. Stein, R. de Borst, and T. J. R. Hughes (Eds.), Encyclopedia of Computational Mechanics Second Edition, Volume Part 2. Solids and Structures, Chapter 7, pp. 1–36. John Wiley & Sons.

[26] Shadloo, M., G. Oger, and D. Le Touze (2016). Smoothed particle hydrodynamics method for fluid flows, towards industrial applications: Motivations, current state, and challenges. Computers and Fluids 136, 11–34.

[27] Ubbink, O. and R. Issa (1999). A Method for Capturing Sharp Fluid Interfaces on Arbitrary Meshes. Journal of Computational Physics 153(1), 26–50.

[28] Ulrich, C., M. Leonardi, and T. Rung (2013). Multi-physics SPH simulation of complex marineengineering hydrodynamic problems. Ocean Engineering 64, 109–121.

[29] Wiegard, B., M. König, L. Radtke, J. Lund, S. Netzbandt, M. Abdel-Maksoud, and A. Düster (2021). Fluid-structure interaction and stress analysis of a floating wind turbine. Marine Structures 78, 102970.

[30] Wiegard, B., L. Radtke, M. König, M. Abdel-Maksoud, and A. Düster (2019). Simulation of the fluid-structure interaction of a floating wind turbine. Ships and Offshore Structures 14, 207–218.

[31] Zubeldia, E. H., G. Fourtakas, B. D. Rogers, and M. M. Farias (2018). Multi-phase sph model for simulation of erosion and scouring by means of the shields and drucker-prager criteria. Advances in Water Resources 117, 98–114.

Authors

Prof. Dr.-Ing. Alexander Düster
Technische Universität Hamburg
Institut für Konstruktion und Festigkeit von Schiffen
Am Schwarzenberg-Campus 4 (C)
21073 Hamburg
Tel.: +49(0)40/42878-6083
Fax: +49(0)40/42878-6090
e-mail: alexander.duester@tuhh.de
Web: www2.tuhh.de/skf

Prof. Dr.-Ing. Thomas Rung
Technische Universität Hamburg
Institut für Fluiddynamik und Schiffstheorie
Am Schwarzenberg-Campus 4 (C)
21073 Hamburg
Tel.: +49(0)40/42878-6054
Fax: +49(0)40/42878-6055
e-mail: thomas.rung@tuhh.de
Web: www.tuhh.de/fds

Smart sensor systems – Aspects of low-power devices, energy harvesting, and artificial intelligence

Hoc Khiem Trieu, Johannes Gescher, Kay Smarsly

Abstract: Monitoring of buildings and engineering structures in general, and of adaptive waterside structures in particular, requires smart sensor systems. The temporal as well as environmental constraints associated with long-term monitoring and harsh conditions impose exceptional requirements on the sensor systems. Aspects of low power consumption, long-term stability of sensing devices, autonomous operation by robust energy harvesting concepts and dependable data acquisition for a real-time description of the system behavior by artificial intelligence are key elements for the implementation of smart sensor systems, enabling energy-efficient monitoring and control of adaptive waterside structures. This article addresses the challenges and prospects of novel concepts for the realization of smart sensor systems.

1 Introduction and challenges

The devastating flood disaster in 2021 has once again clearly revealed the consequences of climate change, such as flooding and other extreme weather events, in particular for water-side structures. Most waterside structures represent safety-relevant land/water interfaces that perform vital functions. Therefore, monitoring and inspection of waterside structures is critical to ensure continuous operation, which, however, is associated with a number of specific challenges, as hydrostatic forces, wind, salt spray, currents, tides, waves, and ice contribute to damage and deterioration to a non-negligible degree. As a consequence, significantly more information, acquired at much earlier stages, is required for a safe and sustainable operation of these structures because predictive maintenance measures are all the more successful the earlier they are taken. Particular challenges to be considered are that these structures are used to be unique specimens of enormous size having a considerably longer service life as compared to other technical facilities. Their rate of change due to deterioration is very low and thus hardly measurable. The concept of "digital twins" known from cyber-physical systems has the potential to diagnose and predict the structural behavior based on physical sensory data.

To answer the central question of mechanically adaptive structures of buildings, methods for the long-term monitoring of local overstresses on the sensory side and a methodology for the subsequent control on the actuator side are inseparable. As "long-term" typically means several

decades up to a century, autonomous dependable operation of the system is indispensable. Powering the devices as well as their long-term stability are key issues. The basic engineering challenges on the sensory side with focus on long-term monitoring are the development of (i) sensory methods for detecting overstresses including corrosion and degradation without external electrical energy supply (zero-power sensing), (ii) methods for reading out and evaluating the information stored in the zero-power device and for resetting the device, (iii) an alarm mechanism to inform users in case of emergency. Redundancy and data fusion on the system level of digital twins will ensure consistent data acquisition. For autonomous powering, energy harvesting methods are required. Considering that energy storage also will degrade over that long period by charging and discharging, an absolute strict energy management with minimal power consuming devices is inevitable. Even with the progress in ultra-low-power electronics, autonomous operation over several decades or a century is not yet possible. Hence, strategies for passive sensing without active energy supply have to be addressed. The harvested energy will be used only for the absolutely required tasks of on-demand sensor readouts and data transmissions as well as for alarming users in case of emergencies.

Among the various approaches for energy harvesting, a microbial fuel cell technology for the energy-autonomous operation of sensors and actuators at sea or on structures at shore is appealing to ensure long-term energy supply of such systems for decades. Microbial fuel cells are powered by bacteria that catalyze a direct conversion of chemical energy into electrical energy.

2 State of the art

In recent years, waterside structures, such as bridges, dams, wharves, and port facilities, have been particularly exposed to natural hazards caused by climate change (Wakeman et al., 2015) and several structural health monitoring (SHM) research approaches have focused on protecting waterside structures (Rizzo, 2012). In addition, advances in computer science, particularly in artificial intelligence and data sciences, as well as the increasing use of wireless technologies, have stimulated discussion of SHM of critical infrastructure (including waterside structures) into a new perspective. In modern wireless SHM systems sensor nodes are equipped with a high degree of „intelligence“, which allows the embedding of sophisticated algorithms and models to analyze structural behavior (Lynch, 2006). In addition, modern concepts of data management, which enable developing digital representations of physical systems – as “digital twins” (Booyse et al., 2020) – for the early detection of defects in manufacturing, can be advantageously adapted to SHM, which in turn supports the implementation of predictive maintenance measures. These concepts need to be dovetailed and adapted to the specifics of waterside structures. However, active devices for sensing, actuating, and computing as well as wireless data transmission require energy. The trade-off between power supply and long-term operation needs to be solved.

Current progress enables numerous mobile applications, with electronic systems becoming more and more powerful on the one hand, and as low-power systems they consume less and less energy on the other. Even though microelectronics is advancing and components require less electrical power for their operation, autonomous energy supply over several decades is an

unsolved problem. Batteries in the form of electrochemical cells discharge themselves over the years without active use. Accumulators also have finite charging cycles and cannot bridge such time scales. In measurement technology, we are used to measurement data being recorded and available at a more or less constant sampling rate. For this, the sensors must also be continuously supplied with energy. For some years, efforts have been undertaken to develop passive sensors that record and store limit load states without an external electrical energy supply. One example is a sensor for detecting a deflection with an implemented analog AD converter (Schmitt et al., 2020). The approach of passive sensor technology now needs to be further developed using smart materials that change their properties under the influence of environmental parameters and suitable geometries in such a way that a zero-power sensor that can be programmed to record and store multiple events to be read out and reset when required under external electrical power supply.

In electrical engineering, intensive research is being conducted on energy harvesting methods for this purpose, in order to generate electrical energy from the environment by converting light, kinetic energy, from electromagnetic fields or temperature gradients (Cao et al., 2017). For long-term applications, it is of utmost relevance that the harvester works reliably and requires no maintenance. In this regard, it is advantageous that the system operates independently of light conditions, contains no moving parts, and requires no additional infrastructure such as transmission towers. The approach of microbial fuel cells with, in principle, achievable energy densities of several tens of mW/m^2 is suitable for use in and near water (Schrader et al., 2016). Microbial fuel cells for the realization of energy-autonomous systems have existed for several years. Professor Ieropoulos' group at University of Southampton has developed systems that can even power autonomous robotic systems (Philamore et al., 2016). Such systems show amazing robustness. Many systems run stably for hundreds of days (Cristiani et al., 2019). This characteristic is also believed to have led the U.S. Navy to research these systems in order to develop energy-autonomous sensor systems (Tender, 2014). Overall, a large number of implemented systems already exist that measure parameters such as dissolved oxygen concentration or heavy metal concentration (Shantaram and others, 2005). Systems are becoming more powerful, so that wireless provision of measurement data is available (Walter et al., 2020). Despite this progress, generic reactor designs for use in open water are lacking. In contrast to applications in sediment, where sufficient organic material is available to the microorganisms at the anode under anoxic conditions, for use in free water aspects of organic material supply need to be addressed as well as up-conversion the low voltages from the harvester for practical use and temporary storage of the energy. Due to the envisaged service life of several decades, conventionally rechargeable batteries are also reaching their limits. Concepts with super-capacitors have to be investigated and implemented.

3 Prospective approaches

To address the challenges of SHM over several decades with the unsolved problems discussed above, novel concepts for realizing smart sensor systems have to be investigated. Decentralized self-adaptive digital twins for waterside structures with zero-power sensing for long-term mon-

itoring of local overstresses, and microbiological reactors for powering the micro devices are discussed in the following.

Figure 1 shows the concept of decentralized self-adaptive digital twins for waterside structures where sensor nodes detect the response of the structure to environmental impacts and external devices as underwater robots (μAUV) provide additional environmental infor-mation, such as underwater flows. All the data are collected and processed in a decentralized self-adaptive digital twin. Decentralization and self-adaptability enable a stand-alone operation of the SHM system without the need for long-range communication with a central server. With a digital twin the structural behavior can be modelled, diagnosed, and slow minor changes as used for long-term monitoring can be predicted.

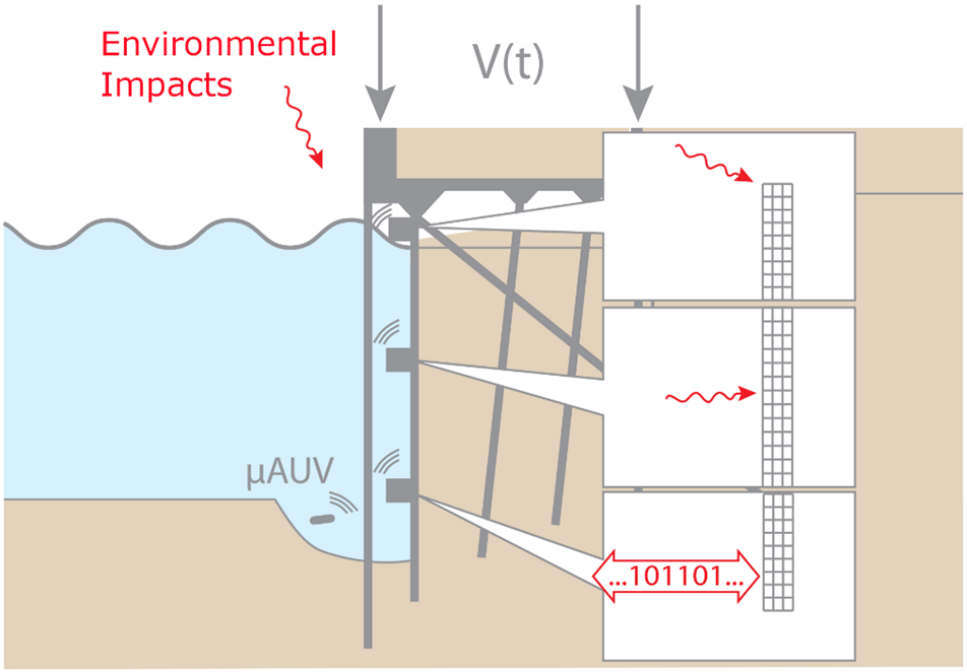

Figure 1: Sensor nodes with decentralized self-adaptive digital twins.

Lessons learned from the past help to consequently hybridize the decentralized physical models by coupling the models with classical data-based models and transfer them to waterside structures as decentralized, self-adaptive digital twins. The physics-based models are coupled with data-based models and implemented as fullfledged digital twins by transferring the physical principles into the digital domain and equipping digital twins with monitoring and control systems. Given the mismatch between physical models and the inherently resource-limited wireless SHM systems (particularly in terms of degrees of freedom to be measured), techniques to reduce the model order for coupling digital twins with structure monitoring systems have to be considered. Finally, for self-adaptation, a multi-agent system approach accompanied by machine learning techniques is used. The decentralization of the digital twins is the focus of interest, i.e., the resource-efficient embedding in wireless monitoring and control systems. The physics-based models of the digital twins are decomposed into partial models, with each partial model embedded in a single wireless sensor node. The overall model composed of the partial models will be validated against the

digital model. In addition, the self-adaptive digital twins can be extended to a smart city in and on the water. As a result, focus on methods for integrating the self-adaptive digital twins into IoT frameworks directs future developments with multisensory data fusion allowing data (or information and knowledge) from heterogeneous, external sources to be integrated to improve the predictive capabilities of the digital twins.

Essential aspects for the development of the digital twin are extraction of information (and knowledge) from SHM data, enabling the structure monitoring systems to perform autonomous self-diagnostics, and the implementation of intelligent structure control mechanisms via actuators. Further aspects focus on the development of multi-agent system approaches to induce collective (swarm) intelligence in wireless sensor networks and to detect structural anomalies on demand using autonomously migrating software entities (Smarsly and Law, 2013). Other research in embedded modeling for wireless structural monitoring systems addresses fault diagnostics in distributed sensor systems (Dragos and Smarsly, 2016) and system identification (Dragos et al., 2018). Artificial intelligence (AI) methods for sensor systems, particularly coupled with traditional methods for pattern recognition and classical structural mechanics, are used to improve the resilience of engineering structures (Law et al., 2014). For this purpose, fully autonomous structural monitoring systems and intelligent structures were implemented, mathematically abstracted in a generally applicable manner, and finally formalized via an engineering-understandable descriptive calculus (Gürlebeck et al., 2019; Theiler and Smarsly, 2018).

The information source for the digital twin are sensors. For long-term operation, sensors have to consume minimal power, ideally zero. This novel concept of zero-power sensor technology has to be considered both on a system level and on a device level. As constant sampling rate will unnecessarily consume power, even no relevant information is available, a new strategy is addressed using smart passive transducers with analog storage of the measured variable. Active readout requiring power is performed only on demand or when set critical limits are exceeded. The approach introduced above reduces the power consumption to an absolute minimum. One of the most power consuming task is the wireless data transmission, hence this should be restricted in operation. Since the system does not continuously send data to users, an alarm mechanism must be implemented to inform the user in case of an emergency. The algorithms of the digital twin also have to be adopted to manage limited data sampling. On device level, passive sensors with integration of smart materials that change their properties under the influence of environmental parameters and appropriate design geometries are used to implement zero-power sensors that can be programmed to record and store multiple events to be read out and reset when required under external electrical power supply.

For the design and fabrication of the zero-power devices, novel 3D patterning and fabrication techniques, such as selected laser-induced etching (SLE) or 2 photon polymerization (2PP) provide an increase in the degree of freedom for the design and integration of polymer-based and non-polymer-based materials. Smart material integration is well known in microsystems technology (Akay et al., 2017; Schlicke et al., 2020). Combination of 2PP and silicon technology has already been successfully demonstrated (Bohne et al., 2019). Complex 3D devices as a spinal cord implant fabricated by SLE have been recently achieved (Rennpferdt et al., 2021; von Poblotzki et al., 2019).

Sensors for the detection of overstress (strain, acceleration, temperature) and corrosion as well as degradation are required. Due to the focus on long-term applications, even with the concept of passive zero-power sensors, a robust energy harvesting schema is inevitable for the on demand readout as well as for the emergency operation. Figure 2 shows the principle of a microbial fuel cell, which can be used in applications at shore.

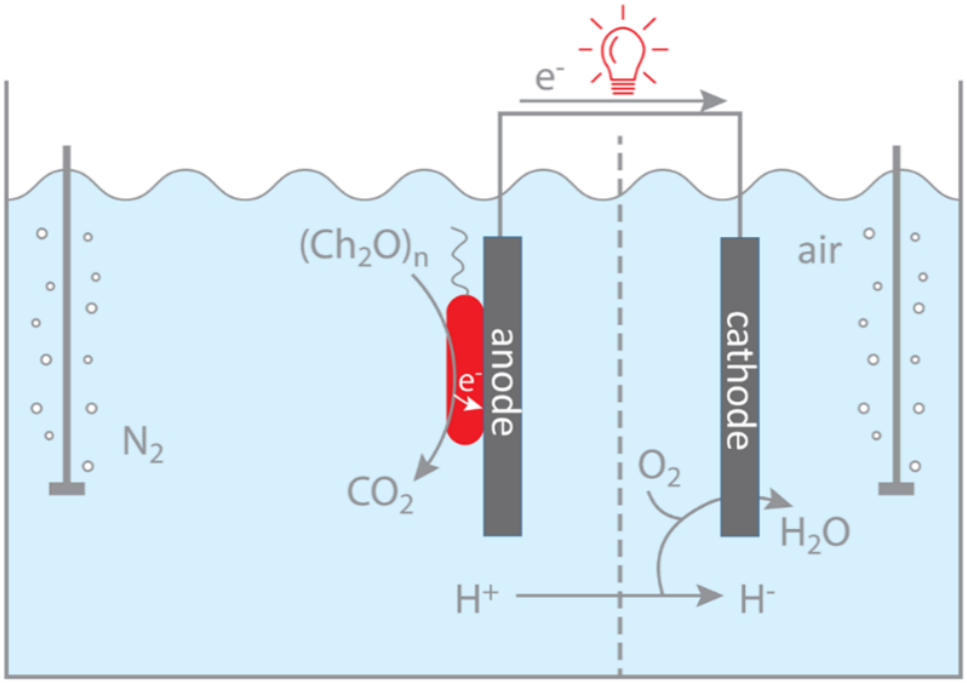

Figure 2: Principle of a microbial fuel cell. Microorganisms thrive on the anode site of the system and couple the oxidation of organic carbon $(CH_2O)_n$ to CO_2 with energy production and growths. The electrons of the oxidative process are transferred to the anode electrode. This electron flow can be used as power source if a cathode is connected at which a reaction with a higher redox potential is catalysed. In microbial fuel cells this process usually is the reduction of oxygen to water. As this process is oxic and the anode process conducted in the absence of any another electron acceptor besides the anode, a separator has to be placed between the two compartments.

Microorganisms have developed a special form of respiration, in which electrons can be delivered to insoluble electron acceptors on the cell surface. In this process, the cytochromes show little substrate specificity, but allow the catalysis of electron transfer to electron accepting surfaces, limited only by the redox potential of the electron acceptor. The electron-transfer mechanisms have been developed during evolution for respiration with iron and manganese oxides. In application, an electrode can be offered to organisms as a surrogate of these metal oxides. Since the process is enzyme-catalyzed, the electrodes can be made from simple graphite materials. The organisms also gain the necessary energy to grow through the process. Therefore, the biocatalyst continuously renews itself and strives to improve through adaptation as part of evolution making this approach being robust for long-term application. Microbial fuel cells have already been developed for many applications in sediment. However, for general use in free water the technology needs to be extended to include free-floating microbial fuel cells where

the small amount of organic carbon in seawater can produce enough energy to power the sensor system. Nature shows that even small amounts of organic carbon in seawater are sufficient to provide food for a large number of organisms by means of filtration. The size spectrum of filter-feeding organisms ranges from sessile organisms such as sponges/corals to large free-living animals such as whale sharks/baleen whales. animals such as whale sharks/baleen whales. This principle of nature could be used to develop microbial fuel cells. The tidal current is expected to carry the water through filtering areas that mimic baleen. The filtered material shall accumulate in the anode compartment of the microbial fuel cell where it shall be oxidized.

Key elements for the development of this free-floating microbial fuel cells are applied bioelectrochemistry (Bursac et al., 2017; Gescher et al., 2014; Edel et al., 2019; Gescher et al., 2013; Simonte et al., 2017) and the expertise for isolation of biocatalysts for organic carbon source elimination.

3.1 Summary and conclusions

Damage and deterioration of waterside structures, affecting structural reliability and safety, typically occur as results of ageing, mechanical impacts, and harsh environmental conditions, the latter increasingly observed as one of the consequences of climate change, such as heavy downpours, floods, storms, or heat waves. To assess damage and deterioration at early stages, monitoring strategies are devised. With recent advancements in information and communication technologies, the monitoring strategies are implemented through smart sensor systems. The harsh environmental conditions as well as the time-variant behavior of adaptive waterside structures, which require coupling monitoring strategies with appropriate control strategies, place exceptional demands on the smart sensor systems. This article, upon analyzing the state of the art, has addressed the challenges and prospects of novel concepts to realize smart sensor systems for adaptive waterside structures. Emphasis has been placed on low-power devices, energy harvesting, and artificial intelligence. It has been concluded that low power consumption, long-term stability of sensors, autonomous operation through robust energy harvesting concepts, and reliable data acquisition for real-time description of system behavior through artificial intelligence are key elements for implementing smart sensor systems enabling energy-efficient monitoring and control of adaptive waterside structures. Last, but not least, it has been illuminated that, to solve the open problems associated with smart sensor systems for adaptive waterside structures, multi-disciplinary collaborations are required between various disciplines, such as civil engineering, electrical engineering, bio-engineering, and computer sciences.

References

[1] Akay, S., Heils, R., Trieu, H. K., Smirnova, I. and O. Yesil-Celiktas (2017). »An in-jectable alginate-based hydrogel for microfluidic applications«. In: Carbohydrate Polymers 161, 228-234. DOI: 10.1016/j.carbpol.2017.01.004.

[2] Bohne, S., M. Heymann, H. Chapman, H. Trieu and S. Bajt (2019). »3D printed nozzles on a silicon fluidic chip«. In: Review of scientific instruments 90.035108 (3). DOI: 10.1063/1.5080428.

[3] Booyse, W., D. N. Wilke and S. Heyns (2020). »Deep digital twins for detection, diagnostics and prognostics«. In: Mechanical Systems and Signal Processing 140.106612. DOI: 10.1016/j.ymssp.2019.106612.

[4] Cao, S. and J. Li (2017). »A survey on ambient energy sources and harvesting methods for structural health monitoring applications«. In: Advances in Mechanical Engineering 9 (4). DOI: 10.1177/1687814017696210.

[5] Cristiani, P. et al. (2019). »Long term feasibility study of in-field floating microbial fuel cells for monitoring anoxic wastewater and energy harvesting«. In: Frontiers in Engergy Research 7. DOI: 10.3389/fenrg.2019.00119.

[6] Dragos, K., T. Makarios, I. Karetsu, G. Manolis and K. Smarsly (2020). »Detection and correction of synchronization induced errors in operational modal analysis«. In: Archive of Applied Mechanics 90 (7), 1547-1567. DOI:10.1007/s00419-020-01683-6.

[7] Dragos, K. and K. Smarsly (2016). »Distributed adaptive diagnosis of sensor faults using structural response data«. In: Smart Materials and Structures 25.105019 (10). DOI: 10.1088/0964-1726/25/10/105019.

[8] Dragos, K., M. Theiler, F. Magalhães, C. Moutinho and K. Smarsly (2018). »On-board data synchronization in wireless structural health monitoring systems based on phase locking«. In: Structural Control and Health Monitoring 25. e2248 (11). DOI: 10.1002/stc.2248.

[9] Fitz, T., M. Theiler and K. Smarsly (2019). »A metamodel for cyber-physical systems«. In: Advanced Engineering Informatics 41, S. 100930. DOI: 10.1016/j.aei.2019.100930.

[10] Gürlebeck, K., D. Legatiuk, H. Nilsson and K. Smarsly (2019). »Conceptual model-ling: Towards detecting modelling errors in engineering applications«. In: Mathemati-cal Methods in the Applied Sciences 43 (3), 1243-1252. DOI: 10.1002/mma.5934.

[11] Law, K., K. Smarsly and Y. Wang (2014). »Sensor Data Management Technologies for Infrastructure Asset Management«. In: Sensor Technologies for Civil Infrastructures. Hrsg. von M. Wang, J. Lynch und H. Sohn. Sawston, UK: Woodhead Publishing, Ltd., 2-32.

[12] Lynch, J. P. (2006). »An overview of wireless structural health monitoring for civil structures«. In: Philosophical Transactions of the Royal Society A 365, 345-372. DOI: 10.1098/rsta.2006.1932.

[13] Philamore, H., I. Ieropoulos, A. Stinchcombe and J. Rossiter (2016). »Toward energetically autonomous foraging soft robots«. In: Soft Robotics 3 (4), 186-197. DOI: 10.1089/soro.2016.0020.

[14] Rennpferdt, L., S. Bohne and H. K. Trieu (2021). »Advances in manufacturing spinal cord implant using 3D selective laser induced etching of fused silica«. In: Transactions on Additive Manufacturing Meets Medicine, 3 (1), 574, DOI: 10.18416/AMMM.2021.2109574

[15] Rizzo, P. (2012). »NDE/SHM of underwater structures: a review«. In: Advances in Science and Technology 83, 208-216. DOI: 10.4028/www.scientific.net/AST.83.208.

[16] Schlicke, H., S. Kunze, M. Rebber, N. Schulz, S. Riekeberg, H. Trieu and T. Vossmey-er (2020). »Cross-linked gold nanoparticle composite membranes as highly sensitive pressure sensors«. In: Advanced Functional Materials 30.2003381 (40).

[17] Schmitt, P. et al. (2020). »Direct binary encoding of displacements on the nano-scale«. In: IEEE 33rd International Conference on Micro Electro Mechanical Systems (MEMS), Vancouver, BC, Canada, January 18, 2020. DOI: 10.1109/MEMS46641.2020.9056116.

[18] Schrader, P. S. u. a. (2016). »Independent benthic microbial fuel cells powering sensors and acoustic communications with the MARS underwater observatory«. In: Journal of Atmospheric and Oceanic Technology 33 (3), 607-617. DOI: 10.1175/JTECH-D-15-0102.1.

[19] Shantaram, A., H. Beyenal, R. R. A. Veluchamy und Z. Lewandowski (2005). »Wireless sensors powered by microbial fuel cells«. In: Environmental Science & Technology 39 (13), 5037-5042. DOI: 10.1021/es0480668.

[20] Smarsly, K. and H. Law (2013). »A migration-based approach towards resource-efficient wireless structural health monitoring«. In: Advanced Engineering Informatics 27 (4), 625-635. DOI: 10.1016/j.aei.2013.08.003.

[21] Tender, L. M. (2014). »Microbial fuel cells for powering Navy devices«. In: Techn. Ber. NRL/FR/6930—14-10,241. Naval Research Laboratory United States Navy.

[22] Theiler, M., D. Legatiuk, S. Ibanez and K. Smarsly (2020). »Metaization concepts for monitoring-related information«. In: Advanced Engineering Informatics 46.101158. DOI: 10.1016/j.aei.2020.101158.

[23] Theiler, M. and K. Smarsly (2018). »IFC Monitor – An IFC extension for modeling structural health monitoring systems«. In: Advanced Engineering Informatics 37, 54-65. DOI: 10.1016/j.aei.2018.04.011.

[24] von Poblotzki, J. M. and K. K. Trieu (2019). »Integration of subtractive 3D printing in-to micromolding of biodegradable implants for spinal cord treatment«. In: Transactions on Additive Manufacturing Meets Medicine 1 (1), DOI: 10.18416/AMMM.2019.1909S03P17.

[25] Wakeman, T., J. Miller and G. Python (2015). »Port resilience: overcoming threats to maritime infrastructure and operations from climate change«. In: Techn. Ber. UTRC/RF Grant No: 49997-47-25. Stevens Institute of Technology.

[26] Walter, X. A., J. Greenman und I. A. Ieropoulos (2020). »Microbial fuel cells directly powering a microcomputer«. In: Journal of Power Sources 446 (227328). DOI: 10.1016/j.jpowsour.2019.227328.

Authors

Prof. Dr.-Ing. Hoc Khiem Trieu
Hamburg University of Technology
Institute of Microsystems Technology
Eißendorfer Straße 42
21073 Hamburg
Germany
Tel.: +49 (0) 40 - 42878 / 4398
e-mail: trieu@tuhh.de
Web: www.tuhh.de/mst

Prof. Dr.-Ing. Johannes Gescher
Hamburg University of Technology
Institute of Technical Microbiology
Am Schwarzenberg Campus 4
21073 Hamburg
Germany
Tel.: +49 (0) 40 - 42878 / 3634
e-mail: johannes.gescher@tuhh.de
Web: www.gescher-lab.de

Prof. Dr.-Ing. Kay Smarsly
Hamburg University of Technology
Institut of Digital und Autonomous Construction
Blohmstraße 15
21079 Hamburg
Germany
e-mail: kay.smarsly@tuhh.de
Web: www.tuhh.de/idac

Towards coupling land-based and water-based mobile robots for monitoring and inspection of waterside structures

Robert Seifried, Kay Smarsly, Kosmas Dragos, Daniel A Duecker, Marc-André Pick

Abstract: Waterside structures represent vulnerable and often safety-relevant land/water interfaces that fulfill critical operations, such as facilitating commute across natural impediments or protecting and managing marine traffic. Therefore, monitoring and inspection of waterside structures are essential to ensure continuous operation. With recent technological advancements, robotic systems have been devised to execute monitoring and inspection tasks. However, robotic monitoring and inspection of waterside structures, compared to monitoring and inspection of land-based civil infrastructure systems, is associated with a number of challenges because of the specifics of waterside structures. In particular, the collaboration of land-based and water-based robots must be ensured, which, so far, has received little attention in robotics research. This paper proposes a concept to couple land-based and water-based robots for monitoring and inspection of waterside structures. The concept is centered around the collaborative analysis of the structural condition, and it builds upon embedded computing considering the semantics provided by digital twins and building information models. Finally, future research directions are discussed that need to be investigated to transfer the proposed concept into engineering practice.

1 Introduction

Safety and reliability, thus the life-cycle performance, of civil infrastructure is crucial to societal health, safety, security, and well-being. Damage and deterioration of civil infrastructure, affecting structural reliability and safety, occur as a result of operation failures, poor design, mechanical impact, or physical destruction due to man-made events or extreme natural phenomena. The latter represent one of the most visible consequences of climate change, such as heavy downpours, floods, storms, or heat waves (Urlainis et al., 2014).

Monitoring and inspection measures have been devised to assess damage and deterioration at early stages (Nguyen et al., 2018). Monitoring systems deployed for civil infrastructure systems usually rely on sensors installed in the structures at fixed locations, while infrastructure inspection is commonly conducted visually by human inspectors (Dragos and Smarsly, 2016). On the one hand, sensor systems in continuous long-term operation may be prone to sensor faults and are costly to install (Smarsly and Petryna, 2014). On the other hand, visual inspections, depending

on the individual expertise of the human inspectors, may be subjective, time-consuming, and costly (Frangopol and Kim, 2019). Therefore, with the advancements in information and communication technologies, both monitoring and inspection tasks have been conducted by mobile robots, ensuring objectivity, cost-efficiency, and accuracy (Charron et al., 2019). Moreover, mobile robots may reach locations that may be hard to reach for human inspectors. Essentially, mobile robots have the potential to advance both monitoring and inspection of civil infrastructure by (i) collecting data relevant to monitoring (e. g. accelerations, strains, displacements) that is continuously recorded by sensor systems installed at remote locations in the structure and transferred to the robots on demand and by (ii) recording data relevant to inspections, e. g. based on laser scans or photogrammetry.

As opposed to land-based civil infrastructure systems, waterside structures, such as dry docks, flood protection structures, fleet moorings, seawalls, groins, jetties, quay walls, underwater foundations, and breakwaters, represent vulnerable and often safety-relevant land/water interfaces that fulfill critical operations. Therefore, monitoring and inspection of waterside structures is vital to ensure the continuous operation of the structures. However, monitoring and inspection of waterside structures are associated with a number of specific challenges because, as compared to land-based civil infrastructure systems, hydrostatic forces, wind, salt spray, currents, tides, waves, and ice contribute to damage and deterioration to a non-negligible extent. Furthermore, many waterside structures are dynamic systems composed of multiple subsystems susceptible to vibrations, such as distribution lines for compressed air, electricity, steam, water, waste, fuel, and fender systems (Dean and Geusic, 2021).

For monitoring and inspection of waterside structures with mobile robots, the robots must execute both land-based and water-based operations due to the specifics of waterside structures. Therefore, proper communication, coordination, cooperation, and collaboration between land-based and water-based mobile robots must be ensured by coupling both robot types. At the same time, existing semantic information about civil infrastructure systems, as provided by digital twins and building information models, should advantageously be used when coupling both robot types. This paper proposes a concept to couple land-based and water-based mobile robots for monitoring and inspection of waterside structures. In the remainder of this paper, the characteristics of robotic monitoring and inspection of waterside structures are described, taking into account the semantics provided by digital twins and building information models. Thereupon, the concept for coupling land-based and water-based mobile robots is presented. The paper concludes with a summary and an outlook on the research required to implement the concept into engineering practice.

2 Monitoring and inspection of waterside structures

Civil infrastructure inspection, a legal basis for maintenance and life-cycle assessment, is typically performed by leveraging the information obtained by human inspectors, combined with decision-making criteria (Spencer et al., 2019). Furthermore, inspections are frequently supported by remote sensing approaches, e.g. lidar or photogrammetry, coupled with computational methods,

such as computer vision approaches or tools to create point clouds, in an attempt to advance conventional inspections. Nevertheless, as illuminated previously, inspections may be time-consuming, laborious, expensive, and/or dangerous. Representing a supplement to inspections, monitoring may provide quantitative insight into the condition of civil engineering structures by measuring physical quantities. These include acceleration, strain or displacement. On the implementation side, the sensors are organized in wireless sensor nodes or cable-based data acquisition units permanently installed in a structure. The sensor data, analyzed either manually or automatically using engineering algorithms, is then transformed into information (and probably into knowledge) used for decision-making. For many years, monitoring has matured into a reliable basis for continuously assessing the structural health in real-time, increasing safety and reliability while reducing maintenance and inspection costs (Lynch and Loh, 2006). Although monitoring provides reliable sensor data, it is associated with high installation costs and suffers from limited spatial resolution, as the sensors are installed at fixed locations. Furthermore, the limited power of the wireless sensor nodes represents another constraint when implementing monitoring concepts for large-scale civil infrastructure systems. Efforts have been underway to improve monitoring and inspection of civil infrastructure systems by deploying mobile robots to overcome the critical constraints.

It must be emphasized that, from a conceptual perspective, both monitoring and inspection can be reduced to the same general process steps: (i) Data is collected by sensors and (ii) transformed into information/knowledge used for decision making. Both process steps can be conducted by mobile robots with a certain degree of autonomy. Regarding monitoring and inspection of waterside structures, distinctions must be made regarding the type of mobile robots. To cover all elements of the structures, land-based and water-based robots must be deployed and coordinated. For land-based robotic monitoring and inspection, legged or wheeled robots are typically used either to retrieve sensor data stored in sensor nodes, whose sensors are continuously measuring at remote locations, or to execute remote sensing operations using, e.g. lidar or photogrammetry (Figure 1a). For water-based robotic monitoring and inspection, unmanned underwater vehicles are used, which, depending on the specific task, possess different actuation concepts to allow for either rapid environment coverage or accurate hovering for detailed inspection (Figure 1b).

(a) Legged robot equipped with a lidar system.

(b) Torpedo-shaped micro underwater robot.

Figure 1: Mobile robots used for land-based and water-based monitoring and inspection.

Both robot types have in common, besides collecting data (process step i), the application of internal algorithms and models for data analysis (process step ii) and the use of communication protocols as a technical basis for coordination, and thus cooperation, to solve the robotic monitoring and inspection tasks collaboratively. To couple land-based and water-based robots, the robotic tasks need to be coupled, considering the algorithms and models as well as the communication protocols. With the recent technological advancements, centralized algorithms and models describing the behavior of a structure, organized as a single "digital twin" (DT), which is interfaced with the physical structure by leveraging Internet of Things (IoT) concepts, are frequently used by the robots. Therefore, existing DT and IoT approaches representing waterside structures to be monitored and inspected also need to be considered when coupling land-based and water-based mobile robots. A concept towards coupling land-based and water-based mobile robots for monitoring and inspection of waterside structures is presented in the following section.

3 Towards coupling land-based and water-based mobile robots

Each environmental domain comes with its specific challenges, particularly in environments with domain transitions, such as waterside structures. As a consequence, highly optimized guidance, navigation, and control approaches have been developed to best address the domain challenges same yields for the robot sensory equipment. For example, coupling robotic systems at domain interfaces of waterside structures constitutes a challenging task. Specifically, new interfaces need to be defined to build a common ground between both domains (land and water). While terrestrial and aerial protocols often allow for high bandwidth communication, this is not the case for underwater communication. In fact, underwater communication bandwidth is very limited, unreliable, and data packages are subject to considerable latencies, posing direct constraints on the communication protocols. The impact of the lacking interfaces at waterside structures on the design of the overall inspection and monitoring framework is considerable since the data processing becomes heterogeneous with regard to various parameters including accuracy, update rate, and latency.

As a result, common approaches using a single centralized model are expected to achieve only limited performance. Thus, centralized models may be hardly suitable for coupling land-based and water-based mobile robots due to the high computational capacity and the reliable communication links required, which scale poorly with an increasing number of mobile robots. As a solution, a hybrid concept is proposed, which combines traditional centralized models with decentralized (embedded) models that can run onboard the mobile robots. The hybrid information-based monitoring and inspection concept is illustrated in Figure 2. Specifically, a *centralized model*, i.e. a high-fidelity representation of the structure (e.g. a digital twin), is implemented in a centralized server equipped with powerful computation hardware and provides detailed information on the structure. The centralized model fuses information gathered by mobile land-based and water-based robots. The robots run embedded partial *decentralized* models of the DT using the onboard processing capabilities. The decentralization comes with various advantages: First, data transmission from the robots towards the centralized server is

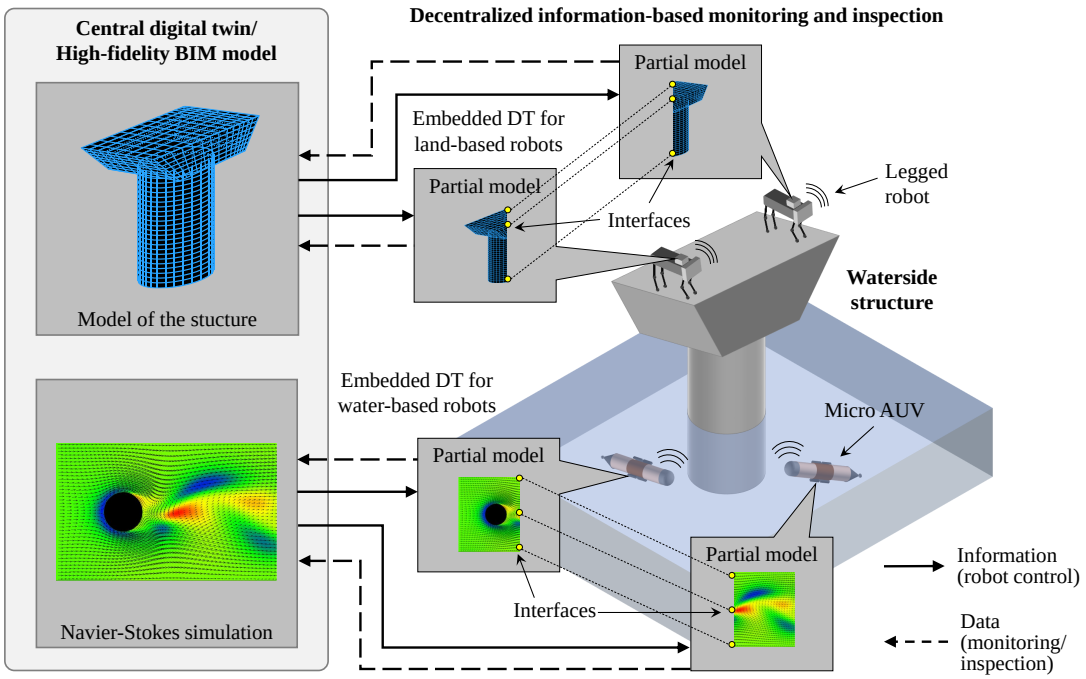

Figure 2: Hybrid decentralized information-based monitoring and inspection. Data gathered by the robots is send to a central DT; vice versa, the central DT provides high-level commands to the robots.

considerably reduced, e.g. instead of raw measurement sequences, the robots transmit only results from data analysis. Second, the data transmissions towards the robots, e.g. control commands, is reduced, owing to the decentralized models. This allows the robots to conduct short-horizon informative path planning locally onboard while the centralized server provides updates on high-level and long-term mission goals. As a result, the dependence of the robots on a reliable high-rate communication link to the centralized server is reduced.

Regarding the overall monitoring and inspection system, combining robots from multiple domains also raises new interesting research questions. For instance, methods need to be developed to decide which information can be efficiently gathered by which robot type. For this purpose, new heterogeneous cost-functions need to be designed, which trade off the importance of collecting new data against the individual effort invested, e.g. time and energy, for gathering data. Furthermore, the question of how the individual model representations can be coupled is raised. This includes considerations regarding potential new communication protocols and interfaces required to allow effective collaboration among various robot types.

4 Summary and conclusions

Monitoring and inspection of waterside structures are imperative to ensure continuous operation. With recent technological advancements, robotic systems are devised to execute monitoring

and inspection tasks. However, robotic monitoring and inspection of waterside structures are associated with a number of challenges because of the specifics of waterside structures, as compared to land-based civil infrastructure systems. In particular, the collaboration of land-based and water-based robots must be ensured, which has received little attention in robotics research so far.

In this study, a concept has been proposed to couple land-based and water-based robots for monitoring and inspection of waterside structures. The concept builds upon collaborative analyses of land-based and water-based mobile robots, using embedded computing and considering the semantics provided by digital twins and building information models. To transfer the concept into engineering practice, research needs to focus on designing interfaces for efficient communication between both types of mobile robots. Last but not least, coupling land-based and water-based robots for monitoring and inspection of waterside structures, representing a heterogeneous and complex research problem, requires integrating expertise from several engineering fields, such as robotics, computer science, mechanical engineering, civil engineering, marine engineering, environmental engineering, and electrical engineering.

5 Acknowledgments

This research has been sponsored by the German Research Foundation (DFG) under grant SM 281/20-1 and Kr 752/36-1. Any opinions, findings, conclusions, or recommendations expressed in this paper are those of the authors and do not necessarily reflect the views of DFG.

References

[1] Urlainis, A., Shohet, I.M., Levy, R., Ornai D., and Vilnay, O., 2014. Damage in critical infrastructures due to natural and man-made extreme events – A critical review. Creative Construction Conference. Prague, Czech Republic, June 21, 2014.

[2] Nguyen, A., Kodikara, K.A.T.L., Chan, T., Thambiratnam, D., 2018. Deterioration assessment of buildings using an improved hybrid model updating approach and long-term health monitoring data. Structural Health Monitoring, 18(1), pp. 5-19.

[3] Dragos, K. and Smarsly, K., 2016. A hybrid system identification methodology for wireless structural health monitoring systems based on dynamic substructuring. In: Proceedings of the SPIE Smart Structures/NDE Conference: Sensors and Smart Structures Technologies for Civil, Mechanical, and Aerospace Systems. Las Vegas, NV, USA, March 24, 2016.

[4] Smarsly, K. and Petryna, Y., 2014. A Decentralized Approach towards Autonomous Fault Detection in Wireless Structural Health Monitoring Systems. In: Proceedings of the 7th European Workshop on Structural Health Monitoring. Nantes, France, July 8, 2014.

[5] Frangopol, D.M. and Kim, S., 2019. Life-cycle of structures under uncertainty: Emphasis on fatigue-sensitive civil and marine structures. CRC Press, Boca Raton, FL, USA.

[6] Charron, N., McLaughlin, E., Phillips, S., Goorts, K. Narasimhan, S., and Waslander, S. L., 2019. Automated bridge inspection using mobile ground robotics. Journal of Structural Engineering, 145(11), 04019137.

[7] Dean, J.C. and Geusic, S., 2021. Waterfront and coastal structures knowledge area. National Institute of Building Sciences. Available at https://www.wbdg.org/ffc/dod/cpc-source/waterfront-coastal-structures-knowledge-area, accessed March 13, 2022.

[8] Spencer, B.F., Hoskere, V., and Narazaki, Y., 2019. Advances in Computer Vision-Based Civil Infrastructure Inspection and Monitoring. Engineering, 5(2), pp. 199-222.

[9] Lynch, J.P. and Loh, K.J, 2006. A summary review of wireless sensors and sensor networks for structural health monitoring. Shock and Vibration Digest, 38 (2), pp. 91-130.

Authors

Univ.-Prof. Dr.-Ing. Robert Seifried
Hamburg University of Technology
Institute of Mechanics and Ocean Engineering
Eißendorfer Straße 42 (M)
21073 Hamburg
Germany
e-mail: robert.seifried@tuhh.de
Web: www.tuhh.de/mum

Univ.-Prof. Dr.-Ing. Kay Smarsly
Hamburg University of Technology
Institute of Digital and Autonomous Construction
Blohmstraße 15
21079 Hamburg
Germany
e-mail: kay.smarsly@tuhh.de
Web: www.tuhh.de/idac

Dipl.-Ing. Kosmas Dragos, M.Sc.
Hamburg University of Technology
Institute of Digital and Autonomous Construction
Blohmstraße 15
21079 Hamburg
Germany e-mail: kosmas.dragos@tuhh.de
Web: www.tuhh.de/idac

Daniel A. Duecker, M.Sc.
Hamburg University of Technology
Institute of Mechanics and Ocean Engineering
Eißendorfer Straße 42 (M)
21073 Hamburg
Germany
e-mail: daniel.duecker@tuhh.de
Web: www.tuhh.de/mum

Dr.-Ing. Marc-André Pick
Hamburg University of Technology
Institute of Mechanics and Ocean Engineering
Eißendorfer Straße 42 (M)
21073 Hamburg
Germany
e-mail: pick@tuhh.de
Web: www.tuhh.de/mum

Autonomous robotics using microbial energy harvesting

Ioannis A. Ieropoulos

The contribution was not available by the time of printing.

smartBRIDGE Hamburg – the digital twin of the Köhlbrand Bridge revolutionizes the infrastructure maintenance of bridges

Niklas Schwarz, Dr. Marc Wenner

Abstract: Ports are responsible for providing and operating a variety of infrastructure assets. The usability and security of this infrastructure is of crucial importance. In order to improve the management and maintenance process of one of its main infrastructure objects the Hamburg Port Authority AöR (HPA) and its project partners developed smartBRIDGE Hamburg - the digital twin of the Köhlbrand Bridge. The digital twin combines the advantages of traditional bridge inspection and digital technologies such as monitoring and diagnostics. Thereby a single point of information is established. The condition information of the bridge is objective and available in real time.

1 Introduction

Ports are responsible for providing and operating a variety of infrastructure assets, such as quay walls, locks, waterways, railways, roads and bridges. These infrastructure objects are exposed to extraordinary loads and some of them are outdated. The safety and usability of the port infrastructure is of vital importance. One of the most important infrastructure objects in the port of Hamburg is the Köhlbrand Bridge (Figure 1). The Köhlbrand Bridge is not only a landmark, but also the main artery for the traffic flowing through the Port of Hamburg. Built in the 1970s, the structure is exposed to a high impact of stress resulting from the increasing level of traffic. Up to 38,000 vehicles are crossing the bridge every day. Constant and precise monitoring of the structure is required. Performing conventional inspection and maintenance presents an enormous and challenging task. To improve the maintenance process the Hamburg Port Authority AöR (HPA) and its project partners launched the project smartBRIDGE Hamburg – the digital twin of the Köhlbrand Bridge. The digital twin revolutionizes the infrastructure maintenance of bridges. By combining the advantages of traditional inspection, diagnostics, and monitoring smart-BRIDGE Hamburg provides objective real-time condition information of the entire bridge. Furthermore, smartBRIDGE Hamburg creates a single point of information regarding the condition information concerning the whole structure and its parts.

Traditional bridge inspections in Germany are standardized procedures according to DIN 1076 (1999), which is valid since 1930. Since the 1990s the inspections are usually documented digitally in the software SIB-Bauwerke, according to RI-EBW-PRÜF (RIERHING, 2017). The

Figure 1: The Köhlbrand Bridge (©HPA-Bildarchiv: Martin Elsen) Status Quo: the maintenance process of bridges in Germany

inspection process is conducted by qualified engineers and is based on the detection of visible and audible damage. The audible damages are detected by tapping on the structure with a hammer. Every six years a major inspection is mandatory. 3 years after a major inspection a minor inspection is executed, usually without the aid of inspection equipment. A major inspection, on the other hand, includes the manual inspection of almost inaccessible parts. If necessary, the major inspection is supported by utilizing inspection equipment. The bridge inspection in Germany is a proven procedure, which ultimately summarizes results of the inspection in a report and provides an overview on the status of the whole structure. However, the classic testing process reveals potential for improvement. The traditional inspection process only enables reactive maintenance. Damages are detected and repaired before more serious damages occur. Predicting damages is not possible with traditional inspection. Furthermore, the manual approach does not allow automation. Moreover, the documentation occurs in data silos. The data is not connected, which makes interoperability difficult. Finally, the classic inspection process ignores current and promising developments such as Building Information Modeling or structural health monitoring.

2 The Concept of the Digital Twin

The digital twin promises to precisely fulfill this potential for improvement in infrastructure maintenance. In other industries, such as mechanical engineering and automotive construction, the digital twin has already been established. Despite this, the term digital twin is used differently and requires a clear definition.

The Digital Twin Consortium defines the digital twin as follows: “A digital twin is a virtual representation of real-world entities and processes, synchronized at a specified frequency and fidelity. Digital twin systems transform business by accelerating holistic understanding, optimal decision-making, and effective action. Digital twins use real-time and historical data to represent the past and present and simulate predicted futures. Digital twins are motivated by outcomes, tailored to use cases, powered by integration, built on data, guided by domain knowledge, and implemented in IT/OT systems” (Olcott, 2020).

A common mistake in people’s understanding of the digital twin is to interpret a simple 3D or even a BIM model as a digital twin. That is not the case at all. The digital twin is based on a BIM model, but the digital twin has a connection to the real world, which is frequently updated. Furthermore, the digital twin performs a bidirectional information flow between the physical and virtual twin. In case of bridges this means that the sensors, which are installed on or in the structure, report their data to the virtual twin. The virtual twin processes the data and aggregates it to condition information. As soon as the sensor parameters exceed a certain threshold, the software alerts the asset managers that measures need to be performed. After these measures are performed and changes on the physical object are made the data sent by the sensor now changes again.

3 The pilot project smartBRIDGE Hamburg

The HPA is constantly working on optimizing its infrastructure maintenance procedures. Therefore, the HPA initiated smartBRIDGE Hamburg in 2019. This included the creation of a large-scale demonstrator to implement and experience the concept of the digital twin, aiming for an innovative improvement of the maintenance for bridges regarding the transferability to other asset classes. The bridge is the perfect demonstrator for testing the concept of the digital twin in a challenging way, because of its size and complex structure.

The main objective of the project was to create a digital twin of the bridge, which includes the data from traditional inspection as well as digital data sources such as diagnostics and monitoring. This digital twin had to show all this information combined in one model and located at the structure of the twin. Another requirement was that the condition of the bridge should be accessible in real time.

In conclusion the main benefits targeted by the interdisciplinary project team were:

- The combination of traditional inspection, diagnostics and monitoring and thereby using the advantage of each procedure (Figure 2)
- A Single Point of Information concerning the bridges condition and locating the information at the bridge structure
- A real time and objective overview of the whole bridge.

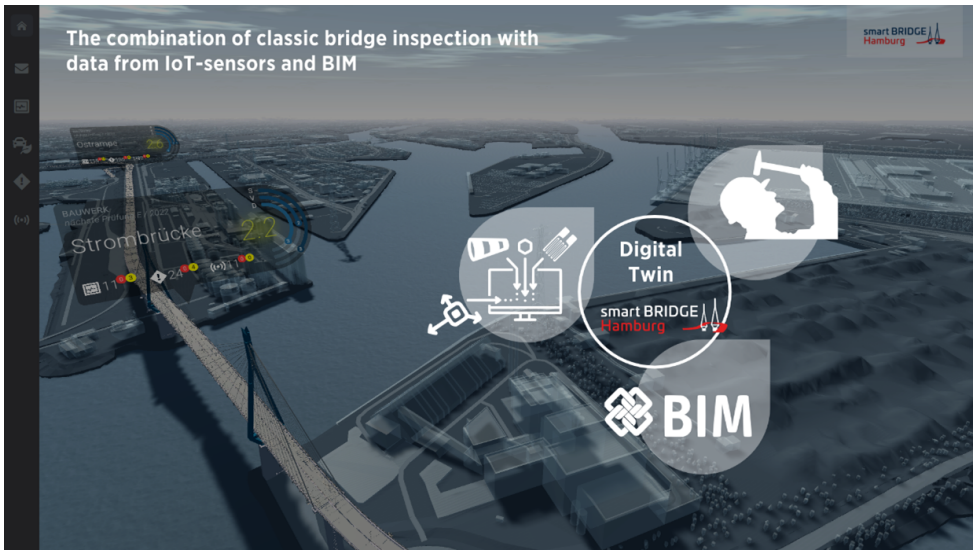

Figure 2: The combination of bridge inspection with data from IOT-sensors and BIM (© HPA AöR / MKP GmbH)

4 Key factors to successfully establish a digital twin

To realize a digital twin of an infrastructure asset six key factors have been identified. These factors will be presented in the following section.

4.1 Structural Health Monitoring (SHM) as a major source of condition information

The monitoring of the structure and its components aim to generate the required historic database to

- objectively and precisely evaluate the actual bridge condition in real time and
- forecast its future development.

The main benefits of SHM by utilizing sensors are:

- "The data history allows for a better analysis of the cause of observed damages during inspection and a target-oriented determination of necessary maintenance measures,
- the influence of changes of use or special uses (heavy goods transports, overloading) can be tracked,

- the continuous automated monitoring in dedicated areas (e. g. damaged areas or areas difficult to access) can relieve or replace an inspection,
- the concept of the digital twin to revolutionize the infrastructure maintenance: the pilot project
- the effectiveness of compensatory measures can be monitored or optimized,
- the data can be used to identify additional dysfunctions, damage or critical developments of damage that need to be assessed during an inspection." (Olcott, 2020)

To achieve these advantages, it is of crucial importance to plan and implement SHM carefully. Every bridge is unique and requires a fitting approach answering the following key questions:

1. Which parts of the structure need to be monitored to identify the structural behaviour and to detect changes?
2. Which sensors and which layout is adapted to measure the structural response?
3. Which analysis processes are necessary to derive the expected features from measured data?

4.2 The aggregation of the measurement data, the key to generate consumable information

Traditional bridge inspection evaluates existing damages and can integrate findings based on visual inspection and inspection by hand, sometimes supported by inspection equipment. Traditional inspection focuses on evaluating the surface of the structure.

Calculation methods, on the other hand, determine the theoretical condition of the entire bridge. However, these methods are based on a large number of assumptions. Thus, they are only able to calculate the theoretical bridge condition and do not necessarily represent the actual condition. Thus, these calculations do not necessarily represent the actual condition.

Sensor based monitoring can support both methods: traditional inspection and numerical analysis. To support traditional inspection existing damages can be monitored to detect degradation or to predict a point in time for maintenance measures (e. g. for elastomer bearings). To support numerical analysis, sensor-based data can be used to verify the structural model or to derive custom structural action models, e. g. for traffic, wind, or temperature (Olcott, 2020).

The important question (as soon as you reach a certain density of sensors) is how to analyse and aggregate numerous raw data into usable information.

The procedure at smartBRIDGE Hamburg is the following: First, possible damage scenarios (e.g. buckling, fatigue) were defined for the various components. Secondly, the measured sensor

information that are linked to specific scenarios, including threshold values for the appearance of certain scenario, were evaluated (sensor values such as tension values, load factor). Then the condition assessment of a component results from the various partial assessments of different damage scenarios. Each partial assessment is then subjected to a rating system (numerical values from 1 to 4). These partial assessments result in a Partial Condition Indicator (PCI). The PCI is the condition rating of a single component. If several partial condition indicators are aggregated to form a higher-level indicator, this is then called the condition indicator (CI).

In conclusion it is important to follow this data aggregation process:

- Sensor raw data: analysing the raw data using damage scenarios
- Partial Assessment: Determine a Partial Condition Indicator by evaluating the results of the damage assessments.
- Condition aggregation: Aggregate Partial Condition Indicators to Condition Indicators.

4.3 The fusion of information coming from conventional bridge inspection and from SHM

A very significant benefit of the project was the fusion between traditional inspection and monitoring data. Whereas the traditional inspection is a sequential event (every 3, 6 years), the monitoring data resulted in real time condition information.

The combination results in a condition assessment, which is composed of damage detected by the inspection and measured and processed sensor information.

This results in objective and real time condition indication of the bridge in one single point of truth: the digital twin.

Furthermore, it was very important to transfer the logic of the traditional inspection to the PCIs and CIs resulting from sensor information. Thereby a consistent logic applies, relying on the numeric evaluation values from one to four which is known to the traditional inspection for decades (Figure 3).

4.4 The role of BIM in realizing a digital twin

The BIM model has a very important role in realizing the digital twin. Nevertheless, a BIM model on its own is far from being a digital twin. A digital twin interacts automatically with its physical twin whereas a BIM model doesn't.

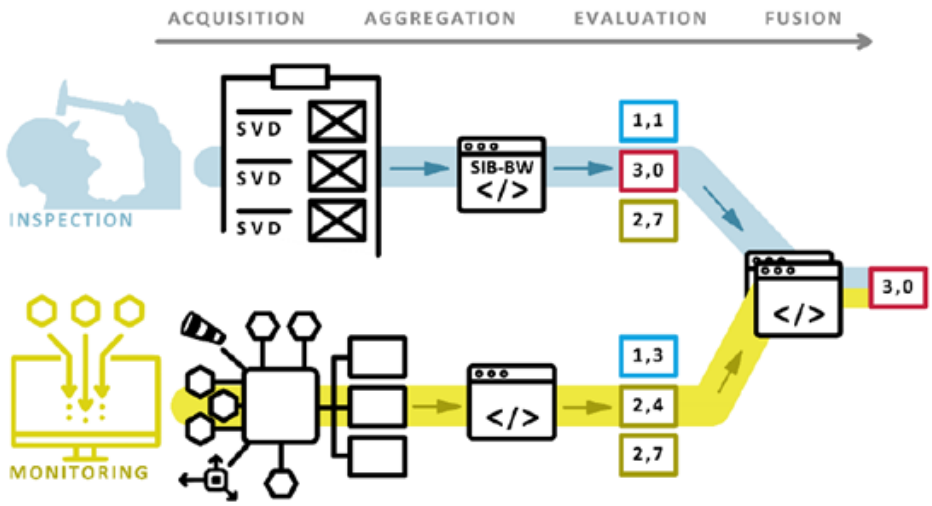

Figure 3: Data fusion from bridge inspection and SHM (© HPA AöR / MKP GmbH)

The BIM model is the skeleton of the digital twin. The BIM model enables the digital twin to:

- Visualize the geometry of the bridge in the front end,
- Provide structural classification, thereby enabling navigation and highlighting of individual parts of the structure and
- Localize damages, diagnostic information and sensor information (Figure 4).

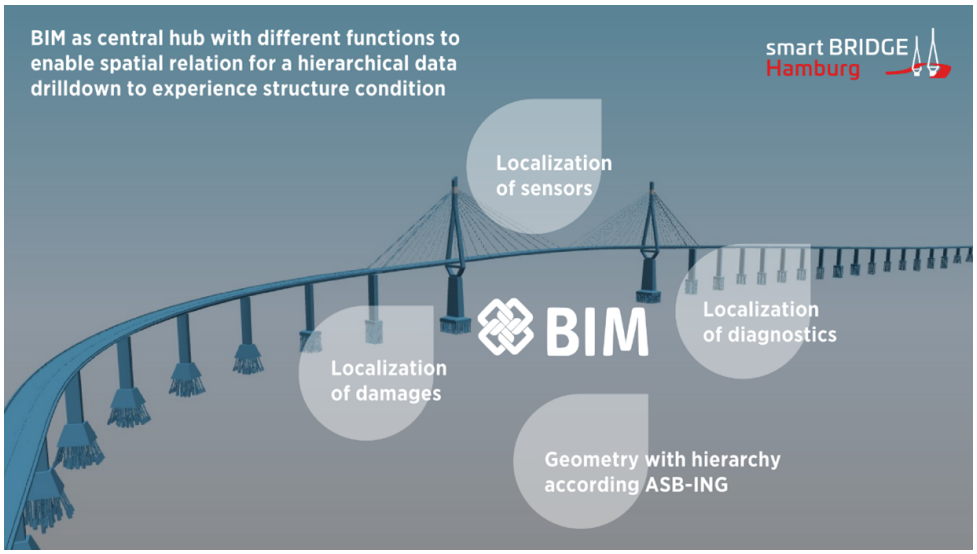

Figure 4: BIM: the skeleton of the digital twin (© HPA AöR / MKP GmbH)

4.5 The data architecture and data management as technical backbone of the digital twin

The data architecture and management are of vital importance for the digital twin. Information from multiple data sources need to be connected. Therefore, a strong backend database is needed (e.g. OGC Sensor things-Server). By using specific interfaces IOT devices can transfer their information into the database. A process engine controls the data processing.

The goal of processing the data are the PCIs and CIs.

4.6 The Human Machine Interface: key of the success and acceptance of the digital twin

The key to the success of each software is the acceptance of its users. This is no different with the digital twin. If the users don't find the digital twin intuitive and easy to operate the concept has failed. To gain user acceptance, we developed a multi-level Human-Machine Interface / a multi- level front-end.

This consists of the following parts:

- Condition Control (Figure 5)
- Expert Control

Condition Control is the intuitive visualization of the bridge and its condition indicators. Condition Control is easy to understand and to navigate. Condition Control's target audience ranges from senior management (who are not involved in engineering workflows) to subject matter experts. There are two ways for the user to navigate through the digital twin: exploring the digital twin by clicking through the 3D Model itself or a guided approach by using the structured menu, called "Tour Layer".

By the successful approach of data aggregation (5.2) smartBRIDGE Hamburg provides the user with consumable information, even if the database is very complex. This consumable information combined with the main focus on usability of Condition Control and Expert Control results in a high acceptance of smartBRIDGE Hamburg within the HPA.

5 Conclusion

smartBRIDGE Hamburg is still at a pilot stage and is not adaptable by drag and drop to other bridges, but we installed smartBRIDGE Hamburg in the HPA. Our asset managers and structural

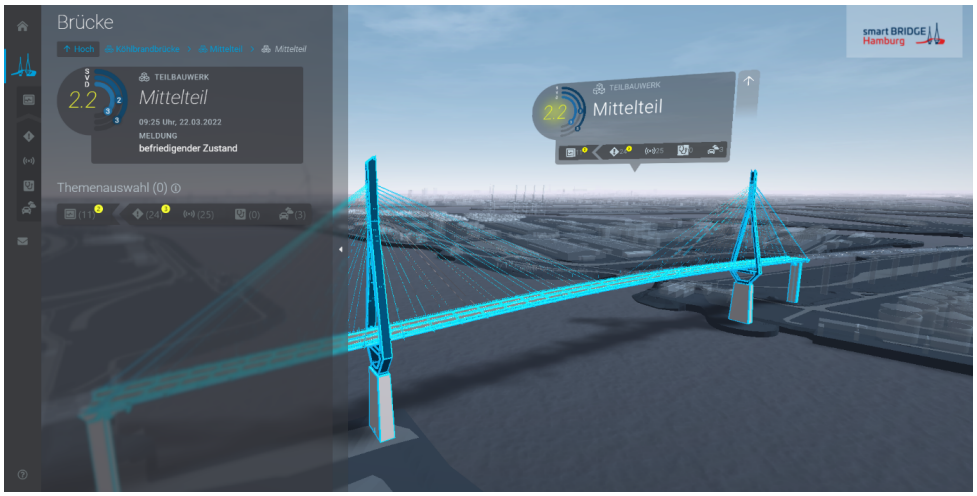

Figure 5: The web interface: Condition Control (© HPA AöR / MKP GmbH) Expert Control focuses on the needs of specialized engineers. They are provided with deeper information about the sensor data and its history, as well as more advanced building information.

engineers use smartBRIDGE Hamburg in their daily working routines. In Chapter 4 the main benefits the HPA and its project partners wanted to achieve by developing smartBRIDGE Hamburg were highlighted. We addressed all the goals that were set during the initiation of the project. The software can combine the data from traditional inspection, diagnostics, and monitoring. The sensors send data in real time. This results in an objective and real time overview of the bridge's condition. The condition information is located at the bridge structure and combined in one Single Point of Truth. Furthermore, the collected historic data is the basis for predictive maintenance.

The digital twin optimizes the maintenance of bridges. The proven traditional inspection is supported by digital methods such as diagnostics and monitoring. The work of the specialized engineers is simplified.

The project as it is presented is a pilot, which led to the realizations as described above. But due to this pilot project it was also possible to gain an understanding towards the possibilities which the digital twin of infrastructure objects will fulfil in the future:

- Lower costs in maintenance due to intelligent predictive measures replacing reactive procedures,
- Reduced maintenance backlog due to predictive measures and
- Increased sustainability by extending the life cycles of structures

Even though the described concept is modelled to fit the Köhlbrand bridge, it is powerful enough to be transferred to other assets and to integrate further innovation such as automatic databased anomaly detection (self-inspection), automatic generation of a 3D model with photogrammetry

or LIDAR technology, and application of artificial intelligence (AI) to analyze measurement data and make forecasts.

To meet the future challenges of increasing usage and loads of bridges it is necessary to invest in further development of the digital twin concept to support the specialized engineers and raise the infrastructure maintenance to a new level.

References

[1] DIN Deutsches Institut für Normung (1999). Ingenieurbauwerke im Zuge von Straßen und Wegen, Überwachung und Prüfung, DIN 1076, Berlin, Beuth Verlag GmbH.

[2] Bundesministerium für Verkehr und digitale Infrastruktur (2017). Richtlinien für die Erhaltung von Ingenieurbauten (RI ERH ING) Richtlinie zur einheitlichen Erfassung, Bewertung, Aufzeichnung und Auswertung von Ergebnissen der Bauwerksprüfungen nach DIN 1076, RI EBW PRÜF.

[3] Olcott, S., Mullen, C. (2020). Digital Twin Consortium Defines Digital Twin, https://blog.digitaltwinconsortium.org/2020/12/digital-twin-consortium-defines-digital-twin.html (consulted 04.01.2021)

[4] Marc Wenner, Christof Ullerich, et. al. (2021). The Concept of Digital Twin to Revolutionise Infrastructure Maintenance: the Pilot Project smartBRIDGE Hamburg, 27th ITS World Congress, Hamburg, Germany, 11-15 October 2021

Authors

M. Sc. Ing. Niklas Schwarz
Hamburg Port Authority AöR
Neuer Wandrahm 4
20457 Hamburg
Tel.: +49 (0) 40 – 42847 - 5238
e-mail: niklas.schwarz@hpa.hamburg.de
Web: hamburg-port-authority.de

Dr. Ing. Marc Wenner
Marx Krontal Partner GmbH
Zum Hospitalgraben 2
99425 Weimar
Tel.: +49 3643 43 96-0
e-mail: info.weimar@marxkrontal.com
Web: https://marxkrontal.com/de/

Adaptive Bridge Design through Additively Manufactured Modular Laminated Metal Composites

Marcus Rutner, Jakob Brunow, Niclas Spalek

Abstract: Adaptive bridge design through wire arc additive manufacturing (WAAM)-modular components addresses the possibility to replace critical bridge components and connections, aiming at preventing specific failure modes, thus creating a longer lifetime of the global structure. WAAM opens up two approaches to tailor the structural component or connection a) through shape-optimization or b) through locally embedding enhanced material properties. The enhanced material properties are achieved by WAAM-fabricated laminated metal composites (LMCs). Laminated metal composites enable superior and tailorable material properties compared with bulk material. The article introduces laminated metal composites consisting of multiple bilayers of alternating layers of ductile and high-strength steel processed by wire arc additive manufacturing. Governing parameters in the fabrication process affecting the material properties and enhanced material properties of the laminated metal composites fabricated by WAAM are discussed and investigated under static tensile, impact and tension-tension high-cycle-fatigue loading in the context of adaptive bridge design.

1 Introduction

The benefits of wire arc additive manufacturing (WAAM) in respect to shape optimization have been discussed in the literature (e.g. Feucht et al., 2021; Kühne et al., 2019; Müller et al., 2019). Through the layer-to-layer section buildup, individual shapes are possible avoiding notches, which reduce the life time of components and connections. Figure 1 shows exemplarily a connection in a brigde, which is also shown as FE Model in Figure 1b. Given the case that the bolt hole is a fatigue-critical detail, WAAM enables to manufacture a shape-optimized design of the component, as shown in Figure 1c left. The WAAM-component installed into the bridge and replacing the original component would remove this particular failure mode, e.g. shear-out failure, hence, increasing the life time of the bridge. However, WAAM allows also multi-material design (Treutler et al., 2019) through the generation of anisotropic behavior in the welding direction welding single strands of dissimilar metal or locally embedding well plasticizable material to increase material strength under cyclic loading. Treutler and Wesling (2021) provide a summary on functionally graded structures and the possibility to locally embed adapted material properties. Reisgen et al. (2019) fed multiple wires of different chemical compositions into the molten pool

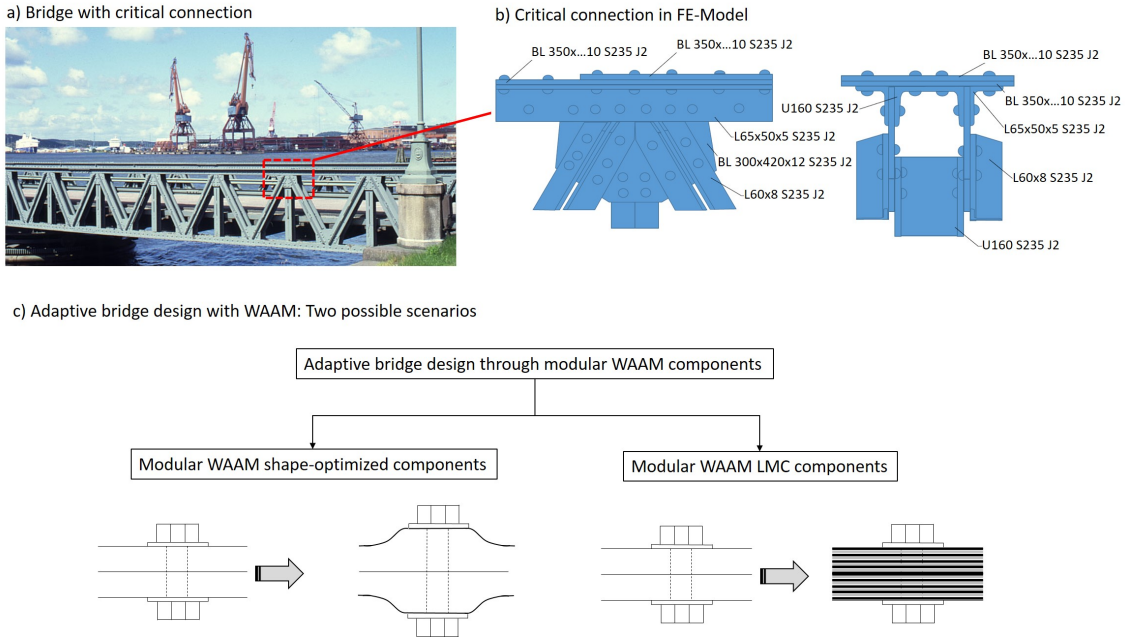

Figure 1: Modular bridge design using WAAM.

of the welding process producing chemically graded structures by constantly alternating the wire feed speed in the multiwire WAAM process. This paper explores the WAAM-manufactured laminated metal composites (LMCs). Laminated metal composites (LMCs) enable superior and tailorable material properties compared with bulk material (Spalek et al., 2021). Figure 1c right shows an example of material-optimized design of a critical component by embedding WAAM LMCs. The process of material-tailoring, producing and building modular WAAM LMC components or connection detailing into the global structure and replacing the respective critcal component or connection is introduced as adaptive bridge design through modular WAAM LMCs.

Various methods exist to produce LMCs with single layer thicknesses in the macroscale, such as rolling and pressing, deposition and spraying. Only very limited literature exists about LMCs fabricated by arc welding based additive manufacturing using a collaborative robot. The study presented herein explores LMCs consisting of multiple bilayers of alternating layers of two materials processed by wire arc additive manufacturing (WAAM). Hence, the LMCs fabricated by WAAM are also referred to as WAAM LMCs herein.

The enhanced mechanical properties of steel-based LMCs manufactured by rolling and pressing are an improved fracture strain, increased tensile strength, toughness and better fatigue resistance compared to the homogenous weld metal material (Carreño et al., 2003; LeSuer et al., 1996; Leedy et al., 2001; Koseki et al., 2014). The literature names reasons for the enhanced material properties of LMCs manufactured by rolling and pressing compared with homogenous weld metal materials. On the one hand, delamination is seen as reason for the improved mechanical properties (Carreño et al., 2003; LeSuer et al., 1996; Leedy et al., 2001; Koseki et al., 2014). On the other hand, a high interface toughness which suppresses delamination in LMCs and enables

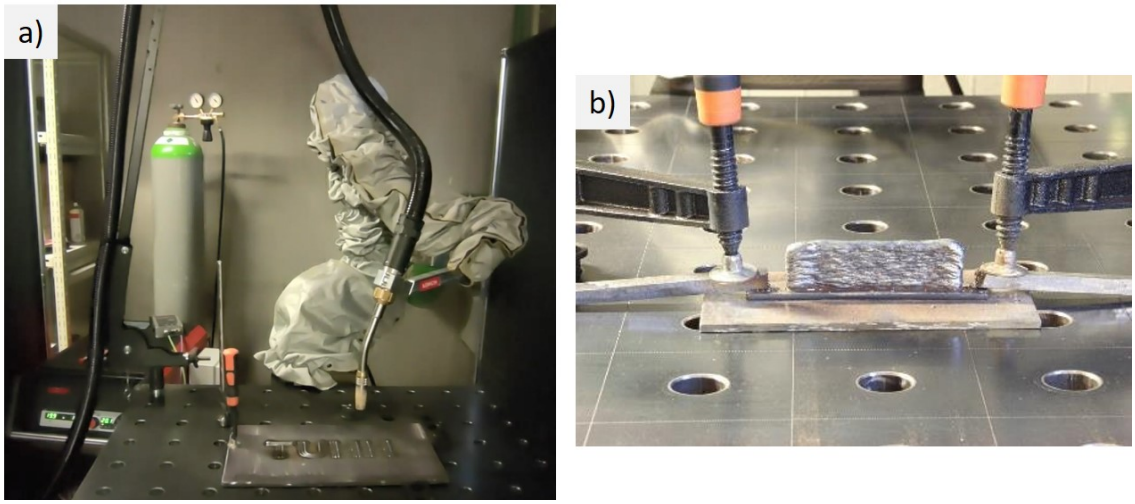

Figure 2: (a) Collaborative robot (Universal Robot UR10e) guiding the welding equipment (Lorch S5 Speedpuls XT); (b) WAAM LMC (Spalek et al., 2021).

load transfer between ductile and brittle layers of the laminate (Ojima et al., 2012; Nambu et al., 2009; Kümmel et al., 2016), is argued to be the key parameter. Hence, in this context, this article provides insights into section build-up, material properties and occurrence of delaminations of WAAM LMCs when exposed to static, impact or fatigue loading. The objectives of the study presented herein are

- to provide insights into the fabrication of laminated metal composites by WAAM,
- to investigate parameters affecting the material parameters of WAAM LMCs,
- to provide information on the failure mechanisms of WAAM LMCs and
- to point out the use of WAAM LMCs for adaptive bridge design.

2 Materials and Methods:

The WAAM LMC is fabricated by a collaborative operative robot (Universal Robot UR10e, Universal Robots, Odense, Denmark) guiding the welding equipment (Lorch S5 Speedpuls XT, Lorch Schweisstechnik GmbH, Auenwald, Germany) which allows highly precise and reproducible welds, as shown in Figure 2. The robot arm is mounted on a quadratic steel table which provides a plane working surface.

For the WAAM-fabricated LMC, two different weld materials are used, a 1-mm-diameter ductile steel wire, hereafter named SG2 (EMK 6 D, Böhler, material No. 1.5125) and a 1mm-diameter high-strength steel wire, hereafter named X90 (DT-X90, DRATEC GmbH, Material No. 1.6834). The filler wires SG2 and X90 are identified by EN ISO designations and the chemical

compositions of each wire are provided in Table 1. The LMC presented herein is built up by alternating deposits made of ductile steel and high-strength steel type wires. The WAAM LMC is built up onto a steel substrate (S355), as shown in Figure 2.

Table 1: Designation and chemical compositions of filler wires (Spalek et al., 2021).

Name	Designation	C (%)	Si (%)	Mn (%)	Ni (%)	Mo (%)	Cr (%)
X90	EN ISO 16834-A: G89 4 M21 Mn4Ni2CrMo	0.1	0.7	1.7	2.0	0.5	0.3
SG2	EN ISO 14341: G42 4 M G3Si1	0.1	0.85	1.45	0	0	0

The layup of the WAAM LMC is governed by various process parameters, among others, the interpass temperature which affects the weld bead thickness. The interpass temperature is higher when the pause time, which is the time interval before the next weld layer is set, becomes shorter. There is a significant incremental reduction of the weld bead thickness in dependence of pause time and number of welds, as shown in Figure 3. A defined pause time controls the interpass temperature which directly affects the weld geometry and flowability of the weld. In this study, the initially defined weld height is h = 1.75 mm. The welds are set on top of each other and the weld bead thickness is measured after cooling by means of a Vernier caliper. The diagram in Figure 3 shows that the measured weld bead thickness decreases with increasing number of layers. Figure 3 (left) shows the section of the WAAM LMC as manufactured as well as cut and polished for fatigue testing. The cross section shows distinguishable alternating weld layers of ductile and high-strength steel. The thickness of the weld layer varies and wavy sharp interfaces of the weld layers are visible, as annotated in Figure 3. The interpass temperature not only affects the weld bead thickness, moreover, it also affects the dilution between SG2 and X90. The decreasing weld bead thickness with subsequent deposition of weld bead on top of each layer implies an increase in dilution between the two dissimilar deposits.

A pause time between $t_P = 40$ s and $t_P = 120$ s leads to meaningful data. At small pause times of $t_P = 20$ s or less, the substrate plate deforms because of high energy input, thermally induced stresses in weld and substrate plate essentially causing weld defects. A pause time of 300 s results in a weld bead thickness which corresponds well with the weld bead thickness created by a pause time of 120 s, hence it is uneconomical. A reduced pause time results in a smaller weld bead thickness. The incremental change of the weld bead thickness with increasing number of layers is larger between the first and fifth weld layer, however, it eventually approaches a final weld bead thickness of about 1.3 mm using a pause time of 60 s. Maintaining a constant current throughout the welding process is seen as crucial for receiving reproducible weld beads and a constant welding procedure. The contact-tip-to-work-distance (CTWD) is found to be a key parameter in tailoring weld bead geometries and is itself governed by welding parameters, e.g., the amperage. A suitable set of those parameters is determined and used throughout testing, as summarized in Table 2.

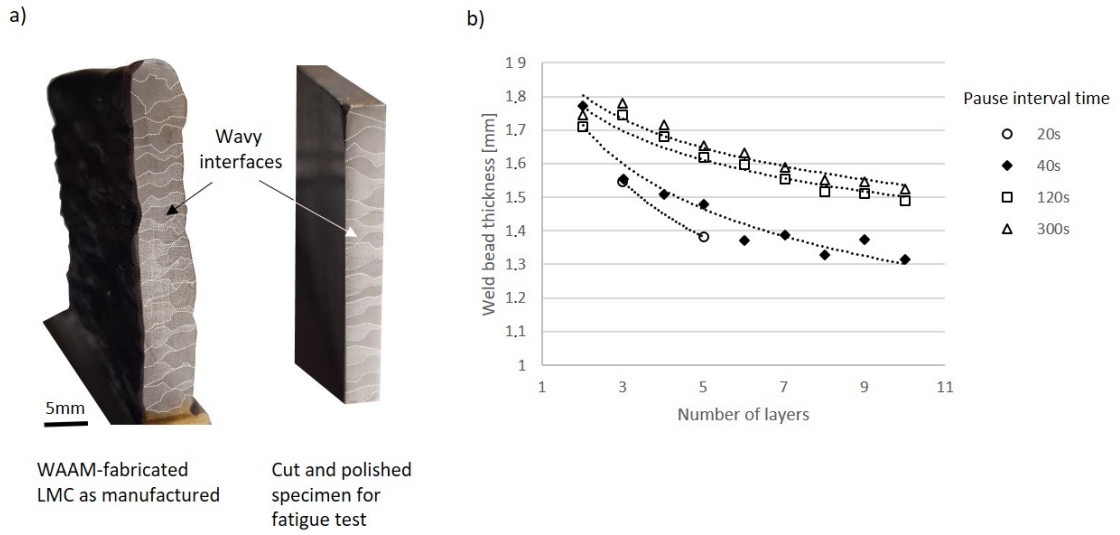

Figure 3: (a) WAAM LMC cross section—as manufactured and cut and polished for fatigue testing; (b) relation of weld bead thickness, pause time and number of layers (Spalek et al., 2021).

Table 2: Parameters for WAAM-fabricated LMCs (Spalek et al., 2021).

Specimen	Electric Current (A)	Wire Feed Speed (mm/s)	Welding Speed (mm/s)	Pause Time (s)	Heat Input (J/mm)	CTWD (mm)	Weld Bead Thickness (mm)
WAAM LMC	150	7.2	10	60	270	13	1.3
X90-WAAM	150	7.2	10	60	270	12	1.3
SG2-WAAM	150	7.2	10	60	270	13	1.3

Table 3 presents the measured Vickers hardness (HV3) of the WAAM-fabricated LMC at three different equidistant measurement positions in the middle of a weld layer, as shown in Figure 4. Two layers of each material are measured for comparison. Interestingly, the observed hardness is almost identical for both steel types. The hardness corresponding to high-strength steel is about 188.65 (HV3), and the hardness of the mild steel is about 179.65 (HV3). The mechanical properties of the LMC are strongly influenced by the dilution between the unalloyed SG2 and X90 weld beads causing the hardness of both SG2 and X90 steel to fall in the same range of hardness. The applied welding heat input causes a strong dilution of alloy elements especially in the X90 beads and results in a significant decrease in hardness. HV10 measurements are conducted for validation reasons. The HV10 measurements confirm the HV3 measurements.

The results of the hardness measurements are subsequently compared to tensile test results which describe the macroscopic stress–strain behavior of the two steels and the WAAM LMC, as shown in Table 4.

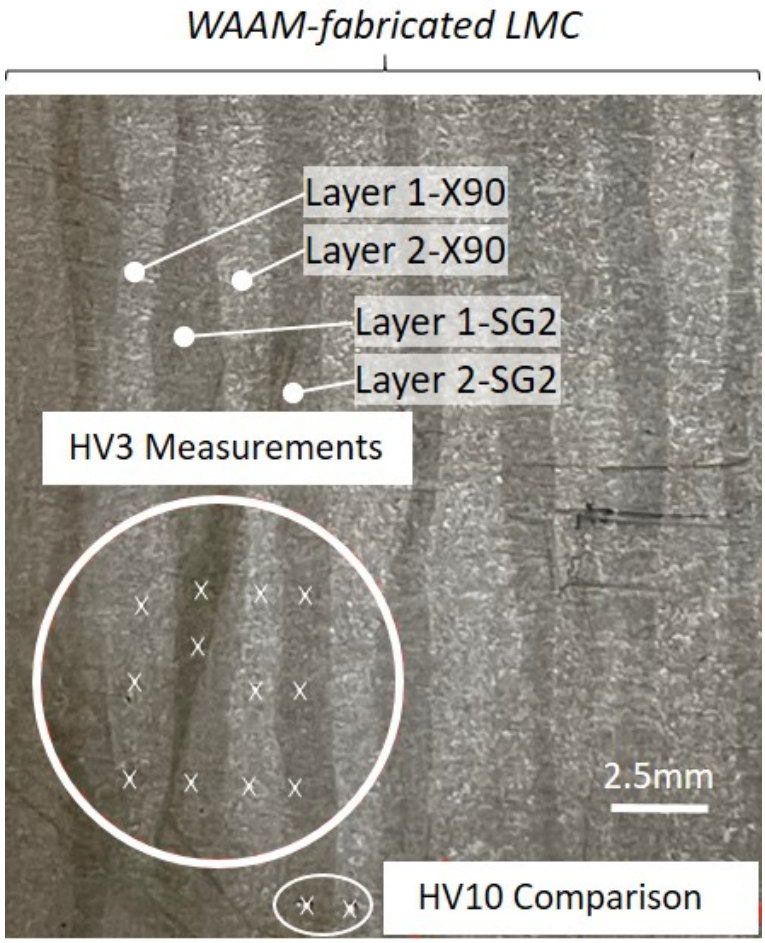

Figure 4: Vickers hardness HV3 and HV10 measurement at equidistant measurement positions in the middle of a weld layer (Spalek et al., 2021).

Table 3: Measured Vickers hardness of SG2/X90-WAAM LMC (Spalek et al., 2021).

HV3 Measurements	SG2-Ductile Steel Layer		X90-High Strength Steel Layer	
Position	Layer 1	Layer 2	Layer 1	Layer 2
0 mm	178	161	202	182
2.5 mm	190	174	182	174
5 mm	193	182	202	190
Mean value	187.0	172.3	195.3	182.0
Standard deviation	7.9	10.6	11.5	8.0

Table 4: Measured Vickers hardness HV of SG2/X90-WAAM LMC with equal spacing between measurement positions (Spalek et al., 2021).

Parameter	SG2-Ductile Steel Layer		X90-High Strength Steel Layer	
	Layer 1	Layer 2	Layer 1	Layer 2
Mean Vickers hardness (HV3)	187.0	172.3	195.3	182.0
Mean yield strength (MPa)	392.4	344.1	419.6	376.0
Mean ultimate strength (MPa)	609.1	560.6	636.5	592.6

Figure 5 provides information regarding the extent of dilution by EDX-spectrum analysis. Figure 5a shows the SEM scan of a part of the WAAM layup with a SG2 layer in the center and X90 layers on both sides, as annotated. A line plot runs across the three layers cutting the interfaces, which are also annotated. The line plots in Figure 5b show the nickel (Ni) and the chromium (Cr) distribution across the interfaces of the laminate. According to the manufacturer, the Ni content of the X90 and SG2 is 2.0 wt% and 0 wt%, respectively, as listed in Table 1. However, dilution causes the concentration in the X90 layers to drop to 1.04 wt% while the Ni-concentration increases in the SG2 layer from 0 to 0.62 wt%. Further, according to the manufacturer, the Cr content of the X90 and SG2 is 0.3 wt% and 0 wt%, respectively. However, dilution causes the Cr-concentration in the X90 layers to drop to 0.24 wt% while the concentration increases in the SG2 layer from 0 to 0.16 wt%. It is concluded that significant dilution is identified which balances the hardness in this study and changes the material properties of the WAAM LMC. Figure 5c shows the EDX-spectrum analysis and Figure 5d lists the concentrations of Ni and Cr, as measured in spectrum 1 and spectrum 2 (see Figure 5a).

3 Results

This study includes static tension tests, Charpy V-notch tests and fatigue tests, in order to better understand the material properties, physical behavior and failure mode of WAAM-fabricated LMCs.

3.1 Static Tension Test

The specimen geometry for the static tension tests follows the DIN 50125. The specimen length is 240 mm. The WAAM-fabricated specimen originally has an uneven surface; hence, it is cut and polished to a thickness of 4 mm. EDM cutting und CNC-milling are used to cut out the dog bone specimen form. The reduced cross-section height of the dog bone specimen is 10 mm and has about seven layers, as shown in Figure 6. The specimen is cut out of the built WAAM-layup as shown in Figure 6c. The WAAM specimen out of ductile steel (SG2) and out of high-strength steel (X90), respectively, as well as the WAAM-fabricated LMC after the static test, are shown in Figure 7.

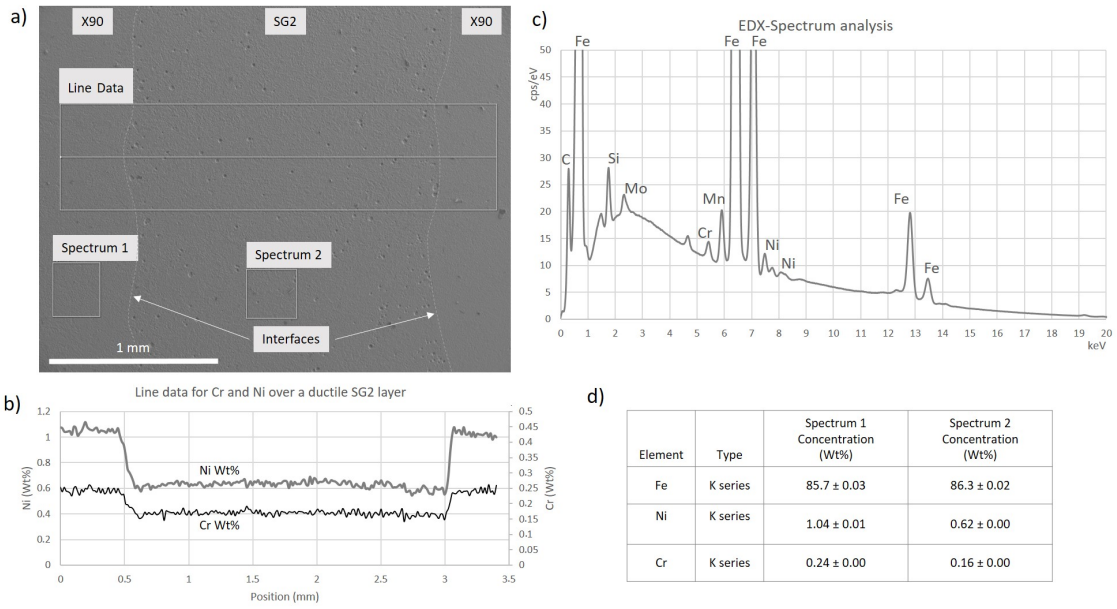

Element	Type	Spectrum 1 Concentration (Wt%)	Spectrum 2 Concentration (Wt%)
Fe	K series	85.7 ± 0.03	86.3 ± 0.02
Ni	K series	1.04 ± 0.01	0.62 ± 0.00
Cr	K series	0.24 ± 0.00	0.16 ± 0.00

Figure 5: EDX-spectrum analysis (a) SEM scan; (b) line plot for Cr and Ni; (c) EDX spectrum analy-sis; (d) table listing Cr- and Ni-measurements in spectra 1 and 2, respectively (Spalek et al., 2021).

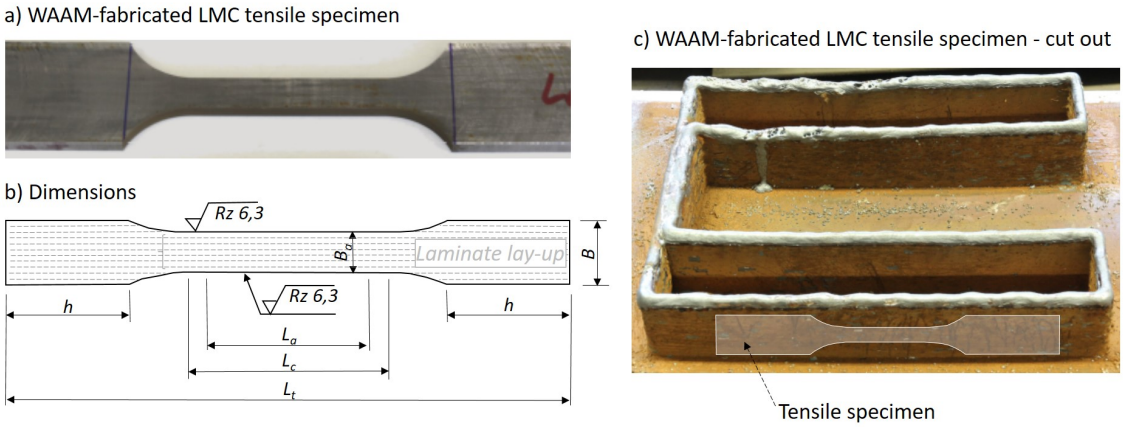

a_0 [mm]	B_a [mm]	L_a [mm]	B [mm]	r [mm]	h [mm]	L_c [mm]	L_t [mm]
4	10	35	34	20	70	55	240

Figure 6: (a) WAAM-fabricated LMC tensile specimen; (b) static tension specimen geometry according to DIN 50125; (c) position of cut-out (Spalek et al., 2021).

Figure 7: Static tension WAAM specimen out of ductile steel (SG2), high-strength steel (X90) and SG2/X90-WAAM LMC after static tension testing (Spalek et al., 2021).

The hydraulic tension machine (Schenck PC400M; Schenck Technologie- und Industriepark, Darmstadt, Germany) is used for the static tension tests. Tension loading is applied displacement with controlled increasing of the displacement constantly by 0.03 mm/s. Yield strength, elastic strain, tensile strength and fracture strain are the parameters measured. The stress–strain curves assessed are shown in Figure 8. Obviously, both steel materials, the ductile SG2 WAAM material and the high-strength X90 WAAM material, show the expected different behavior. While the ductile SG2 shows a fracture strain of 34 %, the high-strength X90 only has a fracture strain of 17.5 %. The ductile SG2 has a pronounced yielding and hardening, with yield strength of about 330 MPa and tensile strength of 440 MPa, while the high-strength X90 has no yielding and a tensile strength of 870 MPa. The WAAM-fabricated LMC has a fracture strain of 23 %, a pronounced yield strength of 490 MPa and a tensile strength of 600 MPa. Since the laminate consists of 50 % ductile and 50 % high-strength steel, the rule of mixture would result in a yield strength of 665 MPa and a fracture strain of 25 %. However, the material properties are much more dependent on dilution, as discussed in Section 3.

Table 5 lists the mechanical properties of the filler wires used for WAAM-fabricating the LMC. In respect to the yield strength, the difference between manufacturer information and measured results is provided. Since the high-strength steel (X90) does not show a yield strength plateau, the offset yield strength (Rp0.2) is assessed at 0.2 % offset strain. Overall, the measured tensile strength by using the homogenous WAAM specimen is larger than the tensile strength average estimated from Vickers hardness tests using the WAAM LMC (Table 4). Accounting for the offset yield strength of high-strength steel, the measured yield strength matches the yield strength average estimated from the Vickers hardness tests quite well.

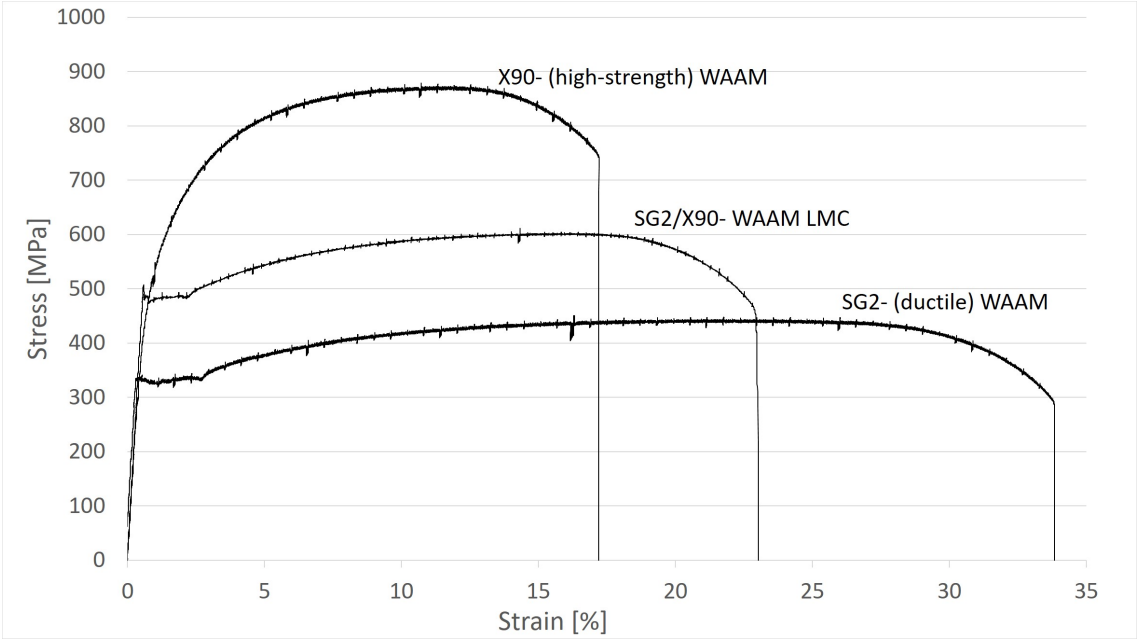

Figure 8: Static tension test; stress–strain curves for all three specimen, homogenous ductile (SG2) WAAM, homogenous high-strength (X90) WAAM and SG2/X90-WAAM LMC (Spalek et al., 2021).

Table 5: Yield strength, tensile strength, fracture strain and impact energy values of the steels applied; manufacturer information (Spalek et al., 2021).

Product name	Yield strength Manufacturer info / measured (MPa)	Tensile strength (MPa)	Fracture strain (%)	Charpy V-notch energy at 20 °C (J)
Böhler EMK (SG2)	Manufacturer info: 440	560	30	160
	Measured (Offset yield point ReH): 330	440		
DRATEC DT-X90	Manufacturer info: 880-920	940–980	16–20	65–95
	Measured (Offset Yield Rp0.2): 475	870		

Figure 9: (a) WAAM LMC sample as manufactured; (b) EDM-cutting the top; (c) Charpy V-notch specimen with its final geometry (H/B/L = 10/10/55 mm) (V-notch annotated) (Spalek et al., 2021).

3.1.1 Charpy V-Notch Impact Test

The specimen geometry is defined by DIN EN ISO 148-1. The specimen length is 55 mm, and the square cross section has a side length of 10 mm. The specimen geometry is produced in two steps, first the WAAM processing and second the post-weld EDM cutting and sanding (Kibria et al., 2019). The processing steps are shown in Figure 9: (a) the WAAM-fabricated LMC specimen, (b) the top surface preparation and (c) the V-notch sample completely cut from the substrate plate and polished with the final measures according to DIN EN ISO 148-1. The location of the V-notch is in crack arrestor orientation and is annotated in Figure 9c. Typically, Charpy V-notch testing is conducted at different tempera-tures. However, in this test series the temperature is held constant at room temperature (20 °C).

Six Charpy V-notch WAAM samples fabricated out of ductile steel (SG2), six Charpy V-notch WAAM samples fabricated out of high-strength steel (X90) and three Charpy V-notch WAAM samples fabricated out of SG2/X90-WAAM LMC are compared in this test series. Figure 10a shows the cross section of the Charpy V-notch sample fabricated out of WAAM LMC. The deformed Charpy V-notch samples out of high-strength (X90) WAAM, ductile (SG2) WAAM and the SG2/X90-WAAM LMC are shown in Figure 10b.

While the Charpy V-notch test splits the high-strength WAAM specimen into two parts, the ductile WAAM and the WAAM LMC specimen are still one piece. The high-strength and the ductile WAAM V-notch specimen fracture along the symmetry plane. However, the WAAM LMC specimen slightly torques during the deformation process. Table 6 provides the energy values from Charpy V-notch testing. As expected, the homogenous high-strength WAAM samples respond brittlely, and show on average a reduced toughness of 62 J, with a ductile

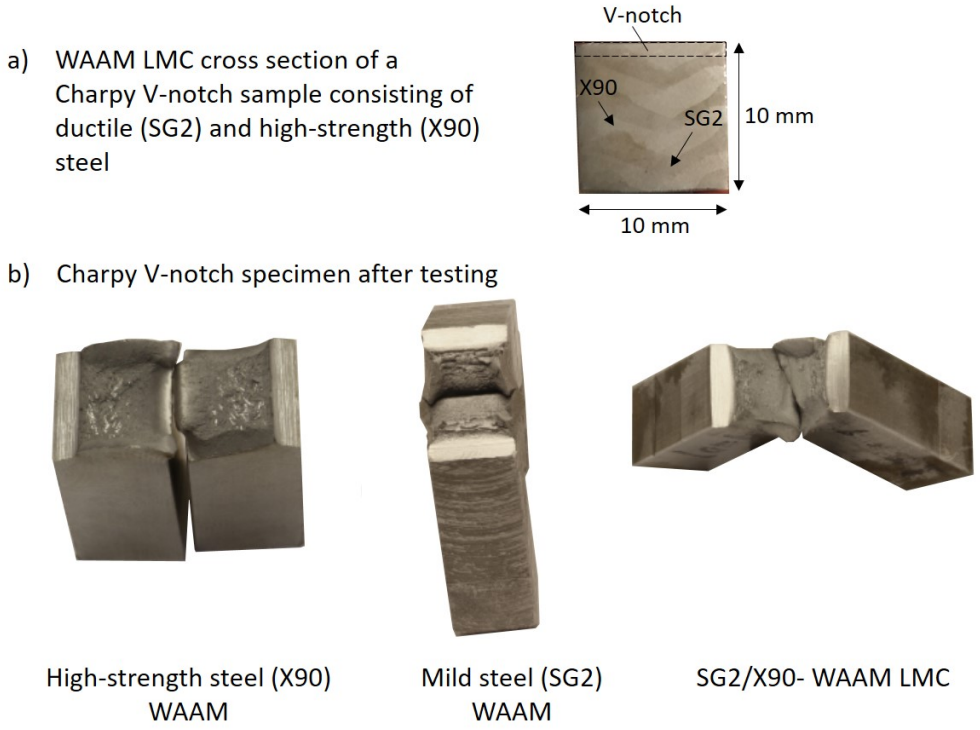

Figure 10: Charpy V-notch test (a) WAAM LMC Charpy V-notch specimen cross section; (b) Charpy V-notch specimen after testing (Spalek et al., 2021).

fracture percentage of 64 %. The homogenous ductile WAAM samples show an average of about 154 J. The WAAM LMC reaches an average toughness of 144 J with a ductile fracture percentage of 81 %, hence very close to the homogenous ductile WAAM samples with a ductile fracture percentage of 90 %. Typically, in Charpy V-notch samples, the energy is found to be proportional to the yield strength ratio (Hosford, 2010), which is not confirmed herein from studying WAAM-fabricated steel samples.

Table 6: Charpy V-notch energy values of WAAM-specimen out of ductile steel (SG2), high-strength steel (X90) and SG2/X90-WAAM LMC (Spalek et al., 2021).

Sample	SG2-Ductile WAAM (J)	X90-High-Strength WAAM (J)	SG2/X90-WAAM LMC (J)
1	149	66	121
2	170	62	156
3	169	62	156
4	158	67	
5	156	60	
6	122	55	
Mean value	154	62	144
Standard deviation	17.60	4.33	20.21

Samples from the Charpy V-notch WAAM LMC are prepared for microscopy, as shown in Figure 11. The samples are sawed out of the specimen and embedded in epoxy with copper content. The specimens are sanded beginning with 180 grit up to 2500 grit on rotating plates with water cooling and then with 4000 grit on a Tegramin-30 (Struers GmbH, Willich, Germany), and then polished in two steps. The first polishing step is done by using a 3μ-diamond suspension, the second polishing step is done by an OP-S suspension (0.04μ), where the OP-S content is mixed at a ratio of 1:2 with ethanol, cleansed by ethanol, treated in an ultrasound bath for about one minute, and finally cleaned with isopropanol and dried. While the crack in the homogenous WAAM specimen cuts straight from the notch through the specimen, the dynamic fracture in the WAAM LMC is rather stair-stepped, as shown in area a (Figure 11). The location of area a is provided in the schematic sketch in Figure 11. The crack progression in area a is explained as follows: The crack in area a is blunted at the interface connecting the high-strength with the ductile layer. The crack diverts, runs along the interface causing delamination. Crack diversion and delamination consume fracture energy which essentially drops below the interface toughness. A crack then nucleates and initiates into the ductile layer leaving no residual delamination at the interface, as shown in Figure 11. Area b shows a similar interface between the high-strength and the ductile layer and a small crack along the interface is noticed. Apparently, delamination initiates here before the fracture energy drops below the interface toughness followed by crack nucleation into the ductile material layer.

3.2 Fatigue Test

DIN EN 6072 recommends various specimen geometries. This study uses rectangular-sized flat specimens with a centered bolt hole for increased local stress at the notch. DIN EN 6072 provides the measures for the specimen, as shown in Figure 12.

The study includes nine fatigue specimens, three WAAM specimens out of high-strength steel (X90), three WAAM specimens out of ductile steel (SG2) and three SG2/X90-WAAM LMC. The specimens are tested in tension-tension constant amplitude loading up to failure. The load ratio R is 0.01 and the frequency is 10 Hz. The maximum stress levels are selected in the high-cycle-fatigue range at $0.7\,f_u$, $0.6\,f_u$, and $0.4\,f_u$. The different stress amplitudes create nine points in the S-N-diagram, as shown in Figure 13. The slopes of the S-N-curves of the ductile (SG2) WAAM, the high-strength (X90) WAAM and the SG2/X90-WAAM LMC are determined by using the pearl-string method as recommended in DIN 50100 for a limited number of data points distributed in the HCF range. Figure 13 shows the S-N curves for ductile (SG2), high-strength (X90) WAAM material as well as SG2/X90-WAAM LMC. The S-N curve for the SG2/X90-WAAM LMC approaches the S-N-curve of the high-strength WAAM specimen. The slope of the SG2/X90-WAAM LMC ($m_{\mathrm{WAAM\,LMC}}$ = 3.04) is smaller than the slope of the high-strength (X90) WAAM material ($m_{\mathrm{high-strength\,WAAM}}$ = 2.64) and similar to the ductile (SG2) WAAM material ($m_{\mathrm{ductile\,WAAM}}$ = 3.08). It is pointed out that these results can only be seen as a first tendency since the number of specimens tested is limited. Currently ongoing

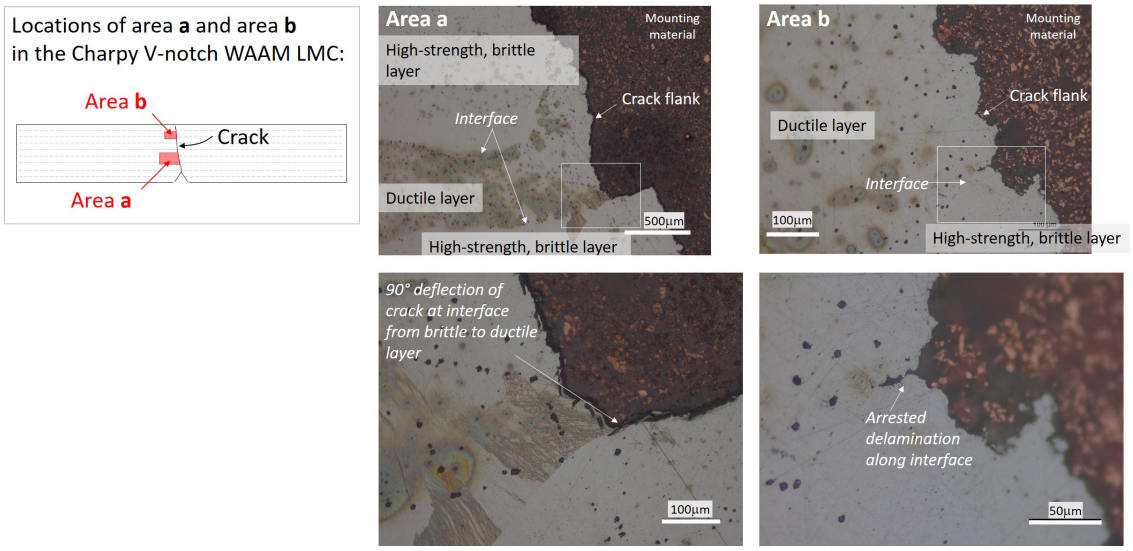

Figure 11: Schematic sketch of area a and area b; area a: crack blunting and diversion, no remaining delamination and crack nucleation at interface between the high-strength and ductile material layers; area b: remaining delamination at interface between high-strength and ductile material layers (Spalek et al., 2021).

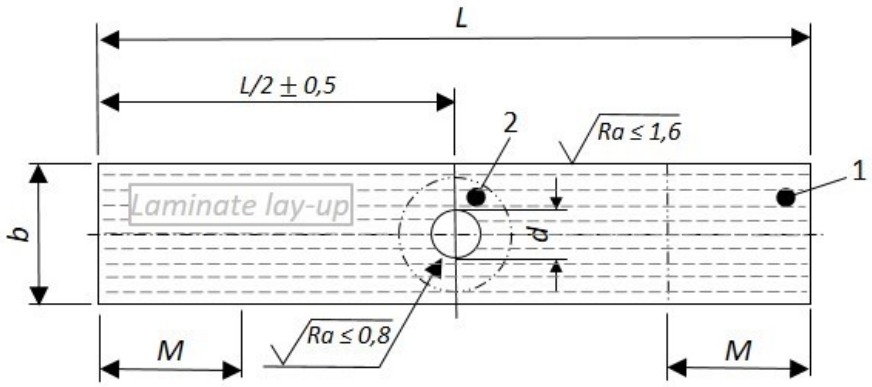

Specimen	L [mm]	b [mm]	d [mm]	M [mm]
Type T	150	30	10	25-35

Figure 12: Fatigue WAAM LMC specimen according to DIN EN 6072 adapted from DIN 50100:2016-12 (Spalek et al., 2021).

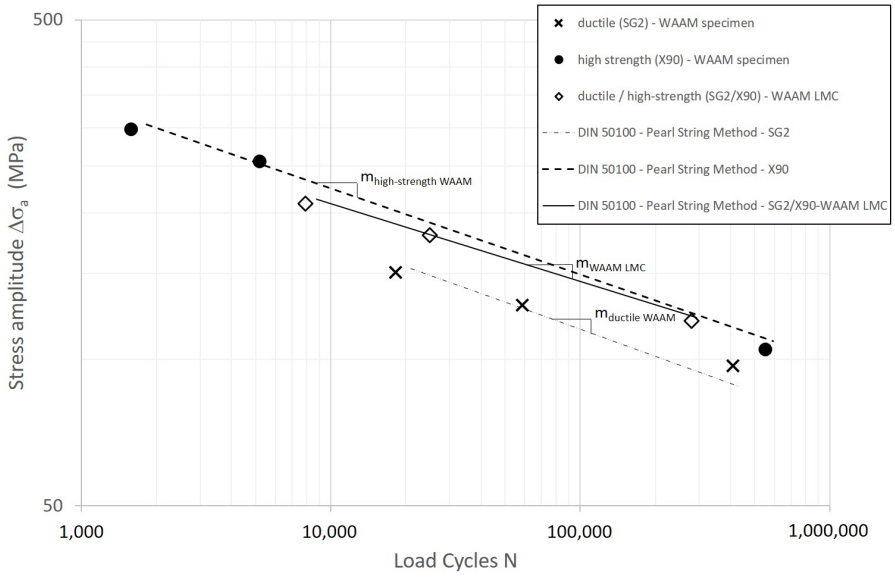

Figure 13: S-N-curves for ductile (SG2) WAAM, high-strength (X90) WAAM and SG2/X90-WAAM LMC; trend lines assessed by pearl-string method (DIN 50100:2016-12)) (Spalek et al., 2021).

further studies will increase the number of data points and enable a statistically stable result. From the fatigue study is concluded that the WAAM LMC seems to have a smaller slope than the S-N-curve of the high-strength steel. No conclusion can be drawn in respect to the level of the endurance limit. The fatigue behavior of WAAM-fabricated LMCs does not follow the rule of mixture, as already found by the Charpy V-notch test.

The location for microscopic investigation is selected left of the bolt hole, as annotated in Figure 14a by a black-framed window. It should be mentioned that the notch (bolt hole) tip in all three WAAM LMCs is located in the high-strength steel (X90) material. Figure 14b shows microscopy scans of the fractured SG2/X90-WAAM LMC after fatigue loading. The scans are assembled by stitching.

In Figure 14b, the layers of ductile (SG2) WAAM steel are colored. No delamination is recognized along the fracture path, not even at the interfaces from high-strength to ductile WAAM steel layers, as it was found in the Charpy V-notch WAAM LMC specimen. The fatigue specimen is loaded parallel to the WAAM layers, hence not in the crack arrestor orientation as in the Charpy-V-notch test. The crack progresses beginning from the notch tip (see arrow) perpendicular to the loading direction and shows elastic fracture behavior. Within a ductile (SG2) layer, the crack path shows a kink (annotated in Figure 14) and progresses not perpendicular to the loading direction. From the kink onwards, the crack shows elastic-plastic fracture behavior. This conclusion is confirmed in fracture surface scans, as shown in Figure 15. The fracture surface up to the kink is generated by elastic crack propagation. The fracture surface from the kink onwards is characterized by ductile tearing, an established 45°-tilted surface which proves shear stress activation and essentially necking of the surface, as annotated in Figure 15. Fatigue loading markings (striations) are visible along the fracture surface, as shown in Figure 14c. The

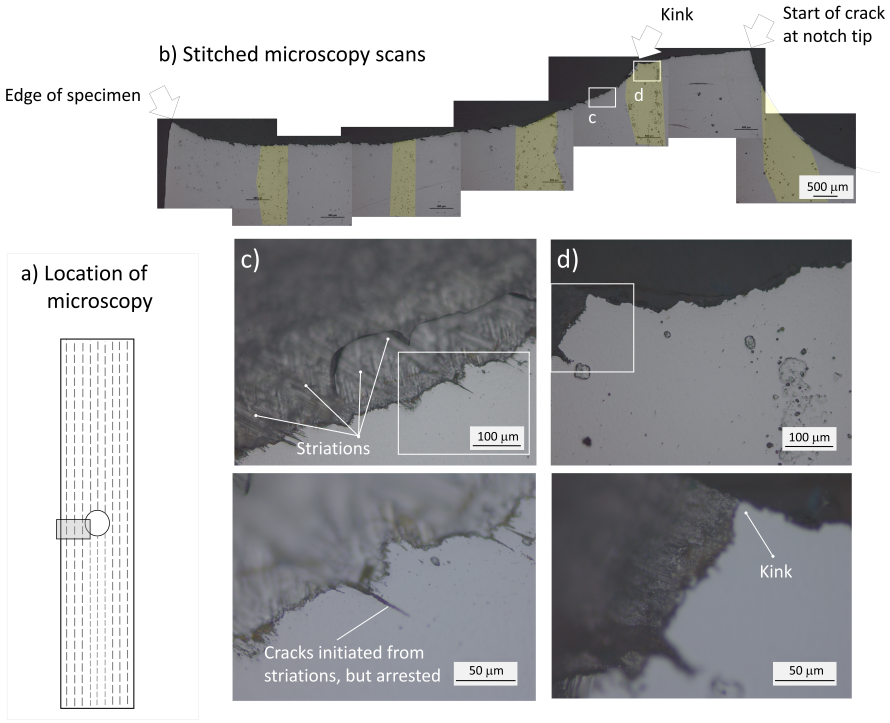

Figure 14: Fatigue fracture of WAAM LMC specimen; (a) location of microscopy; (b) microscopy scans of crack path; (c) striations on fracture surface; (d) kink (Spalek et al., 2021).

striations cause about 50 μm-sized cracks in the section, however these microcracks do not grow further into larger cracks. Apparently, the interface toughness provides a high resistance and delamination does not occur.

4 Conclusions

The processing and the performance of laminated metal composites (LMCs) consisting of multiple bilayers of alternating layers of ductile and high-strength steel and processed by wire arc additive manufacturing (WAAM) using a computer code-guided welding robot have been investigated. The LMC layup is built up by alternating deposits made of ductile steel (SG2) and high-strength steel (X90) type wires. Governing parameters during processing the LMCs are discussed and parameter settings of this study are provided. The pause time is investigated in dependence of weld bead thickness and number of weld layers. The weld layers within the LMC cross section are sharp but wavy. The mechanical properties of the LMC are strongly influenced by the dilution between the unalloyed SG2 and X90 weld beads causing the hardness of both SG2 and X90 steel to fall in the same range of hardness. The performance and failure modes of the LMCs are tested under static, impact and high-cycle fatigue loading. Under static tensile loading, yield strength and strain follow the rule of mixture. Accompanying hardness tests are conducted to also assess yield strength and tensile strength from hardness measurements. Under impact loading, where the loading is in the crack arrestor orientation, the WAAM LMC layup

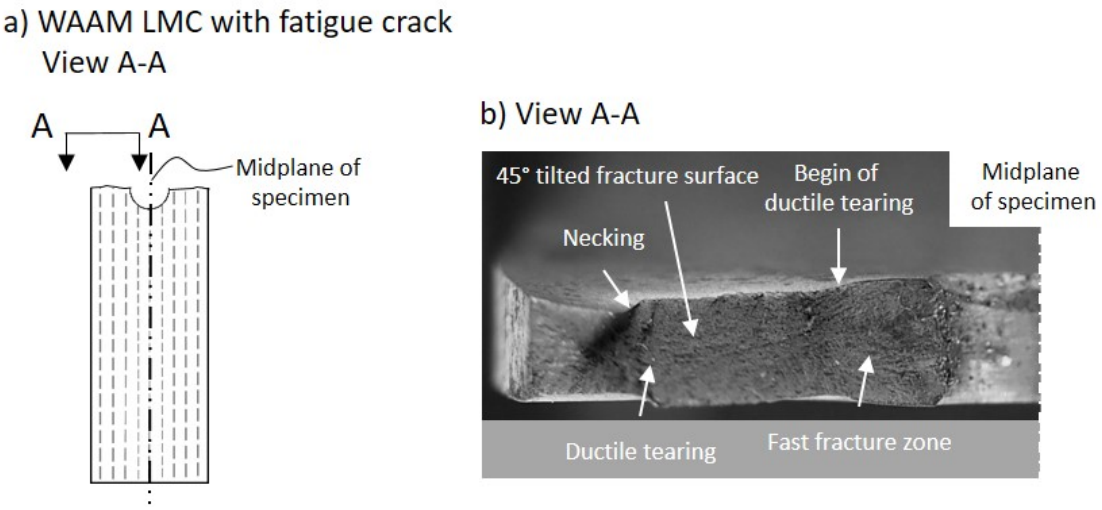

Figure 15: 15. Fracture surface of fatigue-tested WAAM LMC. (a) WAAM LMC with fatigue crack View A-A; (b) View A-A (Spalek et al., 2021).

resists the crack propagation, particularly at the interfaces between high-strength and mild steel layers. Crack blunting, crack deviation and delamination are recognized. Hence, the dynamic fracture cutting through the LMC is rather stair-stepped. The WAAM laminate shows almost the same fracture energy as the homogenous ductile steel WAAM specimen. Under high-cycle fatigue loading, the WAAM LMC seems to perform better than the homogenous steel WAAM specimen. Because of the limited number of specimens in this study, this promising result is seen as a first tendency and needs to be confirmed. Microscopy of the laminate section reveals no delamination. The interplay of deformation in the ductile material layers and high-strength layers is seen as part of the fatigue fracture resisting mechanism. Further research is required to clarify this. The results of the Charpy V-notch tests and the fatigue tests of the WAAM LMCs significantly deviate from the rule of mixture and are strongly affected by dilution, as demonstrated with EDX line plots across the LMC layup. Using WAAM to produce tailored structural components and connection detailing consisting of LMCs to replace critical structural components and connections in fatigue loaded-structures, such as bridges, is seen as a promising way to extend the life time of built metal infrastructure within the framework of modular bridge design.

References

[1] Feucht, T., Waldschmitt, B., Lange, J., Erven, M. (2021) 3D-Printing with Steel: Additive Manufacturing of a Bridge in situ, ce/papers, Volume 4, Issue 2-4, p. 1695-1701, https://doi.org/10.1002/cepa.1475.

[2] Kühne, R., Feldmann, M., Citarelli, S., Reisgen, R., Sharma, R., Oster, L. (2019) 3D printing in steel construction with the automated Wire Arc Additive Manufacturing, NORDIC STEEL 2019 The 14th Nordic Steel Construction Conference, September 18–20, 2019, Copenhagen, Denmark, ce/papers, Volume 3, Issue 3-4, p. 577-583, https://doi.org/10.1002/cepa.1103.

[3] Müller, J., Grabowski, M., Müller, C., Hensel, J., Unglaub, J., Thiele, K., Kloft, H., Dilger, K. (2019) Design and Parameter Identification of Wire and Arc Additively Manufactured (WAAM) Steel Bars for Use in Construction, Metals 2019, 9, 725; doi:10.3390/met9070725.

[4] Treutler, K., Kamper, S., Leicher, M., Blick, T., Wesling, V. (2019) Multi-Material Design in Welding Arc Additive Manufacturing, Metals 2019, 9, 809; doi:10.3390/met9070809.

[5] Treutler, K., Wesling, V. (2021): The Current State of Research of Wire Arc Additive Manufacturing (WAAM): A Review. Appl. Sci. 2021, 11, 8619. https://doi.org/10.3390/app11188619.

[6] Reisgen, U., Sharma, R., Oster, L. (2019) Plasma Multiwire Technology with Alternating Wire Feed for Tailor-Made Material Properties in Wire and Arc Additive Manu-facturing, Metals 2019, 9, 745; doi:10.3390/met9070745.

[7] Spalek, N., Brunow, J., Braun, M., Rutner, M. (2021) WAAM-Fabricated Laminated Metal Composites. Metals 2021, 11, 1948. https://doi.org/10.3390/met1112194.

[8] Carreno, F., Chao, J., Pozuelo, M., Ruano, O. (2003) Microstructure and fracture properties of an ultrahigh carbon steel–mild steel laminated composite. Scr. Mater. 2003, 48, 1135–1140. https://doi.org/10.1016/s1359-6462(02)00602-4.

[9] LeSuer, D.R., Syn, C.K., Sherby, O.D., Wadsworth, J., Lewandowski, J.J., Hunt, W.H. (1996) Mechanical behaviour of laminated metal composites. Int. Mater. Rev. 1996, 41, 169–197. https://doi.org/10.1179/imr.1996.41.5.169.

[10] Leedy, K., Stubbins, J. (2001) Copper alloy–stainless steel bonded laminates for fusion reactor applications: Crack growth and fatigue. Mater. Sci. Eng. A 2001, 297, 19–25. https://doi.org/10.1016/s0921-5093(00)01274-0.

[11] Koseki, T., Inoue, J., Nambu, S. (2014) Development of Multilayer Steels for Improved Combinations of High Strength and High Ductility. Mater. Trans. 2014, 55, 227–237. https://doi.org/10.2320/matertrans.m2013382.

[12] Ojima, M., Inoue, J., Nambu, S., Xu, P., Akita, K., Suzuki, H., Koseki, T. (2012) Stress partitioning behavior of multilayered steels during tensile deformation measured by in situ neutron diffraction. Scr. Mater. 2012, 66, 139–142. https://doi.org/10.1016/j.scriptamat.2011.10.018.

[13] Nambu, S., Michiuchi, M., Inoue, J., Koseki, T. (2009) Effect of interfacial bonding strength on tensile ductility of multilayered steel composites. Compos. Sci. Technol. 2009, 69, 1936–1941. https://doi.org/10.1016/j.compscitech.2009.04.013.

[14] Kümmel, F., Hausöl, T., Höppel, H.W., Göken, M. (2016) Enhanced fatigue lives in AA1050A/AA5005 laminated metal composites produced by accumulative roll bonding. Acta Mater. 2016, 120, 150–158. https://doi.org/10.1016/j.actamat.2016.08.039.

[15] DIN 50125. (2016) Testing of Metallic Materials—Tensile Test Pieces. 2016, 17, Beuth Verlag GmbH, Berlin.

[16] DIN EN ISO 148-1. (2017) Metallic materials-Charpy pendulum impact test-Part 1: Test method. 2017, 40, Beuth Verlag GmbH, Berlin.

[17] Kibria, G., Jahan, M.P., Bhattacharyya, B. (2019) Micro-Electrical Discharge Machining Processes; Springer: Singapore, 2019.

[18] Hosford, W.F. (2010) Mechanical Behavior of Materials; Cambridge University Press (CUP), Cambridge, England, 2010.

[19] DIN EN 6072 (2011) Aerospace series-Metallic materials-Test methods-Constant amplitude fatigue testing. Ger. Inst. Stand. Berl. Ger. 2011, 1, 68.

[20] DIN 50100 (2016) Load controlled fatigue testing–Execution and evaluation of cyclic tests at constant load amplitudes on metallic specimens and components. 2016, 111, Beuth Verlag GmbH, Berlin.

Authors

Univ.-Prof. Dr.-Ing. habil. Marcus Rutner
Technische Universität Hamburg
Institut für Metall- und Verbundbau
Denickestraße 17
21073 Hamburg
Tel.: +49 (0) 40 - 42878 / 3022
e-mail: marcus.rutner@tuhh.de
Web: www.tuhh.de/mvb

Jakob Brunow, M.Sc.
Technische Universität Hamburg
Institut für Metall- und Verbundbau
Denickestraße 17
21073 Hamburg
Tel.: +49 (0) 40 - 42878 / 4327
e-mail: jakob.brunow@tuhh.de
Web: www.tuhh.de/mvb

Niclas Spalek, M.Sc.
Technische Universität Hamburg
Institut für Metall- und Verbundbau
Denickestraße 17
21073 Hamburg
Tel.: +49 (0) 40 - 42878 / 2275
e-mail: niclas.spalek@tuhh.de
Web: www.tuhh.de/mvb

Climate change, sustainability, ship size development - Challenges for the Port of Hamburg

Christian Heitmann, Hamburg Port Authority AöR

Abstract: Change is a tradition at the Port of Hamburg and orientation towards the future is a necessity. In face of enormous technological and social transformations, new answers must be found and megatrends such as urbanisation, climate change and digitalisation must be actively shaped. Solutions must be found to ensure the accessibility and availability of the Port of Hamburg, to keep the infrastructure resilient and functional and to plan in advance.

1 Sustainability and Climate change

The Hamburg Port Authority (HPA) has set the goal of developing the port sustainably and using the success factors resulting from its geographical location to secure its future.

The megatrends of urbanisation, climate change and digitalisation are influencing the configuration of infrastructures and the intensity of land use. Climate-related resource scarcity and the decision to phase out coal are prompting tenants and port players to make their business models and business areas more flexible and adaptable.

Whether the Port of Hamburg remains fit for the future will not depend solely on changing trade flows, new technologies or the effects of climate change. This development is largely determined by the decisions of companies, authorities and people in the region. The focus is on further developing the port economically, socially and ecologically, and on driving trendsetting innovations in the process. Sustainability can thus become a rewarding competitive advantage for the Port of Hamburg.

An efficient infrastructure and traffic management in the heart of Hamburg is of central importance. The vision is, that the port of Hamburg must be accessible all the time. To make infrastructure resilient and sustainable, three dimensions of sustainability are equally important. The infrastructure must be able to adapt changing climate and environmental conditions, and it must ensure reliable availability and safe accessibility to the port based on forward-looking port planning.

With climate change imminent and already foreseeable, the challenges facing the port will be exacerbated in the future. It is expected that climate change will influence the frequency, intensity,

geographical extent, duration and timing of extreme weather and climate events. Many of the most important climate-related changes for ports are caused by global warming.

For example, rising sea levels as a result of glacier melt could lead to changing design water levels in the harbour. Higher sea surface temperatures and increased evaporation result in more intense storms, higher wind speeds, higher tides and more precipitation. Extreme precipitation, wind, waves, heat, humidity and cold threaten lives, economies and the environment. They can cause damage to shipping infrastructure such as breakwaters, quay walls or drainage systems and disrupt daily port operations (PIANC, 2020).

Trouble-free traffic handling is extremely important for the Port of Hamburg as a hub for shipping, rail and truck traffic. Efficient use of existing infrastructure results in a reduction of traffic-related emissions and a reduction in additional infrastructure required for growing traffic volumes.

Parallel to efficiency, high operational quality is also important for the attractiveness and competitiveness of the individual modes of transport. This is expressed above all in punctuality, predictability and reliability. The overall objective of the HPA is the constant improvement of traffic flow management. In the area of cross-traffic management, it is planned to network port traffic even more efficiently. The aim is to link traffic management with movable infrastructures such as locks and bridges as well as data on water levels and wind events (HPA, 2019).

2 Ship size development

The challenges for an efficiently and sustainably operated port are based on a resilient infrastructure. With view to the formulated climate and sustainability goals, the port planner faces enormous challenges. The focus of action is on the one hand on the preservation, maintenance and functionality of the infrastructure and on the other hand on the efficiency and flexibility of the transport infrastructure. This applies to each of the relevant forms of transport: water, rail and road. The major challenge lies in the steadily increasing size of ships and the obvious gaps in the existing standards and recommendations. As early as 1985, Wirsbitzki (1985) pointed out the lack of recommendations by the classification societies, the unclear responsibilities for the dimensioning of mooring equipment and the lack of consensus between shipbuilders and port planners. There is still no concrete cooperation to adapt container ships and the port to the changed conditions. The growth in ship sizes has been rising uninterruptedly for 16 years. In 2006, the largest container ship in the world was the Emma Maersk (E-class) with a capacity of 14,700 TEU (standard containers) and a length of 399 metres. What was considered inconceivably large at the time, calls the Port of Hamburg daily. While the dimensions have mainly developed upwards in recent years with a maximum length of 399 m, the first Ultra Large Container Vessels (ULCVs) with a width of 61.5 m have been put into service since 2020. The terminal operators are already planning with vessels up to 425 m long and 66 m wide, the so-called "Gigamax-26", which is shown in Figure 1.

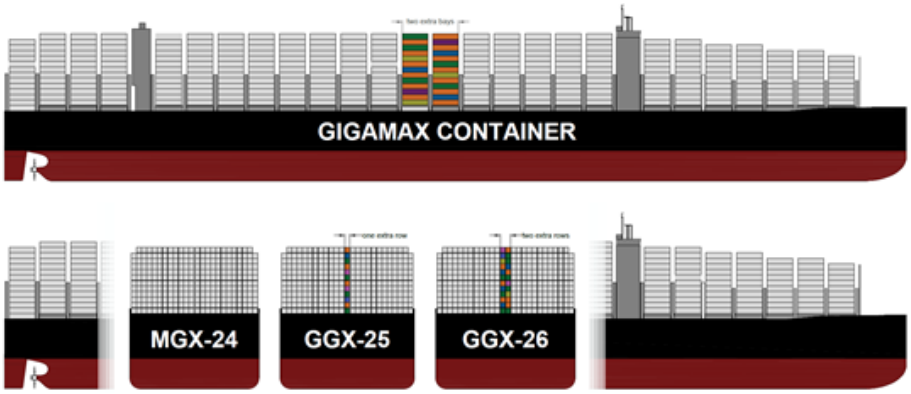

Figure 1: Gigamax-26 Container Vessel (Graphic by Christian Heitmann, HPA)

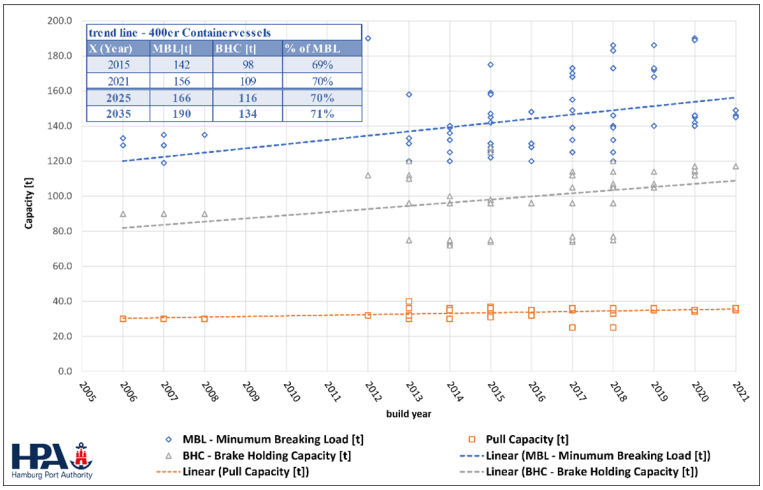

Figure 2: Data collection of MBL and BHC by ULCV in the Port of Hamburg (Graphic by Christian Heitmann, HPA)

Container ships have not only constantly evolved in terms of their main dimensions, but also in the field of mooring equipment on ship's side. In course of the constant data collection in the Port of Hamburg, it could be determined that the capacity of the mooring systems of large ships increases steadily with increasing size and year of construction. While the BHC (brake holding capacity of the winch systems) for 400 m vessels was still around 100 t in 2015, the development of BHC is already approaching the 120 t limit per line in 2025 (see Figure 2).

In consideration due to the development of ship sizes and the current construction recommendations of the International Association of Classification Societies (IACS, 1982), concrete requirements arise for the Port of Hamburg and in particular to the existing infrastructure for Ultra Large Container Vessels. The main issue here is what measures can be taken to prevent damage such as ships breaking loose but also an excessive overloading of the quay wall. The HPA is currently working on various projects to further improve safety and to meet the requirements of climate change and sustainability. Important parts of the safety assessment are fully dynamic mooring analyses and the recalculation guideline for quay walls. The latter is considered an important instrument for assessing the current need for action as well as for reliable statements on

previously uncalculated costs for maintenance, rehabilitation and/or new buildings of quay walls in the Port of Hamburg. Until 2017, the static mooring analysis according to the EAU 2012 (EAU, 2012) was the state of the art. The EAU 2012 describes a very conservative load determination procedure. As a result of new findings and further developments of calculation methods, the fully dynamic analysis has established and provides more accurate estimates regarding the loads caused by ULCVs in the planning, design and recalculation of quay walls. In the near future one topic will be the monitoring of quay walls. Monitoring means the supervision of existing quay constructions by installed measuring sensors. The sensors record the current movement and material conditions. With the obtained data, an assessment of the safety and stability of the structures can be made by using digital computer models (digital twin) of the structures. Looking to the future, the Port of Hamburg is to be managed in a sustainable and resilient manner. The port should generate added value without worsening the CO_2 balance. The sustainable use of resources, the use of alternative, renewable energies and the responsible treatment of the environment and nature will be defining factors for the future. At the same time, we can confidently demonstrate where the HPA has already added value to society and will make its contribution to achieving the United Nations Sustainable Development Goals (SDGs) (WPSP, 2020). The ultimate goal is and remains to ensure accessibility, availability, safety and lightness in the Port of Hamburg.

References

[1] PIANC (2020); PIANC EnviCom WG Report n° 178-2020 “Climate Change Adaptation Planning for Ports and Inland Waterways”; The World Association for Water-borne Transport Infrastructure, Belgique

[2] HPA (2019); Nachhaltigkeitsbericht des Hamburger Hafens 2017/2018, Hamburg Port Authority AöR; Hamburg

[3] Wirsbitzki, (1985); Die Trossenausrüstung und das Vertäuen von Seeschiffen; HANSA-Schiffahrt-Schiffbau-Hafen-122. Jahrgang, Heft 10

[4] IACS No. 10 (1982); Chain Anchoring, Mooring and Towing Equipment - Rev. 4 Sep 2020; International Association of Classification Societies, London

[5] EAU (2012); Empfehlungen des Arbeitsausschusses „Ufereinfassungen“ Häfen und Wasserstrassen EAU 2012; HTG Hafenbautechnische Gesellschaft e. V.

[6] WPSP (2020); World Ports sustainability report 2020; World Ports Sustainability Pro-gram

Authors

Christian Heitmann (Naval Architect)
Hamburg Port Authority AöR
Technical Division
Neuer Wandrahmen 4
20457 Hamburg
Tel.: +49 (0) 40 - 42847 / 5713
e-mail: christian.heitmann@hpa.hamburg.de
Web: www.hamburg-port-authority.de

Smart quay walls & trends in quay-wall engineering

Alfred Roubos

Abstract: Numerous marine structures such as quay walls, jetties and flexible dolphins have been constructed all over the world to accommodate ships' berthing, mooring and loading operations. The reliability of these structures has played an essential role in the global transhipment of goods and is the cornerstone of a well-functioning port. New quay walls are equipped with modern sensors, such as fibre-optic strain sensors installed on soil-retaining walls or anchor systems, and can therefore become potentially more intelligent and reliable. Global digitisation has already created smart port infrastructure using 'internet of things' technologies. However, the biggest challenge is neither to collect data nor to facilitate connections, but to translate the available data into useful information and to identify which data is lacking in order to resolve uncertainty. This extended abstract briefly describes the sensor stagey of the port of Rotterdam and presents the state of the art of the 'smart' port infrastructure.

1 Introduction

In port engineering, many uncertainties must be taken into consideration in order to ensure the effective, safe and efficient handling of ships during their service life. Port authorities and terminals have to guarantee quay-wall functionality in accordance with service-level agreements with their clients. Quay walls are generally designed in such a way that they are likely to survive for at least 50 years (Roubos, 2019), whereas the duration of these service-level agreements is normally 25 years. As a result, adjustments may be necessary to improve functionality – for instance, by increasing water depths or enhancing terminal loads, since ships are evolving constantly.

New port infrastructure will still be developed, although the focus is shifting towards the maintenance, repair, rehabilitation and adaptation of existing structures in fully up-and-running terminals (Roubos, 2019). In the coming years, thousands of quay walls will have to be reassessed as part of lifetime extension programmes throughout the world. Numerous existing marine structures, including half of the 85 kilometres of quay walls in the port of Rotterdam (Fig. 1), which represent a value of approximately 2 billion euros, will approach the end of their design lifetime in the next few decades. However, the end of their design lifetime does not automatically align with the end of their service life, because most of the quay walls are still in good condition.

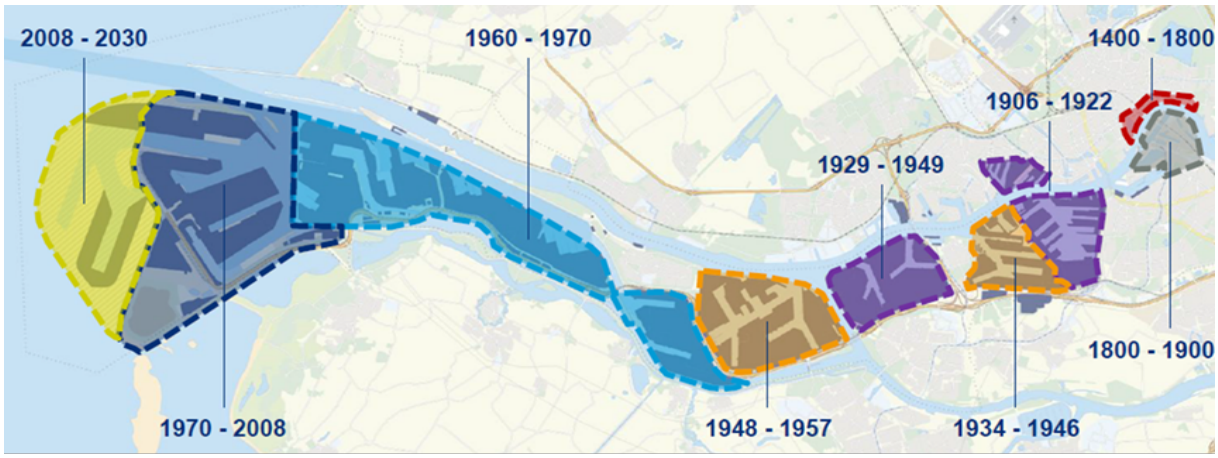

Figure 1: Development of the port of Rotterdam

Nonetheless, these structures may have undergone alteration, deterioration, misuse and other changes during their service life. Consequently, port authorities and terminals frequently perform inspections and have to maintain their assets to guarantee safety. The Port of Rotterdam Authority has already addressed an urgent need to focus on asset management. They equip their new quay walls with modern sensors and has developed a quay-wall monitoring system for their existing assets. This system objectively supports the decision-making process, focusing on budgeting and prioritising the maintenance of quay walls. Over the years, the Port of Rotterdam Authority has collected a great deal of data, which has been used predominantly for asset-management purposes.

2 Sensor Strategy smart quay walls

This section briefly discusses the sensor strategy of the port of Rotterdam. In 2008, the port of Rotterdam realized the 1st smart quay wall (Fig. 2). This quay wall was mainly equipped with fibre optic strain and pressure sensors, which were mainly installed for asset management purposes, e.g. alarm and intervention values in order to prevent functional misuse. Currently, 10 smart quay walls have been built and a new sensor strategy has been developed. The motivation for investing in smart quay walls is sixfold: i) to improve functionality of the quay wall; ii) to guarantee safety; iii) to predict extreme loads; iv) to predict degradation and extent the service life of existing quay wall; v) to reduce construction and maintenance costs, and to optimise the carbon footprint; vi) to enhance our level of knowledge and improve the design codes and standards that are presently in use.

Since new quay walls are increasingly equipped with sensors, a great deal of data has become available. This data now facilitates predictive modelling and reverse engineering, but also fosters reliability and safety. Fig. 2 shows how port authorities or terminals can make use of sensor data and reliability-based assessments by distinguishing and connecting commercial, asset-management and data-management cycles

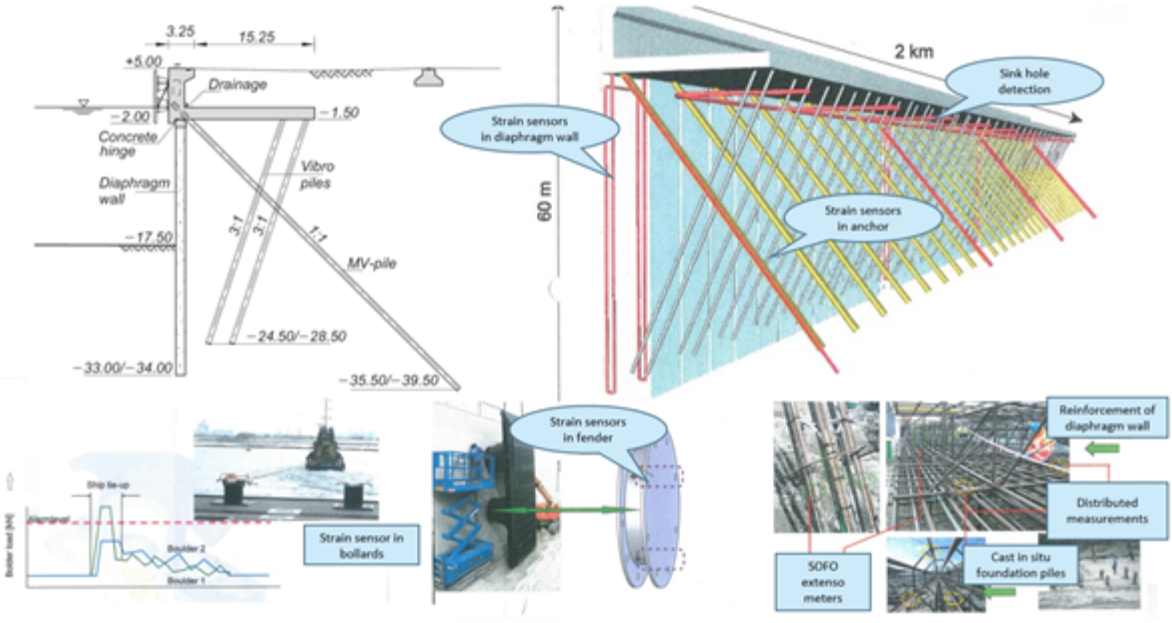

Figure 2: Impression of the 1st smart quay wall realised in 2008

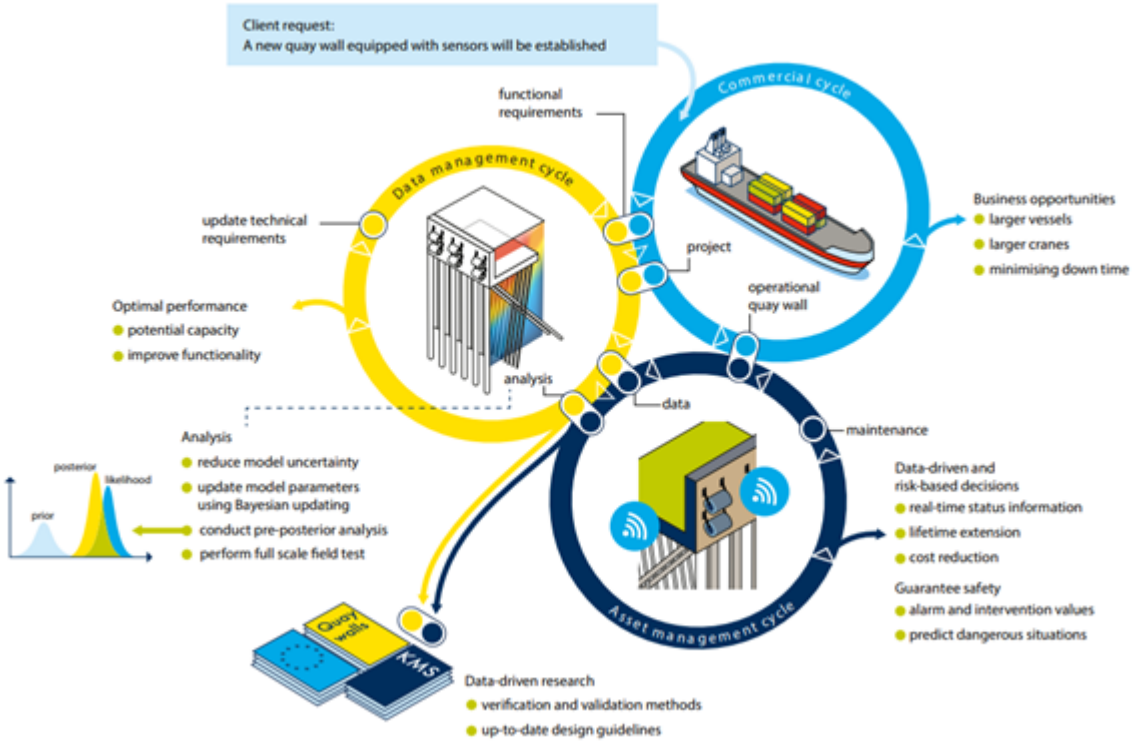

Figure 3: Optimising functionality, maintenance and guidelines using quay-wall data

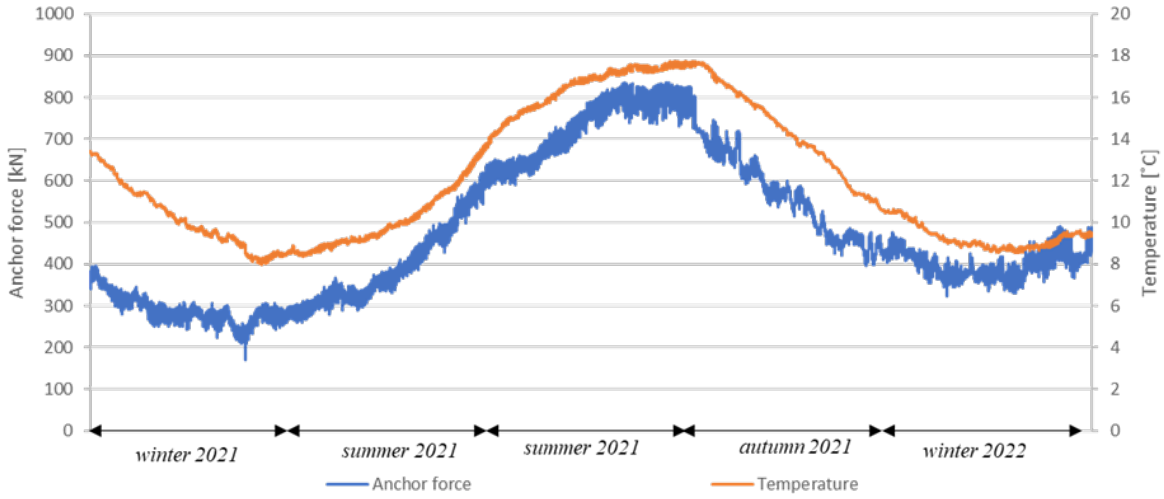

Figure 4: Relation between temperature and anchor force MV pile of a quay wall in the Mississippi-haven port basin

In the asset-management cycle, sensor data allows us to lay foundations for data-driven and risk-based decisions to optimise the required maintenance. In addition, data-driven information will enable us to continuously improve our understanding of quay walls and can be used in the application of Bayesian updating. In the data-management cycle, data analytics in combination with finite element models can be used to update the functional requirements of a specific quay wall, which boosts the commercial cycle, e.g. by creating new business opportunities. Furthermore, data-driven research is of the utmost importance to maintain design guidelines and to validate new methods.

3 Main findings and conclusion

In general, the sensors data show that the stresses and deformations are slightly lower compared to the original design of the quay walls. The sensor data can be used to reduce model uncertainty and the epistemic uncertainty in strength properties of materials, for instance the soil parameters (angle of internal friction and/or soil stiffness). In addition, the sensor data is used, in conjunction with as-built information and test results, as input for reverse engineering. After a period of about a year the design report of the quay wall is updated including a detailed description for the geotechnical and structural behaviour in a soil-structure log file. In general, the functionality of the quay walls can be increased. The results of reverse engineering show that it is possible to deepen most of the quay walls with about 1 to 2 meters and/or to increase the terminal loads by about 25 % or install a larger crane.

The sensor data provides us also with new insights into the quay-wall behaviour, which seems to differ per season. Differences in anchor forces and bending moments of about 10 to 15 % have been measured between summer and winter, e.g. higher forces summer time. However, the

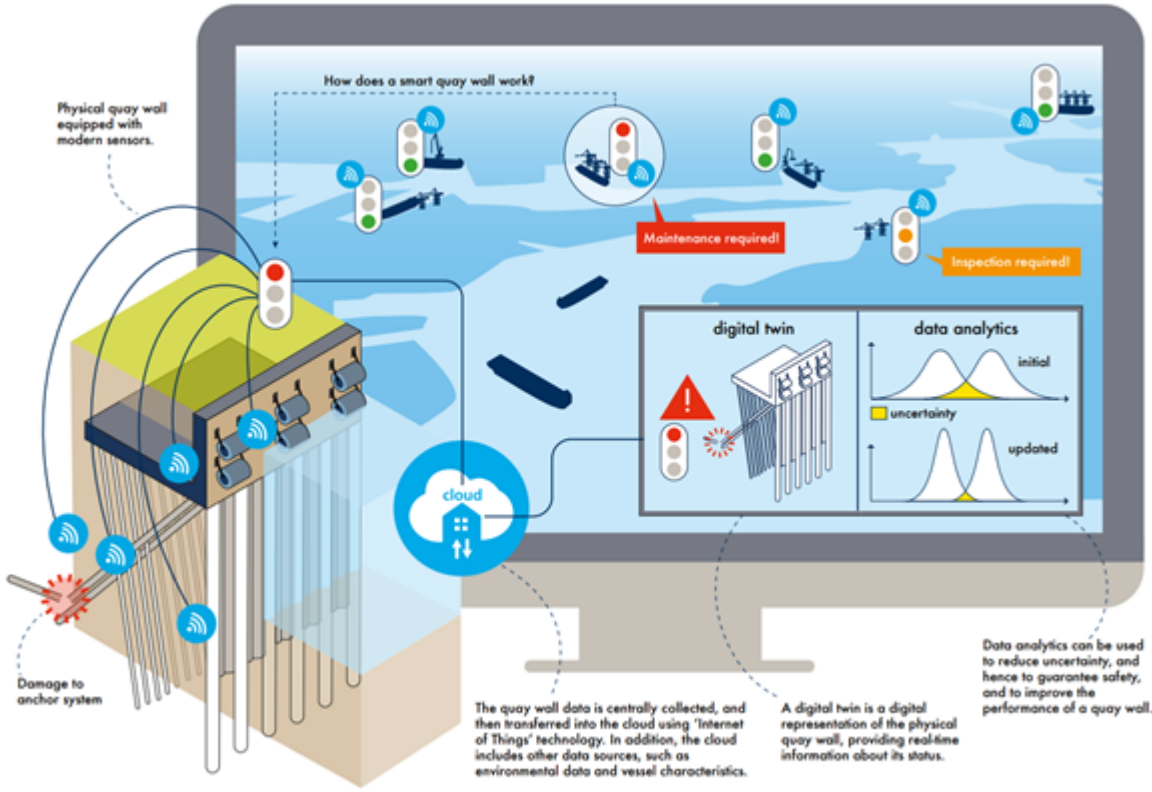

Figure 5: Risk-based and data-driven decisions using real-time quay-wall data

effects of temperature are not taken into account in the design methods that are presently in use. Smart quay walls can help us to derive insight into the effects of climate change on quay-wall behavior.

The asset management department of the port of Rotterdam expects that the inspector of the future will be sensor. Ideally they have digital twin of the real quay wall (Fig. 5), which provides the asset owner information about the performance of the quay wall and whether maintenance is required.

References

[1] Roubos, A.A., (2019): Enhancing Reliability-based assessment of quay walls. Delft, The Netherlands: Delft University of Technology.

Authors

Dr. Alfred Roubos, MSc
Port of Rotterdam Authority & Delft
University of Technology
Port Devellopment, Port Engineering
Wilhelminakade 909
3072 AP, Rotterdam
The Netherlands
e-mail: aa.roubos@portofrotterdam.com
e-mail: a.a.roubos@tudelft.nl

Floating wind turbines – developments and challenges

Kimon Argyriadis

The contribution was not available by the time of printing.

Generation of Tailored Wave Sequences by Data-driven Techniques

Marco Klein, Marc-André Pick, Merten Stender

Abstract: The applicability of data-driven machine learning techniques for the generation of tailored wave sequences is addressed in this paper. For this objective, a fully convolutional neural network was applied to find a functional relation between a certain tailored wave sequence at a specific position in a wave tank and the corresponding wave sequence at the wave board. The synthetic training and validation data were acquired by applying the high-order spectral method featuring wave groups of short duration with varying wave steepness, wave period and enhancement factor. The accuracy of the trained model was evaluated by means of unseen validation data.

1 Problem Definition and Concept

Model tests on waves and their effects on ships and offshore structures are still indispensable, both in the field of research and development and industrial application. Accurate modelling of waves is a crucial prerequisite for model tests in realistic maritime environments. Hereby, the objective is to evaluate the design of a ship or offshore structure in terms of operability and survivability.

In most cases, the standard model of ocean waves (St. Denis and Pierson, 1953) is sufficient for wave generation, e.g., regular waves, transient wave packets and irregular sea states with random phases. The theoretical foundation is the superposition of linear wave components, so that the linear dispersion relation of the independent wave components enable the description of the wave sequence in space and time. Based on this, each wave sequence being defined at a specific location in the wave tank (so-called target location) can be transformed in time and space by means of linear wave theory. Thus, for the determination of the wave maker control signal, the desired wave sequence needs to be transformed with regards to the position of the wave maker, and multiplied with the wave maker response amplitude operator (Biesel and Suquet, 1951; Svendsen, 1985; Schäffer, 1996).

The generation of deterministic sea states, i.e., the reproduction of a predefined tailored wave sequence at a desired target location in the wave tank, requires complex approaches, particularly for steep wave groups which do not obey linear wave theory. In contrast to the standard procedure of generating irregular sea states, where the phase shift of the variance spectrum is supposed to

be random, the phase spectrum of tailored wave sequences is an important deterministic quantity and is responsible for all local wave characteristics at the target location. Consequently, the aim is to determine a control signal for the wave maker by manipulating amplitudes and phases which results in the desired wave sequence at target location. So far, only complex, empirical or time-consuming methods are available hindering a straightforward plug-and-play solution for test facilities (e.g., Chaplin (1996); Trulsen et al. (2000); Schmittner (2005); Clauss et al. (2006); Schmittner et al. (2009); Clauss and Klein (2009); Schmittner and Hennig (2012), among others).

Recently, the topic of machine learning (ML) has also been increasingly applied in the field of classical engineering for a wide variety of problems. A large number of different applications, approaches and methods have been presented. In the field of sea state propagation, there is a focus on wave detection and sea state prediction (Law et al., 2020; Wu et al., 2020; Mohaghegh et al., 2021).

The objective of this study is to explore the potential of ML methods for deterministic wave generation of critical wave sequences. The study was conducted using synthetic data, with emphasis on data generation that mimics the physical problem realistically. Generally, the ML problem is conceptually similar to the physical problem – the target is to find a functional relation between a wave sequence at target location and the required wave board motion. The wave board generates the wave systems that evolve to the target wave sequence. As aforementioned, the simplest functional relation for physics-based wave generation is linear wave theory which fails for steeper wave sequences.

For the intended data-driven wave generation through ML, a fully convolutional network (FCN) was implemented. FCNs are widely used in image processing due to their pattern recognition capability through representation learning (LeCun et al., 2015). For the generation of synthetic data, the accurate and numerically efficient high-order spectral (HOS) method was applied in order to take non-linear wave propagation into account. The JONSWAP spectrum was utilised as basis for the determination of the short wave sequences and the sea state parameter space consisted of varying peak period, enhancement factor and wave steepness.

2 Synthetic Data

The starting point of physics-based wave generation is a wave sequence that is to be reproduced at a specific point in the wave tank. Based on this, the corresponding wave maker motion must be determined. Transferred to the proposed data-driven approach, this means that the complexity of the physical wave propagation between the wave board and the target location has to be taken into account during training data generation through the selection of suitable numerical methods. Hereby, the contrary aspects accuracy and numerical efficiency need to be balanced in order to arrive at sufficient data quality and quantity. The availability of such training data is a crucial and challenging issue as it must meet high qualitative and quantitative standards representing the time-consuming part of the proposed data-driven wave generation.

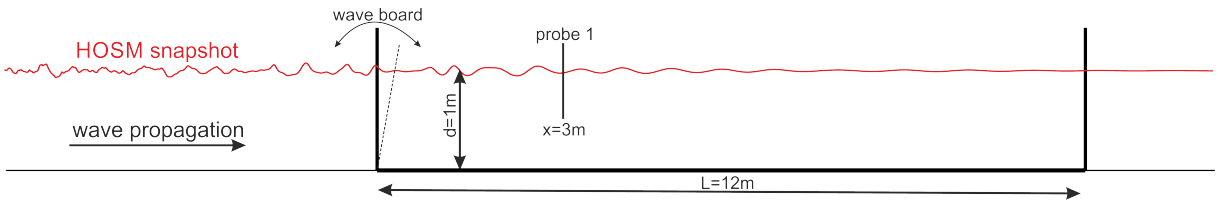

Figure 1: Set-up of the numerical experiment.

For this study, the HOS method (West et al., 1987; Dommermuth and Yue, 1987) was applied as it is a numerically efficient method for the simulation of non-linear wave propagation. The HOS method can take all non-linear interactions, resonant and non-resonant, into account. In addition, wave-current as well as wave-bottom interactions can be considered. The numerical implementation of the pseudo-spectral method followed the procedure presented in West et al. (1987). „The (near) linear computational effort“ as well as „exponential convergence (...) are notable characteristics of the computational efficacy of HOS method“ (Mei et al., 2005) illustrating the motivation why this method was used for this study.

2.1 Set-up of Numerical Experiment

The selected main dimensions and set-up of the numerical wave tank were based on the TUHH physical wave tank at the Institute of Mechanics and Ocean Engineering. The wave tank features a length of $L = 15\,\mathrm{m}$, a width of $B = 1.5\,\mathrm{m}$ and a height of $H = 1.5\,\mathrm{m}$. The water depth is variable, but for the presented investigations it was fixed at $d = 1\,\mathrm{m}$. A flap-type wave maker is installed on one side, with its point of rotation at the bottom of the tank. On the other side, a beach is positioned to reduce wave reflections. The parabolic curved slope of the beach is very efficient in cancelling out the waves, but a complete prevention of wave reflection is not possible. Figure 1 presents a sketch of the set-up of the numerical experiment. The bold black line illustrates the side view of the considered wave tank main dimensions including the flap-type wave maker on the left and the position of the reference wave probe. The sketched wave tank (bold black line) is displayed only for illustrative purpose and not included into the numerical problem. This denotes that the HOS method was applied exclusively for the wave simulation in the space domain (red wavelike line). Thus, the wave tank is displayed to give a better understanding of the overall problem. For this study, one wave probe position was selected at which time series of the sea states simulated in the space domain (red wavelike line) were determined. The position of the wave probe was chosen with a focus on later model tests in order to avoid influences caused by reflections. In addition, the wave sequence at the location of the wave maker was also determined as ground truth for the ML to be trained, i.e., the determination of the wave maker motion was excluded in this study due to the availability of an analytical solution.

2.2 Sea State Parameters

For this study, a large number of irregular sea states of short duration were generated based on the finite depth variant (TMA) form (Bouws et al., 1985) of the JONSWAP spectrum (Hasselmann et al., 1973). Hereby, the sea state parameters peak period T_p, wave steepness $\epsilon = {k_p}^{H_s}/_2$ and enhancement factor γ were systematically varied in order to cover a wide variety of sea state characteristics for the model training process. H_s represents the significant wave height, $k_p = {}^{2\pi}/_{L_p}$ the peak wave number, and wavelength and wave period are linked via the linear dispersion relation $\omega = \sqrt{gk \tanh kd}$ with $\omega = {}^{2\pi}/_{T}$. Note that this relationship between k and ω is only assumed for the definition of the initial surface elevation snapshot, the wave field evolution is performed according to the HOS equations at the considered order of non-linearity without further assumption.

Altogether, 126 sea state parameter combination were used as input for the wave generation with

- $\omega_p = \{3, 4, 5, 6, 7, 8, 9\}$,
- $\epsilon = \{0.1, 0.075, 0.05, 0.0375, 0.025, 0.0125\}$ and
- $\gamma = \{1, 3, 6\}$.

Each sea state parameter combination was used to generate 500 independent wave sequences starting with random phase initialisation resulting in a data set of $63\,000$ individual synthetic wave sequences. After the data set was generated, the simulations were checked for plausibility and in the end $62\,981$ individual wave sequences were identified as error-free, then forming the basis for the ML training.

In the following, a short description of the general procedure of the wave generation process is given. Referring to Figure 1, the initial snapshot of each individual sea state was tailored in such a way that spatial waves were exclusively defined on the left hand side, i.e., outside the black bold line (wave tank). On the right hand side, i.e., in the assumed wave tank, the surface was defined as zero to simulate calm water at the beginning. In addition, the snapshot on the left hand side was prepared with a start and end ramp to ensure a smooth transition between the wave sequence and the calm water part. The length of the wave snapshot on the left hand side was chosen based on the linear dispersion relation under the consideration that wave reflection should be avoided. This self-imposed limitation was not necessitated by the HOS method (periodic boundary conditions) but by the objective that the training scenario should be transferable to the assumed physical wave tank. However, once the initial conditions were defined, the HOS method was applied to evolve the initial snapshot in in the time domain. Based on this simulation, the time series at the position of the wave maker and the reference wave probe (see Figure 1) were obtained.

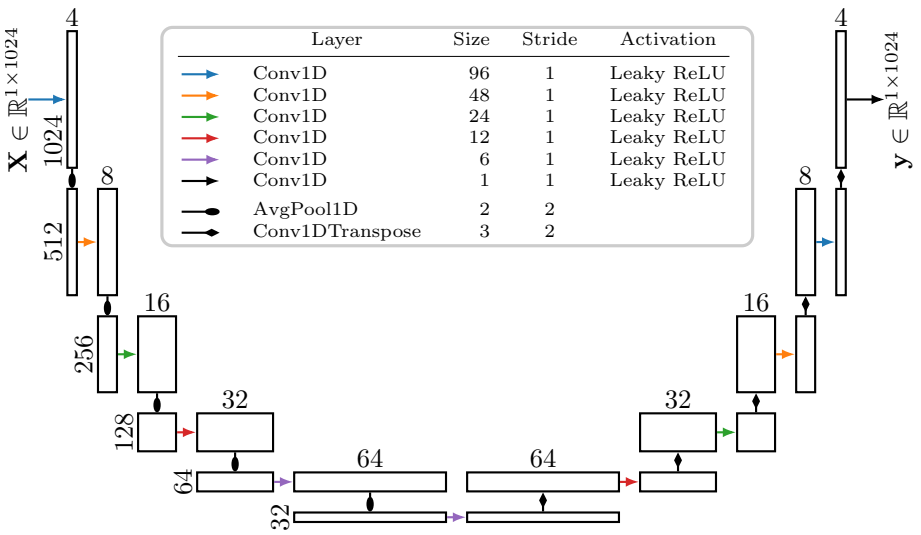

Figure 2: Schematic of the fully convolutional neural network architecture.

3 Machine Learning Model

The following paragraph introduces the machine learning set-up chosen for this work. Given the plethora of neural architectures and different building blocks therein, the choice of a fully convolutional neural network (FCN) is a classical one. Several hyperparameter studies have been performed upfront to find a suitable architecture and parameterization.

3.1 Set-up of ML Model

The FCN is set up as an encoder-decoder structure, see schematic shown in Figure 2. The encoder acts as the sematic pathway, where data representations are learned by successive convolutional blocks. Average pooling reduces the feature maps in order to arrive at higher abstraction levels in the bottleneck layer. The decoder path takes care of restoring details at the original resolution of the physical domain. The kernel sizes are chosen individually for each convolutional block in order to have control over the receptive field that each convolution operation will take into account when processing the input data. Large kernels in the first layers take large spatial neighborhoods into account, while the local receptive field is gradually decreased the higher the data abstraction becomes in the encoder path. In contrast, the number of convolutional kernels is increased along the encoder, thereby allowing the network to learn more descriptive modes and diverse feature maps. Overall, this neural architecture features $110\,825$ trainable parameters. The input data $X = \zeta(x_1, t) \in \mathbb{R}^{1\times1024}$ are set up to contain the desired surface elevation $\zeta(x_1, t)$ of probe 1 sampled at 1024 time instances. The output data $Y = \zeta\left(x_{\mathrm{wm}}, t\right) \in \mathbb{R}^{1\times1024}$ are taken as the wave sequence at the wave maker. Overall, the learning task is defined as an univariate sequence-to-sequence regression. As the experimental set-up comprises one probe, one model $\mathcal{M}_1$ was trained for translating the desired surface elevation at the reference probe to the wave sequence at the wave maker.

3.2 Model Training Process

Table 1: Overview on the training process results.

Model	SSP training loss		$\mathrm{n}_{\mathrm{epochs}}$	
	min ($\mathrm{n}_{\mathrm{epochs}}$)	max ($\mathrm{n}_{\mathrm{epochs}}$)	min	max
$\mathcal{M}_1$	$0.016\,(1965)$	$0.021\,(1380)$	1150	2008

Model training was performed using the `adam` optimiser (learning rate $\alpha = 0.001$) (Kingma and Ba, 2014). `adam` is one of the most commonly used optimizers in the field of machine learning owing to its computational efficiency. It comes with every available open-sourced ML library, mostly set as default optimization technique. The overall 62981 samples available from the numerical simulations were divided on a $0.7/0.3$ training-validation split. The surface similarity parameter (SSP) (Perlin and Bustamante, 2016; Wedler et al., 2022) was employed as loss function. The SSP compares the amplitude as well as the phase difference of two signals or surfaces. The calculated normalized error ranges between 0 (perfect agreement) and 1 (perfect disagreement). Early stopping was utilized at a patience value of 100 epochs on the training loss, allowing for a maximum number of 1500 epochs. Using a batch size of 750 samples, training was performed on a regular desktop workstation (NVIDIA GeForce RTX 2080 Super GPU, 64 GB RAM, i9-10900 CPU) using TensorFlow $2.5.0$. For cross-validating the results and reducing the bias introduced by weight initialization, 10 independent training runs were performed on independent data splits. Throughout all model training, no overfitting was observed.

Table 1 presents details of the training process. The double-column SSP *training loss* displays the minimum and maximum loss value of the 10 independent training runs and the corresponding number of epochs is displayed in parenthesis. The double-column $\mathrm{n}_{\mathrm{epochs}}$ shows the minimum and maximum number of epochs of the 10 independent training runs.

Using our hardware and software configuration, a single training epoch took on average $< 5\,\mathrm{s}$. Model inference for a batch size of 750 samples took $< SI0.13s$, i.e., $< SI0.17ms$ for predicting a single wave sequence at the wave maker. Although inference timing results greatly depend on hardware and software aspects, these numbers indicate the large potential of an universal data-driven wave maker module to be used in test facilities.

4 Results

Following, the trained model was applied on the validation data set, i.e., the unseen data outside the training distribution, for a detailed analysis. For this purpose, each sea state within the validation data set was used as input for the trained model and the prediction was compared to the ground truth via the SSP. Afterwards, the results were sorted by the sea state parameters wave steepness ε and peak wave frequency ω_p resulting in approximately 450 sea states per

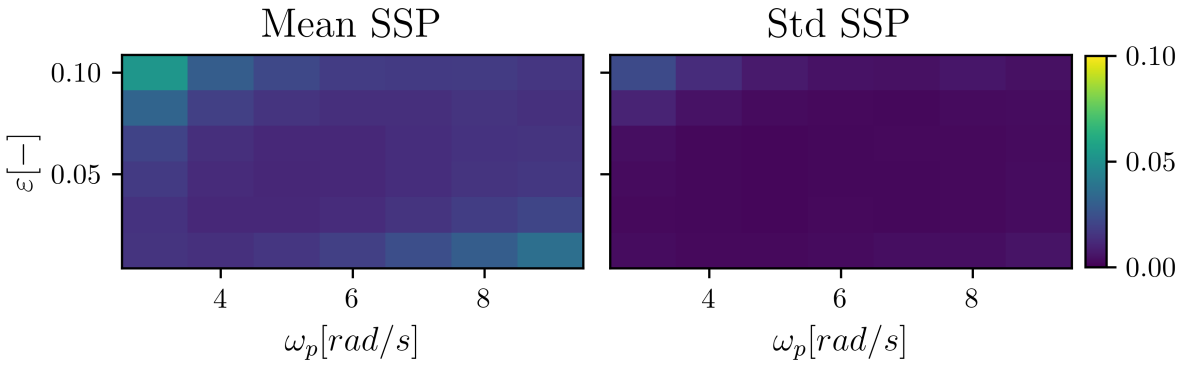

Figure 3: Validation results – the left diagram displays the mean SSP and the right diagram represents the corresponding standard deviation for specific parameter combinations.

combination. In order to evaluate the results, the mean SSP and its standard deviation were determined for each combination.

Figure 3 presents the results of the investigations. The left diagram presents the mean SSP for the trained model. The abscissa represents the peak wave frequency ω_p and the ordinate the wave steepness ε. Each parameter combination is represented by a coloured square. The mean SSP per combination/square is shown according to the colour scale on the right hand side. A $\mathrm{SSP} = 0$ denotes that the predicted signal and the ground truth are identical. The diagram on the right hand side is identically arranged and presents the associated standard deviation (STD) for each combination.

Analysing the left diagram in detail reveals that the accuracy is very good over all combinations. However, the accuracy is not the same across all combinations and becomes less accurate, especially towards the boundaries of the data range. This can be explained by the fact that less data were available at the boundaries of the selected physical data domain, particularly in terms of the existing neighbouring sea state parameter combinations. During the training process the model hence adapted to the over-represented physics in the data set. To accomplish even better generalisation properties, one will need more training data that is covering an even wider range of physical parameters. In this context, only the sea states that are displayed in the upper left and lower right of Figure 3 show significant differences compared to the rest of the parameter combinations. The upper left sea state represents the sea state with the longest peak wavelength and the highest wave steepness. Interestingly, the sea state at the bottom right is exactly the opposite – it is the sea state with the shortest peak wavelength and the smallest wave steepness. One may speculate if these errors on the boundaries of the physical parameter domain not only stems from the bias-variance trade-off engaged in any machine learning approach but also from the configuration of filters and kernel sizes. Both, filter and kernel size configuration, may have some disadvantages for specific pattern so that very fine details may not propagate into all feature maps and therefore can be missed in the prediction.

The diagram on the right shows a very similar pattern. The standard deviation is very small over the entire parameter range, but somewhat larger at the boundaries. Overall, however, the standard deviation is so small that it can be assumed that the prediction for most sea state combinations will also be very good for a large number of variations. Only at the top left, the standard deviation is somewhat larger, so that it can be assumed that the overall prediction of this sea state parameter combinations is less accurate.

5 Conclusions

This study addressed the question if data-driven ML methods can be used to generate tailored wave groups of short duration for wave tank experiments. It was investigated whether a functional relationship between the wave sequence at the target location and the corresponding wave sequence at the wave maker could be established by means of a fully convolutional neural network. The synthetic data generation was carried out using the non-linear HOS method. The basis for the generation of the wave sequences was the JONSWAP spectrum, whereby the wave steepness, wave peak period and enhancement factor were systematically varied.

The investigation showed that the implemented FCN model was suitable for the prediction of the desired wave sequence at the wave maker based on the surface elevation given at the target location. However, it turned out that the accuracy was not the same over the entire parameter domain. The accuracy was significantly worse in certain boundary areas. Nevertheless, it can be concluded that the data-driven approach can be an alternative procedure for the generation of complex wave sequences.

Future steps are the extension of the data set in terms of steeper wave sequences. So far, the physical parameter space ends at $\varepsilon = 0.1$ which is probably not steep enough for critical wave groups. In this context, the trained models are also to be validated in the physical wave tank.

References

[1] Biesel, F. and Suquet, F. (1951). Les appareils générateurs de houle en laboratoire. Houille Blanche-revue Internationale De L Eau, pages 147–165.

[2] Bouws, E., Günther, H., Rosenthal, W., and Vincent, C. L. (1985). Similarity of the wind wave spectrum in finite depth water: 1. Spectral form. 90(C1):975–986.

[3] Chaplin, J. R. (1996). On Frequency-Focusing Unidirectional Waves. International Journal of Offshore and Polar Engineering, 6(2), pages 131–137.

[4] Clauss, G. and Klein, M. (2009). The New Year Wave: Spatial Evolution of an Extreme Sea State. Journal of Offshore Mechanics and Arctic Engineering, 131(4).

[5] Clauss, G. F., Schmittner, C. E., and Klein, M. (2006). Generation of Rogue Waves with Predefined Steepness. In 25th International Conference on Offshore Mechanics and Arctic Engineering, Hamburg, Germany. OMAE2006-92272.

[6] Dommermuth, D. G. and Yue, D. K. P. (1987). A high-order spectral method for the study of nonlinear gravity waves. Journal of Fluid Mechanics, 184:267–288.

[7] Hasselmann, K. F., Barnett, T. P., Bouws, E., Carlson, H. C., Cartwright, D. E., Enke, K., Ewing, J. A., Gienapp, H., Hasselmann, D. E., Kruseman, P., Meerburg, A., Müller, P. M., Olbers, D. J., Richter, K., Sell, W., and Walden, H. (1973). Measurements of wind-wave growth and swell decay during the joint north sea wave project (jonswap).

[8] Kingma, D. P. and Ba, J. (2014). Adam: A method for stochastic optimization. Law, Y., Santo, H., Lim, K., and Chan, E. (2020). Deterministic wave prediction for unidirectional sea-states in real-time using artificial neural network. Ocean Engineering, 195:106722.

[9] LeCun, Y., Bengio, Y., and Hinton, G. (2015). Deep learning. Nature, 521(7553):436–444. Schmittner, C., Kosleck, S., and Hennig, J. (2009). A Phase-Amplitude Iteration Scheme for the Optimization of Deterministic Wave Sequences. In 28th International Conference on Ocean, Offshore and Arctic Engineering, Honolulu, Hawaii. OMAE2009-80131.

[10] Schmittner, C. E. (2005). Rogue Wave Impact on Marine Structures. Dissertation, Technische Universität Berlin (D 83).

[11] Mei, C. C., Stiassnie, M., and Yue, D. K. P. (2005). Theory and Applications of Ocean Surface Waves: Nonlinear aspects. Advanced series on ocean engineering. World Scientific.

[12] Mohaghegh, F., Murthy, J., and Alam, M.-R. (2021). Rapid phase-resolved prediction of nonlinear dispersive waves using machine learning. Applied Ocean Research, 117:102920.

[13] Perlin, M. and Bustamante, M. D. (2016). A robust quantitative comparison criterion of two signals based on the Sobolev norm of their difference. Journal of Engineering Mathematics.

[14] Schäffer, H. A. (1996). Second-Order Wavemaker Theory for Irregular Waves. Ocean Engineering, 23(1):47–88.

[15] Schmittner, C. and Hennig, J. (2012). Optimization of short-crested deterministic wave sequences via a phase-amplitude iteration scheme. In 31stInternational Conference on Ocean, Offshore and Arctic Engineering, Rio de Janeiro, Brazil. OMAE2012-83150.

[16] St. Denis, M. and Pierson, W. (1953). On the motions of ships in confused seas. Transactions, SNAME. 61.

[17] Svendsen, I. A. (1985). Physical modeling of in coastal engineering, chapter Physical modeling of water waves, pages 13–47. Balkema.

[18] Trulsen, K., Kliakhadler, I., Dysthe, K. B., and Verlade, M. G. (2000). On weakly nonlinear modulation of waves in deep water. Phys. Fluids 12 (10), pages 2432–2437.

[19] Wedler, M., Stender, M., Klein, M., Ehlers, S., and Hoffmann, N. (2022). Surface similarity parameter: A new machine learning loss metric for oscillatory sequential data. Neural Networks, 150.

[20] West, B. J., Brueckner, K. A., Janda, R. S., Milder, D. M., and Milton, R. L. (1987). A New numerical method for surface hydrodynamics. Journal of Geophysical Research: Oceans.

[21] Wu, M., Stefanakos, C., and Gao, Z. (2020). Multi-step-ahead forecasting of wave conditions based on a physics-based machine learning (PBML) model for marine operations. Journal of Marine Science and Engineering, 8(12):992.

Authors

Dr.-Ing. Marco Klein
Technische Universität Hamburg
Institut für Strukturdynamik
Schloßmühlendamm 30
21073 Hamburg
Tel.: +49 (40) 42878 2467
e-mail: marco.klein@tuhh.de
Web: https://tore.tuhh.de/cris/rp/rp03241

Dr.-Ing. Marc-André Pick
Technische Universität Hamburg
Institut für Mechanik und Meerestechnik
Eißendorfer Straße 42 (M)
21073 Hamburg
Tel.: +49 (40) 42878 3958
e-mail: pick@tuhh.de
Web: https://www.tuhh.de/mum/home.html

Dr.-Ing. Merten Stender
Technische Universität Hamburg
Institut für Strukturdynamik
Schloßmühlendamm 30
21073 Hamburg
e-mail: m.stender@tuhh.de
Web: https://tore.tuhh.de/cris/rp/rp02552

Numerical and experimental investigations on the dynamic behavior of offshore structures in waves

C. Windt, S. Netzband, C. W. Schulz, M. Abdel-Maksoud, N. Goseberg

Abstract: Climate change on the one hand and the demand to reduce reliance on fossil fuels on the other hand are strong drivers to promote the sector of offshore renewables. In this context, numerical and experimental methods are cornerstones to research and development of offshore renewable energy devices. This work presents recent advances within these two methodological strands, highlighting individual advantages while reflecting on mutual benefits that arise when both methods combine their strength. It is highlighted that a close collaboration during the development of new advances in numerical and experimental methods can be of mutual benefit. In particular, the joint use of data from the large wave flume test facility GWK+ and the *pan*MARE modelling method enables to fully exploit their potential.

1 Introduction and Motivation

Global climate change has largely motivated a recent push to adapt the way humankind attempts to produce its energy. This adaptation aims at decreasing energy sources that emit carbon dioxide and favors renewable, sustainable sources. Onshore renewable energy technologies have been in use for quite some time, while offshore locations for the production of electric energy have only been considered for the past two decades. Offshore renewable energy includes wind, wave, tidal, and thermal energy conversion, among which the offshore wind technology is by far the most commercialized sector in this field (Pelc and Fujita (2002)).

Further development of the offshore production of electric energy is clearly motivated by the vast, abundant, and constant availability of wind and waves, or in the case of tidal currents, its predictability. However, as a drawback, technical frontiers and challenges ranging from installability, over reliability and operability to maintainability exist, all of which have a direct tie to the levelized cost of energy (LCOE) that a certain technology can be operated at (OES, 2021). Aside from technical considerations, environmental concerns are nowadays more clearly voiced; the arguments pertain to the interactions with marine ecosystems (Hammar et al., 2017), effects on migratory birds (Hayes et al., 2015) or negative feedback due to generally increased human activities in marine exploitation hotspots (Kenny et al., 2017).

For tidal energy conversions, a few projects are on a promising trajectory towards commercialisation. Compared to wave energy systems, more advanced technology convergence can be observed, with a trend towards two- to three-bladed rotors on bottom-fixed or floating support structures. Nonetheless, challenges remain, for instance regarding blade shape and material for reduced risk of failure (ETIP Ocean, 2020) or the environmental impact on marine fauna (Pine et al., 2019). Moreover, understanding the effects of tidal turbine arrays is still in its infancy; for both, bottom-fixed and floating turbines alike it remains unclear how they influence each other downstream and how their wakes will affect marine bottom-dwelling communities (Stansby and Ouro, 2022).

To date, challenges of wave energy systems are more severe; a technological convergence towards an optimal energy extraction system has not yet been reached; thus further innovations to reach a competitive LCOE are required (S. Pennock et al., 2022). Challenges lie within the interaction of wave energy devices with extreme loading conditions (waves and currents, often in combination) and its adverse effects on the marine environment (Aderinto and Li., 2018).

Offshore wind energy, by far the most developed and commercially viable form of the technology, currently faces challenges pertaining to deployments in deeper water depth, typically where floating structures show a greater cost efficiency. A recent review on fixed and floating offshore wind structures by Wu et al. (2019) emphasizes the demand for improvement of our understanding of the offshore wind turbine foundations, better validation of numerical models used in design and more elaborate laboratory test conditions. Bottom-fixed offshore wind structures are a long-standing subject of interest; however, there is still considerable demand to better understand combined environmental loading of waves and currents, as well as extreme conditions (Welzel et al., 2020 and Schendel et al., 2016). A higher level of complexity and stronger research demands exist when floating offshore wind technologies are concerned. In this context, interdisciplinary collaborations are required, as aerodynamic and hydrodynamic expertise, along with material sciences, control and structural engineering are needed to achieve sustainable and economically-viable solutions (Y. Liu et al., 2017).

In light of the above outlined challenges and concerns, it is paramount to strengthen research activities with the overall aim to improve the general understanding of technology-induced effects on the marine environment and to develop robust, yet accurate prediction tools. This work addresses the challenges ahead of us from a methodological point of view, (i) discussing and (ii) reflecting the recent advances in numerical and experimental simulations, and (iii) by outlining mutually beneficial aspects of co-modelling. The remainder of this work presents a focused literature review in 2. Next, it presents latest numerical and experimental advances in Sec. 3 and 4, respectively. Sec. 5 draws conclusions and presents mutually beneficial strategies to combine experimental and numerical modelling.

2 Literature Review

2.1 Experimental modelling of floating offshore wind turbines

In the literature, various experimental studies on (floating) offshore wind turbines can be found. A classification of the existing experimental literature can be introduced based on the application of the experimental data sets. Experimental data may be used for the specific analysis of the dynamic behaviour under extreme or operational conditions (F. Madsen et al., 2020) or as input for system identification methodologies (N Hara et al., 2017). Experimental data may also be acquired purely for validation purposes, acting as reference for the validation of numerical or analytical models (D. Walia et al., 2021)

Furthermore, a classification based on the scale of the system under investigation can be performed. While a large number of studies pertain to a small to medium scale (A. Otter et al., 2021), only few studies on the dynamics of offshore wind turbines at large scale (A. Hildebrandt and T. Schlurmann., 2012; C. Lopez-Pavon and A. Souto-Iglesias., 2015) are available – mainly as a result of the limited accessibility of large scale test facilities.

Finally, a classification of the literature can be conducted based on the complexity of the system under investigation, which is commonly linked to the application of the experimental data. Relatively simple model setups may consist of a floating support structure, moored for station-keeping, while data of the incident waves and structural motion is recorded. Such simple setups may be extended by, e.g. including representations of the turbine system, or more advanced measuring equipment (A. Otter et al., 2021). In particular for the experimental investigation of floating offshore wind turbines, more complex experimental setups employing hardware-in-the-loop (HIL) systems are recently moving into the focus. HIL systems, enabling the coupling between a physical system and a numerical modelling framework, are employed in various fields of engineering. For wind turbine tests in wave flumes or basins, an HIL system is commonly employed to overcome scaling discrepancies between the wave and the wind loading. Striking differences between the existing systems can be observed in terms of the underlying numerical model and the actuation systems. The numerical models differ in terms of their level of non-linearity. The actuation can be based, for instance, on ropes–and–pulley systems, single thrusters, or multiple fans. Examples of different HIL systems are documented in Sauder et al. (2016), Urbán and Guanche (2019) and Fontanella et al. (2020).

2.2 Numerical modelling of floating offshore wind turbines

Numerical methods are well established in the assessment of offshore structures, allowing for various specialised approaches to tackle specific questions. A widely-used approach of modern engineering tools for the motion analysis of floating structures is based on frequency domain potential flow solvers (A. Cordle and J. Jonkman., 2011; M. Borg and H. Bredmose., 2015; A. N. Robertson et al., 2020). Basic assumptions of incompressible, inviscid, and irrotational

flow allow for an efficient calculation of characteristic coefficients of the structure which are subsequently applied to calculate the hydrodynamic forces and the dynamic performance of the system in time domain. A series of further methods is based on the Morison approach to estimate the hydrodynamic forces (Borg and Bredmose., 2015; Robertson et al., 2020). This approach particularly applies to slender structures with low impact on the incoming waves.

Wind energy, as well as tidal energy converters, are mostly based on horizontal axis turbines with two or three blades. Due to their computational efficiency and robustness, methods based on the blade element momentum theory (BEMT) are commonly applied to calculate loads and energy yield of such turbines when the computational time is limited. According to BEMT, the rotor area is divided into independent annular rings and empirical coefficients are used to characterise the lift and drag forces on the corresponding blade sections. With the assumptions of an inviscid flow and a uniform distribution of the extracted momentum on the annular rings, a momentum balance between the forces acting on the blades and the flow velocity deficit can be derived for every annular ring. Following, from an integration of the forces on every blade element, power and thrust of the rotor can be computed. A detailed description of the theoretical background can be found in T. Burton et al. (2001). Methods based on this approach are often considered as engineering methods, as only the blade loads are estimated from a rather simple model while no flow simulation is performed.

For floating structures all acting forces can than be integrated with a six-degrees-of-freedom solver (6DOF) to estimate the platform motion. The approach suits well for regular and irregular waves (A. J. Coulling et al., 2013; A. Myhr and T. Nygaard., 2015). However, due to the frequency-based approach and the lack of the three–dimensional flow field, the capabilities of such methods are limited in the investigation of coupled aero-hydro-moor influences.

3 Numerical advances on modelling of floating offshore wind turbines

Compared to the above mentioned engineering methods, a more detailed approach is being adopted at the Hamburg University of Technology (TUHH) with the panel method *pan*MARE. On the same assumptions of an incompressible, inviscid, and irrotational fluid, the three–dimensional potential flow field is solved in time domain. The floating structure, as well as the free water surface, are represented by first-order panels. The unsteady pressure distribution on the platform hull is resolved in each time step by estimating the instantaneous platform position, free surface elevation, and wetted surface area of the hull. This is applied to both the hydrodynamic and aerodynamic problems, allowing the coupled system to be simulated using a single method. A description of the method and its application on floating offshore wind turbines is given in Netzband et al. (2018) and Netzband et al. (2020). A comparison with other methods regarding the hydrodynamic loads are shown in Wang et al. (2021), Wang et al. (2022) and Robertson et al. (2020).

The method is available as a Python library including a C++ core. Computationally expensive

parts are coded in C++ ensure fast generation and solving of the underlying equation systems. The extensive Python interface of the core module allows high flexibility in the applicability of the method. New numerical models can be easily implemented in a first draft within Python scripts. After successful testing of the new implemented models, they can be transferred to the C++ core to benefit from faster processing.

The aerodynamic and hydrodynamic flow fields are considered as potential flow fields, thus it is required that the flow field satisfies the Laplace equation at every point in the solution domain (Katz and Plotkin., 2004). In order to meet this requirement in the aerodynamic domain, the wind turbine (or tidal turbine) blade surface is modelled using panels, each of which is assigned a source and a dipole whose strengths represent the elementary solutions of Laplace equation. While the source panel strength is calculated to the effect that the displacement of the blade geometry is considered correctly in the potential flow field, the dipole panels introduce a certain circulation around the blade. The vortices in the wake of the rotor are also represented by dipole panels. The wake dipole panels are shed from the trailing edge of the blade and move with the local flow velocity downstream. Their strength is determined by the circulation around the blade. Finally, the well-known helix shape of the free vortex system in the wake of a rotor originates from the shed dipole panels. In this way, only the lift force of the rotor blades can be determined, as the drag originates from a viscous boundary layer that is not modelled in potential theory. Therefore, additional drag forces can be included using an approach that utilises the Schoenherr line (Hoerner., 1965). Modelling the flow field allows *pan*MARE to simulate aerodynamic phenomena, such as blade-wake interaction, which is a clear advantage over BEMT methods.

Similar to the aerodynamic part, the surface of the floating structure is modelled with panels. The solution of the hydrodynamic problem under consideration of the incoming waves provides the strength of the source and the dipole at each plate, based on which the unsteady pressure and the hydrodynamic loads, the added mass effects and Froude-Krylov forces are calculated. Due to the initial assumption of a non-viscous flow, an extension of the calculation method is applied for the calculation of the viscous resistance which is based on the drag term of the Morison equation.

Regular waves are represented by analytical formulations of their potential flow and describe up to fifth-order Stokes waves. Irregular waves are generated by a superposing such waves; however, can be applied up to second-order only. Irregular second-order waves include sum and difference frequencies which may have a strong influence on the region of surge or pitch resonance (Robertson et al., 2020). Diffraction and radiation effects of the wave-body interaction are superimposed on the wave potential (González et al., 2021). The vertical deformation of the free surface panels is then calculated and fulfills the kinematic and dynamic boundary condition at their center.

Various different approaches of mooring models are optionally used at present. The most detailed method is a lumped mass model (Hall and Goupee., 2015) where the mass of the line is concentrated onto mass nodes, connected by spring-damper elements representing the structural properties of the line. The node deformation is then solved under the influence of the fairlead motion and fluid flow field.

The forces induced by the aerodynamic loads, the incoming waves and mooring system are

then combined within one 6DOF solver to predict the motion state of the structure under given environmental conditions. Figure 1 shows the procedure of the solving routine with synchronised motion states of all domains and Figure 2 visualises the dynamic pressure on a structure in waves. The time domain approach employed in *pan*MARE closes the gap between the state-of-the-art engineering tools and high fidelity CFD methods. It allows for a detailed and versatile view on the motion behaviour, three-dimensional flow field, and loads of any structure or especially of floating offshore wind turbines.

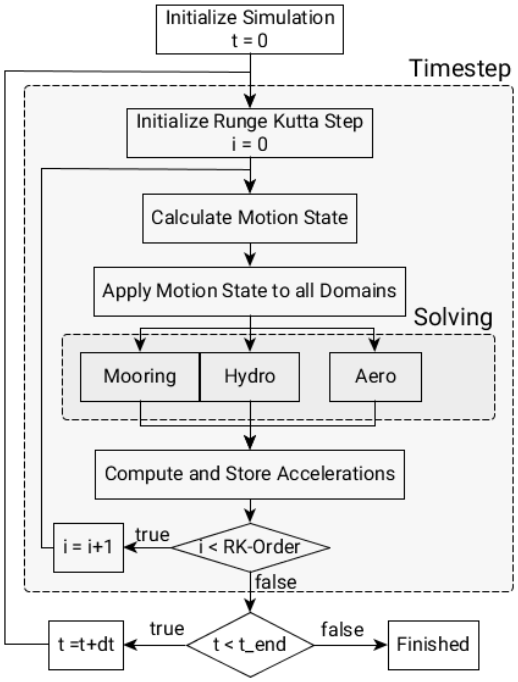

Figure 1: Flow chart of the numerical method with a fully synchronous motion and parallel solving of all domains.

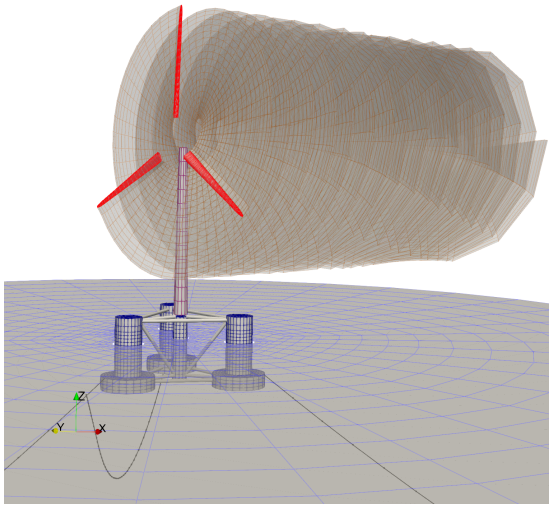

Figure 2: Numerical grid of the simulation of the DeepCWind platform (A. Robertson et al., 2014) equipped with the NREL 5MW reference turbine (Jonkman et al., 2009).

4 Experimental advances on modelling dynamics of offshore structures

This section describes recent developments at a dedicated coastal and ocean engineering test facility, called *Large Wave Flume*+ (GWK+). This wave-current flume has evolved from its predecessor facility, the *Large Wave Flume*, in operation since 1983. It is operated by the Coastal Research Center, a joint research facility of Leibniz University Hannover and Technische Universität Braunschweig, Germany. The described experimental facility includes the main structural and hydro-kinetic devices, as well as dedicated gear to achieve additional, aerodynamic loading for ocean renewable testing.

4.1 Large Wave Flume GWK+

GWK+ is a large-scale coastal and ocean engineering facility, dedicated to testing at very large scale. The large wave flume (dimensions length x width x depth: $307\,\mathrm{m}$ x $5\,\mathrm{m}$ x $7\,\mathrm{m}$, Figure 3(a)) aims to support technology development within the German Energy Research Umbrella (Schlurmann et al., 2018). A 1:10 down-scaled version of the GWK+ is available for pre-testing of complex experimental setups (Brühl et al., 2018). As the challenge of ocean renewables is related to predict responses to extreme conditions, a new wave maker has been procured that is capable of generating wave heights of up to $3.0\,\mathrm{m}$ and periods up to $10.0\,\mathrm{s}$. The wave generation also features state-of-the-art second-order wave generation and reflection compensation.

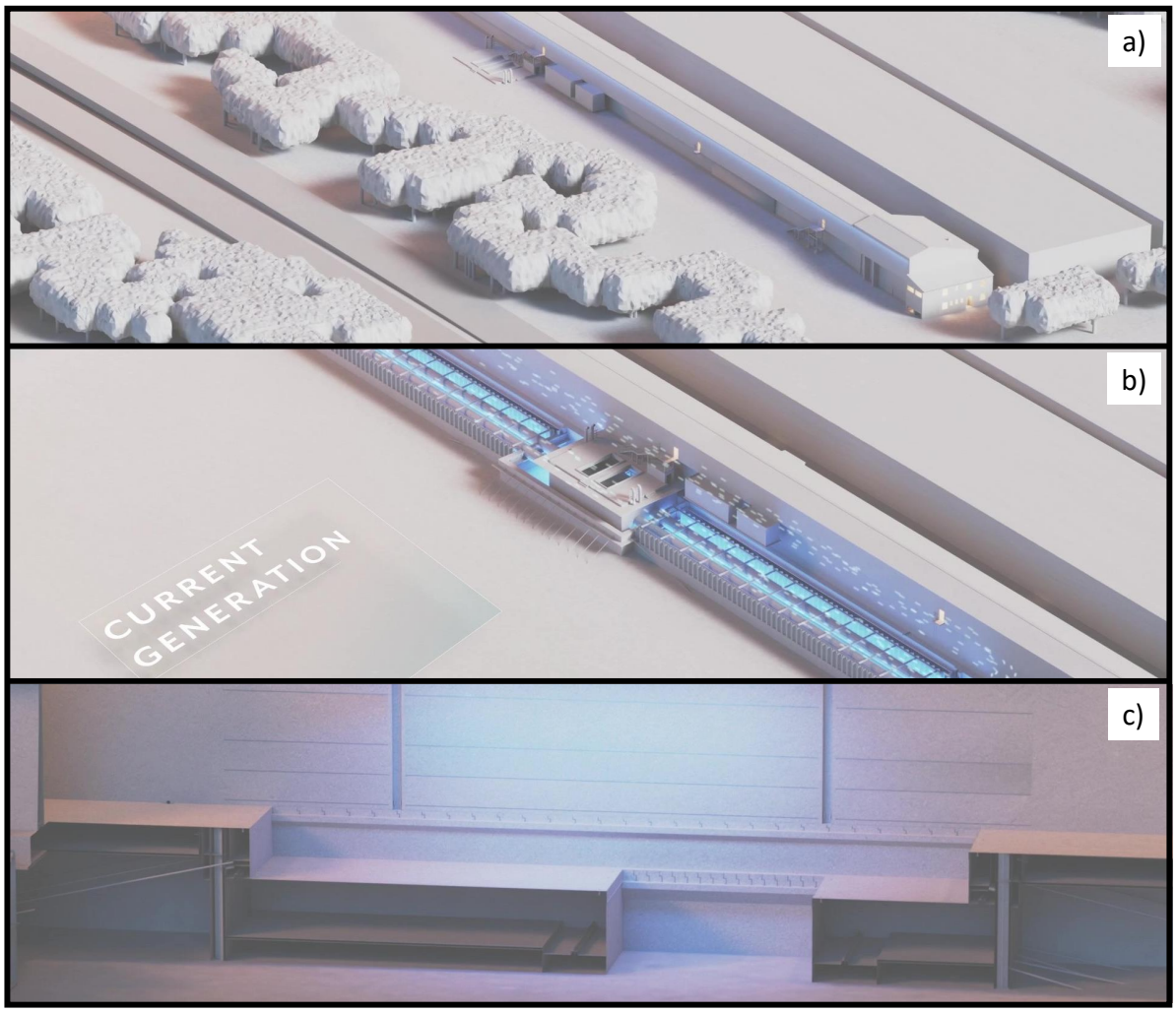

Figure 3: Illustration of the large wave flume. (a) Rendering of the entire facility. (b) Pump facility with re-circulation. (c) Cross-sectional view of the staggered deep section, up to $-6.0\,\mathrm{m}$ below flume bottom

A common in-situ condition at marine offshore sites features combined extreme wave and tidal

current conditions. Wave steepening and energy focusing is a known feature that can lead to more extreme conditions. Such combined environmental loads are often overlooked, yet highly relevant (Quilfen et al., 2018; Barltrop et al., 2007). To that end, GWK+ is expanded with a two-way re-circulation system where currents up to $0.8\,\mathrm{m\,s^{-1}}$ can be super-imposed on waves, in either following or opposing conditions (see Figure 3(b)). Hence, realistic oceanic conditions, with a full spectrum of wave kinematics can be provided at a large scale. Lastly, many floating technologies require realistic mooring properties which are sometimes difficult to provide in shallow water flume facilities. For this purpose, a staggered deep pit is constructed permitting to extended the water depth to about $11.0\,\mathrm{m}$, or in case of fixed structures, to embed marine structures in realistic soil conditions (see Figure 3(c)).

4.2 HIL at GWK+

In the framework of the NuLIMAS project (Numerical modelling of liquefaction around marine structure) (Windt et al., 2022), a dedicated HIL system for the analysis of floating offshore wind systems at large scale is developed for GWK+. In particular, a multi-fan system similar to Urbán and Guanche (2019) is targeted, using four propellers to apply the required wind load on the structure. A block diagram of the entire HIL system and a single drive train of the actuation system is shown in Figures 4 (a) and (b), respectively.

The motion of the floating structure within the physical model (Figure 4 (c)) is captured in real-time with a Qualisys motion-capturing system. Based on the measured motion together with the data of the wind field (e.g. originating from metocean data of a specific deployment site) a numerical model is exercised to calculate the required thrust force. The specific thrust force is then fed back to the physical model via the multi-fan actuating system.

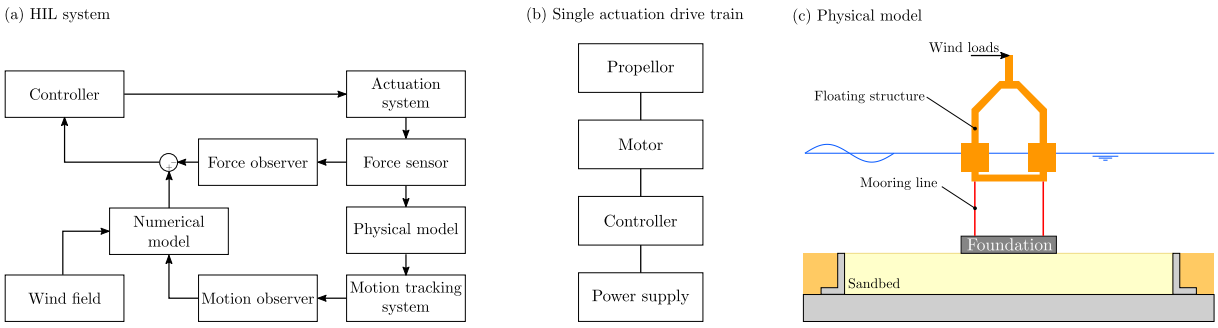

Figure 4: Block diagram of (a) a generic HIL system for floating offshore wind applications (Figure adapted from Sauder et al. (2016)); (b) single drive train of the actuation system.

For the HIL system at GWK+, a simplified low-order numerical model, initially developed by Lemmer (Lemmer, 2018), is employed. Aiming at high computational efficiency to meet real-time requirements, the numerical model is reduced to relevant physics. Here only the aerodynamics are considered via a quasistatic actuator disk model; tower and/or blade dynamics are neglected.

5 Synthesis and Outlook

Large-scale experiments conducted at GMK+ permit thorough and detailed investigations of offshore structures which is deemed as particularly advantageous in case of floating offshore wind turbines with its complex interaction of mooring system, hydro- and aerodynamics. Using the HIL system solves the issue regarding the different scaling approaches of the floating platform and the rotor. Larger wave periods in the large scale experiments also reduce the influence of the time lag of the HIL system, which was observed in smaller scaled experiments (Gueydon et al., 2020). Furthermore, large-scale experiments allow for reduced scale and model effects, particularly when rather extreme environmental loads, with potentially breaking waves are concerned. Thus, experiments with floating offshore wind turbines in the GWK+ can provide very accurate and valuable benchmark data sets for the use in numerical modelling.

Solving the three–dimensional flow field in time-domain tends in the same direction since providing accurate data with numerical methods allows for a more detailed view on the effects around the structure - as compared to two-dimensional and/or frequency domain based methods. *pan*MARE additionally has the advantage of high computational efficiency, while maintaining high accuracy.

Such new advances in both fields can be exploited to the fullest when developed in close collaboration, since numerical and experimental methods benefit from each other when findings on one side improve the quality of the other. For instance, numerical results can already be valuable during the planning and design of the experiments. Knowing the expected range of sensor loads in advance is crucial when dimensioning the sensor. If sensors are oversized, the result is likely to be inaccurate and when undersized they cannot capture important load cases and might fail. The numerical method *pan*MARE is able to determine the expected loads of all potential sensors from the mooring line forces or hull pressure up to the blade root moment. It also allows to verify the aerodynamic loads calculated by the low-order model of the HIL system under the influence of the platform motions and in specific load cases. As the HIL method is still in an early stage of development, the influence of inaccuracies such as time lag or noise on the measured data is currently not fully understood. Utilising a high-fidelity method such as *pan*MARE can also contribute to this understanding when observed inaccuracies arising from the application of the HIL system are incorporated into the simulations. In this way, certain limitations of the HIL method, which are strongly influenced by the scaling ratio, may be identified.

Conversely, the experimental data in the expected quality is highly beneficial for the validation of the higher level simulation method *pan*MARE. In order to numerically reproduce the experiments one-to-one it is feasible to replace the rotor model by the low-order aerodynamic model of the HIL system. In this way, both systems experience the same simplifications on the aerodynamic side, allowing a clearer look on the hydrodynamic problems. The basis of a successful validation is a well-defined setup with low inaccuracies which is more likely to be achieved with larger scale models.

With GWK+ and the HIL system in operation in the second half of 2023, experimental data sets

for a floating offshore wind turbine will be acquired in the framework of the NuLIMAS project. Such data will form the initial basis for a validation of *pan*MARE against large scale physical data. This, in turn, forms the stepping stone towards the above detailed exploitation of the full potential of GWK+ and *pan*MARE in future collaborations.

6 Funding

The authors at Hamburg University of Technology are very grateful to the Federal Ministry of Economics and Climate Protection (BMWK) for the financial support of the VAMOS project [03EE2004C], in which essential development steps of the *pan*MARE method were achieved. For the development of GWK+, funding is received from the German Federal Ministry for Economic Affairs and Climate Action (Grant No. 0324196A). For the development of the HIL system at GWK+, funding is received from the German Federal Ministry for Economic Affairs and Climate Action (Grant No. 03SX524A) in the framework of the ERA-NET Cofund MarTERA (Grant No. 728053).

References

[1] Hoerner S. Fluid-Dynamic Drag: Practical Information on Aerodynamic Drag and Hydrodynamic Resistance. Fluid-Dynamic Drag: Practical Information on Aerodynamic Drag and Hydrodynamic Resistance. Dr.-Ing. S.F. Hoerner, 1965.

[2] Burton T. et al. Wind Energy Handbook. John Wiley & Sons, 2001.

[3] Pelc R. and Fujita R. “Renewable energy from the ocean”. In: Marine Policy 26.6 (2002), pp. 471–479.

[4] Katz J. and Plotkin A. “Low-Speed Aerodynamics, Second Edition”. In: Journal of Fluids Engineering 126.2 (2004), p. 293.

[5] Barltrop N. et al. “Investigation into wave–current interactions in marine current turbines”. In: Proceedings of the Institution of Mechanical Engineers, Part A: Journal of Power and Energy 221.2 (2007), pp. 233–242.

[6] Jonkman J. et al. Definition of a 5-MW Reference Wind Turbine for Offshore System Development. Golden, Colorado, USA, 2009, p. 75. pmid: 11840489.

[7] Cordle A. and Jonkman J. “State of the Art in Floating Wind Turbine Design Tools”. In: 21st International Offshore and Polar Engineering Conference. Maui, Hawaii, 2011.

[8] Hildebrandt A. and Schlurmann T. “Breaking wave kinematics, local pressures, and forces on a tripod structure”. In: Coastal Engineering Proceedings 33 (2012), pp. 71–71.

[9] Coulling A. J. et al. “Validation of a FAST Semi-Submersible Floating Wind Turbine Numerical Model with DeepCwind Test Data”. In: Journal of Renewable and Sustainable Energy 5.2 (2013), p. 023116.

[10] Robertson A. et al. Definition of the Semisubmersible Floating System for Phase II of OC4. Golden, Colorado, USA: National Renewable Energy Laboratory, 2014, p. 38.

[11] Borg M. and Bredmose H. Overview of the Numerical Models Used in the Consortium and Their Qualification. LIFES50+ Deliverable 4.4, DTU WInd Energy Report-E-0097. Kgs. Lyngby, Denmark: Technical University of Denmark, Jan. 1, 2015, p. 36.

[12] Hall M. and Goupee A. “Validation of a Lumped-Mass Mooring Line Model with DeepCwind Semisubmersible Model Test Data”. In: Ocean Engineering 104 (2015), pp. 590–603.

[13] Hayes M. A. et al. “Seasonally-Dynamic Presence-Only Species Distribution Models for a Cryptic Migratory Bat Impacted by Wind Energy Development”. In: PLOS ONE 10.7 (2015), pp. 1–20.

[14] Lopez-Pavon C. andSouto-Iglesias A. “Hydrodynamic coefficients and pressure loads on heave plates for semi-submersible floating offshore wind turbines: A comparative analysis using large scale models”. In: Renewable Energy 81 (2015), pp. 864–881.

[15] Myhr A. and Nygaard T. “Comparison of Experimental Results and Computations for Tension-Leg-Buoy Offshore Wind Turbines”. In: Journal of Ocean and Wind Energy 2 (2015), pp. 12–20.

[16] Sauder T. et al. “Real-time hybrid model testing of a braceless semi-submersible wind turbine: Part I – The hybrid approach”. In: Proceedings of the 35th International Conference on Ocean, Offshore and Arctic Engineering, Busan, Korea. 2016, pp. 1–13.

[17] Schendel A. et al. “Erosion stability of wide-graded quarry-stone material under unidirectional current”. In: Journal of Waterway, Port, Coastal, and Ocean Engineering 142.3 (2016), p. 04015023.

[18] Hammar L. et al. “Introducing ocean energy industries to a busy marine environment”. In: Renewable and Sustainable Energy Reviews 74 (2017), pp. 178–185.

[19] Hara N. et al. “Experimental validation of model-based blade pitch controller design for floating wind turbines: system identification approach”. In: Wind energy 20.7 (2017), pp. 1187–1206.

[20] Kenny A. J. et al. “Assessing cumulative human activities, pressures, and impacts on North Sea benthic habitats using a biological traits approach”. In: ICES Journal of Marine Science 75.3 (2017), pp. 1080–1092.

[21] Liu Y. et al. “Establishing a fully coupled CFD analysis tool for floating offshore wind turbines”. In: Renewable Energy 112 (2017), pp. 280–301.

[22] Aderinto T. and Li. H. “Ocean Wave Energy Converters: Status and Challenges”. In: Energies 11.5 (2018).

[23] Brühl M. et al. “Design and operation of a new small-scale wave-current flume”. In: Proceedings of 9th Chinese-German Joint Symposium on Hydraulic and Ocean Engineering (CGJOINT 2018). National Cheng Kung University. Tainan, ROC, 2018.

[24] Netzband S. et al. “A Panel Method for Floating Offshore Wind Turbine Simulations with Fully Integrated Aero- and Hydrodynamic Modelling in Time Domain”. In: Ship Technology Research 65.3 (Sept. 2, 2018), pp. 123–136.

[25] Quilfen Y. et al. “Storm waves focusing and steepening in the Agulhas current: Satellite observations and modeling”. In: Remote Sensing of Environment 216 (2018), pp. 561–571.

[26] Schlurmann T. et al. “marTech - Development of Renewable Maritime Technologies for Reliable and Sustainable Energy Supply”. In: Proceedings of 9th Chinese-German Joint Symposium on Hydraulic and Ocean Engineering (CGJOINT 2018). National Cheng Kung University. Tainan, ROC, 2018.

[27] Lemmer F.. “Low–Order Modeling, Controller Design and Optimization of Floating Offshore Wind Turbines”. PhD thesis. Institute of Aircraft Design, 20198.

[28] Pine M. K. et al. “Providing ecological context to anthropogenic subsea noise: Assessing listening space reductions of marine mammals from tidal energy devices”. In: Renewable and Sustainable Energy Reviews 103 (2019), pp. 49–57.

[29] Urbán A. M. and Guanche R. “Wind turbine aerodynamics scale-modeling for floating offshore wind platform testing”. In: Journal of Wind Engineering and Industrial Aerodynamics 186 (2019), pp. 49–57.

[30] Wu X. et al. “Foundations of offshore wind turbines: A review”. In: Renewable and Sustainable Energy Reviews 104 (2019), pp. 379–393.

[31] ETIP Ocean. Strategic Research and Innovation Agenda for Ocean Energy. Tech. rep. 2020.

[32] Fontanella A. et al. “A hardware-in-the-loop wave-basin scale-model experiment for the validation of control strategies for floating offshore wind turbines”. In: Journal of Physics: Conference Series. Vol. 1618. 3. IOP Publishing. 2020, p. 032038.

[33] Gueydon S. et al. “Discussion of Solutions for Basin Model Tests of FOWTs in Combined Waves and Wind”. In: Ocean Engineering 209 (Aug. 2020), p. 107288.

[34] Madsen F. et al. “Experimental analysis of the scaled DTU10MW TLP floating wind turbine with different control strategies”. In: Renewable Energy 155 (2020), pp. 330–346.

[35] Netzband S. et al. “Self-Aligning Behaviour of a Passively Yawing Floating Offshore Wind Turbine”. In: Ship Technology Research 67.1 (Jan. 2, 2020), pp. 15–25.

[36] Robertson A. N. et al. “OC6 Phase I: Investigating the Underprediction of Low-Frequency Hydrodynamic Loads and Responses of a Floating Wind Turbine”. In: Journal of Physics: Conference Series 1618 (Sept. 2020), p. 032033.

[37] Welzel M.et al. “Influence of Structural Elements on the Spatial Sediment Displacement around a Jacket-Type Offshore Foundation”. In: Water 12.6 (2020), p. 1651.

[38] González D. F. et al. “Advances on Simulation of Wave-Body Interactions under Consideration of the Nonlinear Free Water Surface”. In: Ship Technology Research 68.1 (Jan. 2, 2021), pp. 27–40.

[39] Ocean Energy Systems. An International Evaluation and Guidance Framework for Ocean Energy Technology. Tech. rep. 2021.

[40] Otter A. et al. “A review of modelling techniques for floating offshore wind turbines”. In: Wind Energy (2021).

[41] Walia D. et al. “Numerical and Physical Modeling of a Tension-Leg Platform for Offshore Wind Turbines”. In: Energies 14.12 (2021), p. 3554.

[42] Wang L. et al. “OC6 Phase Ib: Validation of the CFD Predictions of Difference-Frequency Wave Excitation on a FOWT Semisubmersible”. In: Ocean Engineering 241 (2021), p. 110026.

[43] Pennock S. et al. “Deriving Current Cost Requirements from Future Targets: Case Studies for Emerging Offshore Renewable Energy Technologies”. In: Energies 15.5 (2022).

[44] Stansby P. K. and Ouro P. “Modelling marine turbine arrays in tidal flows”. In: Journal of Hydraulic Research 60.2 (2022), pp. 187–204.

[45] Wang L. et al. “OC6 Phase Ia: CFD Simulations of the Free-Decay Motion of the Deep-Cwind Semisubmersible”. In: Energies 15.1 (2022), p. 389.

[46] Windt C. et al. “Numerical modelling of liquefaction around marine structures – Progress and recent developments”. In: accpeted in the Proceedings of the 41st International Conference on Ocean, Offshore and Arctic engineering, Hamburg, Germany. 2022, pp. 1–10.

Authors

Stefan Netzband
Hamburg University of Technology
Institute for Fluid Dynamics and Ship Theory
Am Schwarzenberg Campus 4
21079 Hamburg
Tel.: +49(0)40/42878-4721
e-mail: stefan.netzband@tuhh.de
Web: www.tuhh.de/fds

Christian W. Schulz
Hamburg University of Technology
Institute for Fluid Dynamics and Ship Theory
Am Schwarzenberg Campus 4
21079 Hamburg
Tel.: +49(0)40/42878-4792
e-mail: christian.schulz@tuhh.de
Web: www.tuhh.de/fds

Prof. Dr.-Ing. Moustafa Abdel-Maksoud
Hamburg University of Technology
Institute for Fluid Dynamics and Ship Theory
Am Schwarzenberg Campus 4
21079 Hamburg
Tel.: +49(0)40/42878-6053
e-mail: m.abdel-maksoud@tuhh.de
Web: www.tuhh.de/fds

Dr. Christian Windt
Technische Universität Braunschweig
Leichtweiß-Institut für Wasserbau
Beethovenstr. 51A
38106 Braunschweig
Tel.: +49(0)531/391-3988
e-mail: c.windt@tu-braunschweig.de
Web: https://www.tu-braunschweig.de/lwi/hyku

Univ.-Prof. Dr.-Ing. Nils Goseberg
Technische Universität Braunschweig
Leichtweiß-Institut für Wasserbau
Beethovenstr. 51A
38106 Braunschweig
Tel.: +49(0)531/391-3930
Fax: +49(0)531/391-8217
e-mail: n.goseberg@tu-braunschweig.de
Web: https://www.tu-braunschweig.de/lwi/hyku